UNIVERSITY OF CALIFORNIA
RIVERSIDE

Flexible Framework for Co-Optimizing Dynamic Traffic Signal Control: Foundation for Adaptive Optimization Strategies

A Dissertation submitted in partial satisfaction
of the requirements for the degree of

Doctor of Philosophy

in

Electrical Engineering

by

Roland David Edger Oswald

September 2023

Dissertation Committee:

- Dr. Matthew J. Barth, Chairperson
- Dr. Peng Hao
- Dr. Hyoseung Kim

The Dissertation of Roland David Edger Oswald is approved:

_____

_____

_____

Committee Chairperson

University of California, Riverside

Acknowledgment

I would like to express my deepest gratitude and appreciation to all those who have supported and guided me throughout the journey of completing this dissertation. This work would not have been possible without the encouragement, assistance, and contributions of numerous individuals and institutions. Therefore, I would like to take this opportunity to acknowledge their invaluable support.

First and foremost, I extend my heartfelt thanks to my advisor, Dr. Matthew Barth, for his unwavering guidance, patience, and encouragement throughout the entire research process. His expertise, constructive feedback, and constant availability have been instrumental in shaping this dissertation into its final form.

I am also grateful to the members of my dissertation committee, Dr. Peng Hao, for his valuable insights, thoughtful suggestions, and critical reviews that have significantly enhanced the quality of this research; and Dr. Hyoseung Kim, it was because of his class that I first worked with some of the equipment mentioned in this dissertation, marking the initial and crucial step in embarking on this research journey.

I would also like to specifically thank Dr. George Scora, Dr. Guoyuan Wu, and Mr. Alexander Vu. The three of you were, and Dr. Peng Hao, were crucial in the research I completed at UCR and I really would not have made it without your help and guidance.

My sincere appreciation goes to the faculty members and researchers at UCR, whose lectures, seminars, and discussions have provided me with a strong academic foundation and inspired my passion for this field of study.

I am indebted to my friends and fellow colleagues who supported me during challenging times, providing encouragement and understanding throughout this demanding academic journey.

Specifically, I would like to mention my TSR group members, including Mike Todd, Dr. Kanok Boriboonsomsin, Dr. Zhouqiao Zhao, Zhensong Wei, Zhengwei Bai, Dr. Ziran Wang, Dr. Chao Wang, Saswat Priyadarshi Nayak, Jacqueline Garrido Escobar, Dr. Xishun Liao, Xuanpen Zhao, Dylan Brown, Pingbo Ruan, and many more. I truly appreciate my friend Dr. Nigel Williams; you were my first friend at CE-CERT and I hope we will continue to be friends for years to come.

I am deeply thankful to my parents and family for their unwavering love, encouragement, and belief in my abilities. Their constant support and sacrifice have been the driving force behind my pursuit of academic excellence.

Finally, I would like to express my gratitude to all the participants who willingly contributed their time, effort, and insights to this research. Without their cooperation, this study would not have been possible.

The successful completion of this dissertation is the result of the collective efforts of many individuals, and I am sincerely grateful to each and every one of them for their support and encouragement. Their contributions have been invaluable, and I am humbled by their generosity.

Thank you all.

The major contents in this dissertation have been published in IEEE Intelligent Transportation Systems Conference, Transportation Research Board Annual Meeting, IEEE Transactions on Intelligent Vehicles, and the National Center for Sustainable Transportation.

ABSTRACT OF THE DISSERTATION

Flexible Framework for Co-Optimizing Dynamic Traffic Signal Control: Foundation for Adaptive Optimization Strategies

by

Roland David Edger Oswald

Doctor of Philosophy, Graduate Program in Electrical Engineering
University of California, Riverside, September 2023
Dr. Matthew Barth, Chairperson

As urban traffic congestion and environmental concerns continue to escalate, there is a growing need for innovative approaches to optimize the performance of signalized intersections. This dissertation presents a comprehensive investigation into the co-optimization of vehicle trajectories and traffic signal timing at isolated signalized intersections. The primary objective is to propose a novel co-optimization framework that integrates eco-trajectory planning and traffic signal timing optimization to improve transportation efficiency and reduce environmental impacts, which we call Eco-friendly Cooperative Traffic Optimization (ECoTOp).

Central to this research are the functional building blocks, including the creation of an Innovation Corridor testbed in Riverside, CA, a Speed Advisory Tablet App, Lane-level GNSS Applications, and the integration of a refined MOVES emission model. These innovative components enable accurate and efficient data collection, advanced traffic control, and precise emission estimation, elevating the ECoTOp approach to new levels of effectiveness and sustainability. Building upon this foundation, the methodology is established, encompassing the development of hybrid co-optimization algorithms and the utilization of a simulation platform, SUMO, for evaluating various experimental scenarios.

The case studies are pivotal in this dissertation, investigating the ECoTOp approach across diverse scenarios with varying traffic volumes, connected and automated vehicle (CAV) penetration rates, and mixed vehicle types. Comparative analyses between ECoTOp and individual strategies are conducted to lay the groundwork for future development of an adaptive optimization strategy. Moreover, the ECoTOp approach is extended to incorporate electric vehicles (EVs), with energy estimated using MATLAB's EV model.

Furthermore, the dissertation explores the concept of an adaptive optimization strategy capable of dynamically selecting the most suitable optimization approach based on real-time traffic conditions and environmental considerations.

The findings of this dissertation demonstrate the potential of the proposed co-optimization approach in enhancing traffic flow and reducing emissions. By comparing the ECoTOp with the individual optimization strategies, this research serves as a precursor for an innovative adaptive optimization strategy that can pave the way for more efficient and sustainable transportation systems in the future. The dissertation contributes valuable insights into the field of traffic signal optimization and vehicle trajectory optimization, encouraging further research and applications in intelligent transportation systems.

Table of Contents

List of Figures

List of Tables

Chapter 1

Introduction

1.1 Motivation

Traffic congestion continues to get worse every year in the United States. The 2019 Urban Mobility Report [1] produced by the Texas A&M Transportation Institute (TTI) predicts that by 2025 the average commuter will waste 62 hours and 23 gallons of fuel because of delay in traffic congestion. Traffic congestion is not only a problem for commuters, but can become a drain on economic growth, because it is predicted that by 2025 the national congestion cost will be $237 billion.

In the field of transportation engineering, the optimization of vehicle trajectories and traffic signal timing at signalized intersections is of paramount importance to improve transportation efficiency and mitigate environmental impacts. Traditionally, two distinct approaches have been explored: vehicle trajectory optimization alone and traffic signal timing optimization alone. However, with the advent of connected and automated vehicle (CAV) technologies and advancements in data-driven methodologies, there is a growing interest in developing integrated co-optimization strategies that can harness the strengths of both approaches. The integration of traffic signal optimization and vehicle trajectory optimization can be a complex task, as these two components can exhibit both synergistic behaviors, enhancing overall traffic efficiency, and conflicting interests, potentially leading to suboptimal outcomes. Striking a balance between these factors is critical to achieving a comprehensive and efficient co-optimization approach.

Transportation accounts for a large percentage of greenhouse gas emissions in the United States. According to the United States Environmental Protection Agency (EPA), mobile sources, such as cars, buses, planes, trucks, and trains, account for 29% of greenhouse gases (GHG) and

over half of all air pollution in the United States [2][3]. Some studies showing as high as 38% [4]. Figure 1.1 shows the GHG emissions by economic sector for 2021. Electricity caused 25% of the GHG emissions in the United States in 2021, but Figure 1.2a shows the power generation by energy source from 2006 to 2022. Electricity produced by coal has been going down, and energy produced by natural gas and renewable energy has been going up causing power (electricity) to produce less GHG since 2005 and transportation actually producing more than 28% of GHG in the coming years, as shown in Figure 1.2b [5].

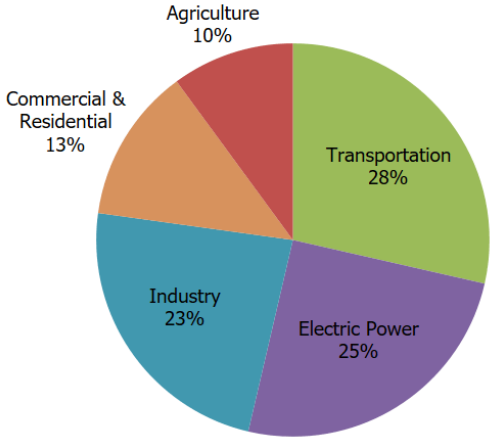

Figure 1.1. Greenhouse gas emissions by sector for 2021, *epa.gov,* 2023.

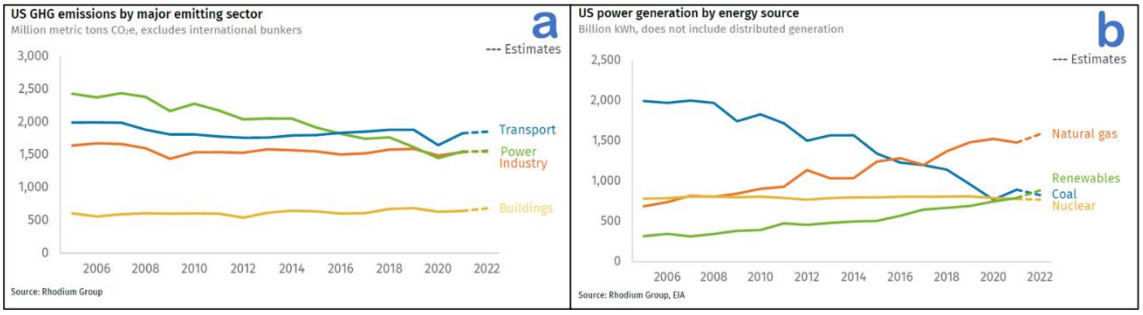

Figure 1.2. (a) Greenhouse Gas Emissions by Sector Since 2006. (b) Power Generation by Energy Source, *rhg.com,* 2023.

One solution to help cut down air pollution from vehicles is to utilize connected vehicle (CV) technology to perform eco-driving techniques. Eco-driving is a combination of different driving techniques to minimize fuel consumption [6].

A connected vehicle (CV) is a vehicle that transmits and receives data through wireless communication. There are four common ways a vehicle can be connected to and communicate with its surroundings: vehicle-to-infrastructure (V2I), vehicle-to-vehicle (V2V), vehicle-to-cloud (V2C), and vehicle-to-pedestrian (V2P). Together, V2I, V2V, V2C, and V2P make up the concept of vehicle-to-everything (V2X) communications, shown in Figure 1.4 [7].

When vehicles on the road can communicate with one another (V2V), it allows vehicles to travel faster and closer to one another in a much safer way. When vehicles can travel closer to each other in a safe manner the vehicles can travel in a platoon formation. Traveling in a platoon formation would help reduce traffic congestion which in turn would reduce fuel consumption and tailpipe emissions [8].

When a vehicle can communicate with the infrastructure (V2I), the vehicle can receive the signal phase and timing (SPaT) from traffic signals, and use the SPaT data to approach the intersection in an eco-manor. Vehicle communication with the cloud, V2C, would allow the vehicle to know upstream traffic and allow for more complex computations. V2P communication would allow for safer travel for walking pedestrians, or pedestrians on bicycles.

1.2 Problem Statement

The primary objective of this research is to propose a novel co-optimization approach for vehicle trajectories and traffic signal timing at isolated signalized intersections. We call this Eco-friendly Cooperative Traffic Optimization (ECoTOp). This approach seeks to strike a balance between intersection efficiency, emissions, and other performance measures, considering the trade-offs inherent in the individual trajectory optimization and signal optimization strategies. Moreover,

this research serves as a precursor to the development of an adaptive optimization strategy that can dynamically select the most appropriate optimization approach based on real-time traffic conditions and environmental impacts.

The development of the adaptive optimization strategy holds significant promise for future transportation systems. By continually monitoring and analyzing traffic data, environmental factors, and relevant parameters, the adaptive strategy can automatically adjust the optimization approach to maximize transportation efficiency while minimizing environmental impacts. This dynamic adaptation ensures that the transportation system remains responsive to changing traffic patterns, varying demand levels, and evolving environmental considerations.

Several studies have investigated aspects of vehicle trajectory optimization ([9][11][12]) and signal optimization ([13][14]) individually. However, limited research has explored the dynamic integration of these optimization strategies, which is critical for adapting to the evolving traffic and environmental conditions. By establishing a foundation for dynamically changing between vehicle trajectory optimization alone, signal optimization alone, and the integrated co-optimization, this research aims to contribute to the development of intelligent transportation systems capable of adapting to real-time traffic conditions.

To achieve the research objectives, a hybrid approach combining model-based and data-driven methodologies is employed. The model-based component incorporates established traffic flow models and optimization algorithms to optimize vehicle trajectories and traffic signal timing. The data-driven component leverages real-time traffic data, CAV technologies, and machine learning techniques to enhance the accuracy and efficiency of the optimization process.

To evaluate the effectiveness and performance of the proposed ECoTOp approach, extensive simulation-based experiments are conducted using the SUMO traffic simulation platform [15]. These experiments encompass various traffic scenarios, including different traffic volumes,

vehicle types, and environmental conditions. Performance metrics such as CO_2 emissions, traffic flow characteristics, and other relevant indicators are meticulously analyzed to assess the benefits and trade-offs of the ECoTOp approach compared to the eco-trajectory planning and signal optimization strategies.

1.3 Contributions

The key contributions of this research are multiple. First, we propose a novel co-optimization approach that integrates vehicle eco-trajectory planning and traffic signal timing optimization, addressing the challenges of balancing traffic flow, emissions, and other performance measures. Second, this research serves as a foundational step towards the future development of an adaptive optimization strategy capable of dynamically selecting the most suitable optimization approach based on real-time traffic conditions and environmental considerations.

To lay the foundation for the ECoTOp approach and the subsequent adaptive optimization strategy, this research also embarked on the development of several functional building blocks that set the stage for innovative advancements in transportation engineering. These building blocks aimed to address critical aspects of transportation efficiency, environmental sustainability, and data-driven decision-making.

One of the key building blocks involved the establishment of an *Innovation Corridor*, a real-world testbed located in Riverside, CA. This testbed served as a unique platform for validating and assessing the proposed co-optimization approach in a practical setting. By leveraging state-of-the-art infrastructure, intelligent transportation systems, and data collection mechanisms, the Innovation Corridor facilitated comprehensive evaluations and analyses, providing valuable insights into the performance and potential of the co-optimization approach.

Another important building block focused on the development of a speed advisory tablet app designed for in-vehicle use. This application provided drivers with real-time speed

recommendations based on traffic conditions, signal timings, and other relevant factors. By utilizing connected vehicle technologies and leveraging real-time data, the app aimed to optimize traffic flow, alleviate congestion, and enhance overall transportation efficiency. The insights gained from this building block were crucial in the formulation of an adaptive optimization strategy that dynamically adjusts vehicle trajectories and signal timings based on real-time conditions and environmental impacts.

Furthermore, the utilization of lane-level Global Navigation Satellite System (GNSS) applications constituted another building block. These applications enabled precise positioning and trajectory tracking, facilitating accurate assessments of the U.S. Department of Transportation's (DOT) MAP message creator tool. The integration of GNSS technology in the co-optimization approach and the subsequent adaptive optimization strategy allowed for fine-grained control and optimization at the intersection level, taking into account the specific conditions and characteristics of each lane.

Additionally, a simple queue estimation application was developed as part of the building blocks. This application employed advanced algorithms and data processing techniques to estimate queue lengths and delays at signalized intersections. Accurate queue estimations played a vital role in optimizing vehicle trajectories and traffic signal timings, leading to enhanced transportation efficiency. The incorporation of queue estimations in the adaptive optimization strategy allowed for responsive and dynamic adjustments to traffic signal timings based on real-time congestion levels and queue lengths.

Finally, an improved Motor Vehicle Emission Simulator (MOVES) model [16] was developed as a key building block. This enhanced model incorporated sub-binning techniques to provide more precise estimates of vehicle emissions. By considering emissions as a crucial performance measure, the co-optimization approach and the subsequent adaptive optimization

strategy aimed to minimize environmental impacts and promote sustainable transportation practices.

Through the establishment of these functional building blocks, this research laid the groundwork for the development of the ECoTOp approach, with the ultimate goal of formulating an adaptive optimization strategy. The subsequent chapters of this dissertation will delve into detailed descriptions of these building blocks, their implementation, and their implications for transportation efficiency and environmental sustainability.

1.4 Organization

The ensuing chapters of this dissertation are organized as follows: Chapter 2 provides an extensive literature review on vehicle trajectory optimization, traffic signal timing optimization, and co-optimization approaches in the context of transportation engineering. Chapter 3 focuses on the establishment of the Innovation Corridor and the development of the functional building blocks. Chapter 4 presents various eco-trajectory planning experiments done in preparation for the eco-trajectory planning algorithm used, as well as the formulation of the eco-trajectory planning optimization objectives. Chapter 5 presents the formulation of the traffic signal optimization objectives. Chapter 6 showcases the methodology adopted in this research, encompassing the formulation of optimization objectives for the ECoTOp approach, as well as preliminary comparison of results. Chapter 7 exhibits a case study for the electric vehicles in this adaptive optimization strategy. Chapter 8 discusses additional case studies conducted to evaluate the performance of the proposed co-optimization approach. Finally, Chapter 9 summarizes the findings of this research, highlights the implications, and outlines potential avenues for future research.

Chapter 2

Background and Literature Review

2.1 Traffic Signal Optimization

The optimization of traffic signal timing has long been recognized as a critical component in improving transportation efficiency and mitigating congestion at signalized intersections [17]. Traffic signal timing optimization aims to determine the ideal allocation of green, yellow, and red signal phases to minimize delays, reduce travel times, enhance traffic flow, and maximize intersection capacity [18]. This section provides a comprehensive literature review on traffic signal timing optimization, highlighting key methodologies, algorithms, and advancements that have contributed to the field of transportation engineering. By examining the existing body of knowledge, this review aims to provide a solid foundation for understanding the state-of-the-art techniques and identifying gaps that can be addressed by the proposed co-optimization approach.

The earliest form of traffic signal optimization can be traced back to the use of manually operated traffic control devices. One such early system was introduced in London, England in 1868, known as the "gas-lit semaphore" [19]. It was developed by John Peake Knight, an engineer and inventor. The semaphore system used movable arms or "semaphores" that were manually operated by police officers stationed at intersections. While this early form of traffic control was an important step in regulating traffic flow, it was limited by the fact that it relied on human operators. The system was prone to errors and inconsistencies due to factors such as human reaction time and subjective judgment.

Further advancements in traffic signal optimization came with the introduction of electrically operated traffic signals in the early 20th century. Over time, traffic signal optimization has evolved significantly, incorporating advanced technologies such as computerized control

systems [20], traffic sensors, and algorithms that analyze real-time traffic data to adjust signal timings dynamically [18].

Traffic-adaptive signal controllers take in real-time detector data to measure traffic flow [13]. This real-time measurement of traffic flow data can then be used to optimize flow. In a connected vehicle environment, CVs can communicate with the infrastructure and the data obtained can be used for signal control [14].

The Multi-Modal Intelligent Traffic Signal System (MMITSS) seeks to provide a comprehensive traffic information framework to service all modes of transportation, including general vehicles, transit, emergency vehicles, freight fleets, and pedestrians and bicyclists in a connected vehicle environment [21]. MMITSS was developed by the University of Arizona in collaboration with Econolite Group, Inc., Savari, Inc., and the University of California, Berkeley PATH program in 2014. An early version of MMITSS was introduced in 1992 called, RHODES, which was a real-time traffic-adaptive signal control system [13].

In 2014 at the World Congress on ITS Technology Showcase, the first demonstration of MMITSS was given, where participants witnessed how connected vehicles enabled a signalized intersection to prioritize and simultaneously accommodate a transit vehicle and two emergency vehicles as they approached the intersection. Then the participants witnessed the pedestrian crossing signal request from a mobile device [22].

In 2015, Feng et al. [14] developed a real-time adaptive signal phase allocation algorithm. The algorithm utilizes vehicle location and speed data to optimize phase sequence and duration. In order to estimate the vehicle states of non-connected vehicles, an algorithm that uses connected vehicle data was developed. A real-world intersection was modeled in VISSIM with CAV penetration rates of 100%, 75%, 50% and 25%. With 100% CAV penetration rate, total delay was

decreased by up to 14.67% when minimizing total vehicle delay, and 16.33% when minimizing queue length.

In 2015, Sun et al. [23] developed a quasi-optimal decentralized QUEUE-based feedback control strategy for a system of oversaturated intersections. This strategy is applied cycle-by-cycle based on measurement of current queue sizes, but its overall result is able to approximate the optimal one derived from off-line studies. Also, this strategy was numerically tested in MATLAB.

The vast majority of the existing studies concerning real-time phase and timing signal optimization attempt to minimize queue length or minimize total delay. This research proposes maximizing throughput at an intersection.

2.2 Eco-Trajectory Planning Optimization

Vehicle trajectory optimization plays a crucial role in enhancing traffic efficiency, safety, and environmental sustainability. By carefully designing vehicle trajectories, it becomes possible to improve the overall performance of transportation systems, enhance fuel efficiency, and mitigate emissions. Over the years, extensive research has been conducted on vehicle trajectory optimization, resulting in the development of various models, algorithms, and optimization techniques. This section provides a comprehensive literature review on vehicle trajectory optimization, exploring the key methodologies and advancements in this field. By examining the existing body of knowledge, this review aims to establish a foundation for understanding the state-of-the-art techniques and identifying areas where further research is needed. The insights gained from this review will contribute to the development of an effective co-optimization approach for vehicle trajectories and traffic signal timing, ultimately leading to more efficient and sustainable transportation systems.

Barth and Boriboonsomsin [9] developed a freeway-based eco-driving system where advice is gen to drivers in real-time based on changing traffic conditions around the vehicle. The

system takes advantage of road sensors to provide real-time traffic conditions, and tests showed up to 20% reduction in fuel consumption and CO_2 emissions.

Mandava et al. [10] suggested a piecewise linear-trigonometric function-based vehicle trajectory planning algorithm. Simulations showed this method reduced emissions by 12-14%.

Asadi and Vahidi [11] developed an algorithm that uses SPaT information and short-range radar to reduce idling times at signalized intersections and fuel consumption. The authors tested the algorithm in three simulated scenarios, two different scenarios with a single vehicle using the algorithm, and one scenario with a fleet of vehicles using the algorithm. The best results for this algorithm showed a 47% reduction in fuel consumption.

Rakha and Kamalanathsharma [12] developed a framework to reduce fuel consumption when approaching a signalized intersection using SPaT information. The algorithm developed used an objective function to minimize the total fuel consumed in passing an intersection safely. The algorithm was tested by running different speed profiles in a microscopic fuel consumption model.

He et al. [24] proposed an optimization for speed trajectory on signalized arterials that considers the impacts of surrounding traffic. The work relied on numerical tests for verification. The tests showed fuel consumption reduced by 29% but increased travel time by 9%, and a 24% reduction in fuel consumption with no sacrifice in travel time.

Huang and Peng [25] developed an algorithm to optimize vehicle speed trajectory over multiple signalized intersections using SPaT to minimize fuel consumption and travel time. The authors in [25] also studied the effects of vehicle motion during turning to show its significant effect on fuel consumption and travel time. The algorithm showed an average fuel consumption reduction of 12.1% and time reduction of 7.5% for single intersection cases. If turning motion is not considered, the resultant fuel consumption is lower by 0.77% and the traveling time is lower by 6.00%.

Xia et al. [26] conducted simulation and field experiments testing the benefits of eco-approach and departure (EAD). In the experiments V2C communication was used to receive SPaT information. The traffic signal controller sent the SPaT information to a cloud-based server and the test vehicle was setup with an LTE interface enabling it to receive the SPaT information from the server. The field tests were conducted on a closed fixed-time intersection. The simulation tests were performed on an intersection identical to the field experiment. Both field and simulation tests showed fuel consumption improved by approximately 14%, and the field tests showed an improved travel time as well.

Altan et al. [27] ran field experiments testing the benefits of EAD using a partially automated vehicle. The test vehicle was equipped with a mechanism that allowed full-range longitudinal speed control. For this experiment, V2I communication was used where the traffic signal controller sent the SPaT information to an RSU that then broadcast the SPaT data via DSRC. The test vehicle was equipped with a DSRC OBU and a computer that used the SPaT information to calculate a new trajectory. The tests were conducted on a closed, fixed-time intersection, and measured the fuel consumption and CO_2 emissions for manual driving with a driver-interface suggesting the calculated speed, and for partially automated driving where the calculated trajectory is given directly to the longitudinal speed control mechanism. The experiments showed an average fuel consumption improvement of 17%, and 5% when only considering manual driving with suggested speed.

In 2015, Hao et al. [28] developed and tested an EAD application for actuated traffic signals, where the traffic signal changes based on traffic rather than a predetermined fixed time. The experiments were run on a closed intersection using DSRC-based V2I communication. The tests concluded that at high speed the energy savings were between 5%-10%, and at lower speed the energy savings were between 6%-26%.

Then in 2018, Hao et al. [29] were able to test the EAD application for actuated traffic signals from 2015 in real-world traffic. The tests were run on a corridor with eight traffic controllers equipped with DSRC-based RSUs. The experiment had two vehicles driving at the same time on the corridor where one vehicle was implementing the EAD application and the other vehicle was not. The EAD application proved to save 2% energy for the entire trip, and saved 6% energy on the DSRC equipped segments of the corridor.

Hao et al. [30] developed a graph-based trajectory planning algorithm (GBTPA) for eco-approach and departure applications. The algorithm computes the speed trajectory with the lowest fuel consumption rate for a vehicle to cross the upcoming intersection. Numerical experiments showed average energy savings of 11% for level terrain.

In 2021, Esaid et al. [31] developed a machine learning trajectory planning algorithm (MLTPA), which trained a machine learning model to approximate the solution from the GBTPA [Peng SAE]. The GBTPA required tens of seconds for computation, the MLTPA reduced that to a few milliseconds. Simulations showed median 5%-6.2% energy savings. It is this algorithm that is used for the eco-trajectory planning module in the ECoTOp system.

2.3 Vehicle Trajectory and Traffic Signal Timing Co-optimization

In recent years, there has been growing interest in developing methods for the co-optimization of traffic signals and vehicle trajectories at isolated signalized intersections. This is because traditional traffic signal control methods, which focus solely on optimizing the traffic signal timings [18], can lead to inefficient vehicle movements and increased fuel consumption [32][33][34][35]. In this literature review, we discuss existing methods for co-optimization of traffic signals and vehicle trajectories, which can improve intersection performance and reduce the environmental impact of transportation.

One of the early methods proposed for combining vehicle trajectory optimization with traffic signal timing was with the use of Cooperative Adaptive Cruise Control (CACC) integrated with an intelligent traffic signal [36]. This controller can dynamically switch between serving a major street and minor street. Vehicle trajectories are determined in order to reduce idling, acceleration, and deceleration. The method significantly reduced vehicle stops, queues, and fuel use. However, the testing was done on a four-legged, single lane through approach intersection, which is unrealistic.

Yu et al., [37] proposed a unified framework for optimizing traffic signals and vehicle trajectories using mixed integer linear programming (MILP). The model optimizes the phase sequence, green start and duration, cycle length, vehicle lane-changing behavior, and arrival times to minimize delays. The proposed model splits vehicles into platoons to ensure they pass through the intersection without stopping, maintaining desired speeds. The study showed that the proposed approach led to a decrease of up to 40% in vehicle delays under low traffic demand and up to 80% under high demand. Additionally, the approach led to a reduction of CO_2 emissions by approximately 7.5% for low demand and 50% for high demand.

In 2019, Xu et al. [38] developed a cooperative method to optimize traffic signal timing and vehicle control simultaneously. The method assumes that all vehicles are equipped with CAV technology and strictly follow the optimized speed profile. The traffic optimization is implemented at the signal controller, where the optimal traffic signal timing and vehicles' arrival times are calculated based on the speed and position of vehicles. Meanwhile, vehicles use the arrival times to compute the optimal speed trajectory. Simulation results demonstrated a reduction in fuel consumption, travel time, and vehicle stops.

Also in 2019, Guo et al. [39] developed a combined dynamic programming and shooting heuristic approach for the joint optimization of vehicle trajectories and intersection controllers. The

approach considered both CAVs and human-driven vehicles. Using numerical experiments, the approach reduced travel time by up to 37% and fuel consumption by up to 31%.

Du et al. [40] offered a method to optimized traffic signal timing and vehicle trajectories simultaneously that implements the GlidePath [27] method for generating eco-driving trajectories. The signal timing optimization method tries to minimize the delay time for all delayed vehicles, and minimize the difference among all phases. Simulation results showed a 13% improvement in intersection efficiency, and a 14% reduction in fuel consumption.

More recently in 2022, Sun et al. [41] presented an eco-driving algorithm based on vehicle to infrastructure (V2I) communications at signalized intersections. The algorithm uses basic kinematic wave and car-following models. The algorithm considers CAVs and human-driven vehicles, and showed an increase in throughput, travel speed, and fuel savings at signalized intersections. However, the algorithm does not consider turning movements, and assumes human-driven vehicles are connected.

The co-optimization of traffic signals and vehicle trajectories at isolated signalized intersections is an important research area with significant potential for improving intersection performance and reducing environmental impact. In the landscape of existing literature, it's notable that various studies have primarily focused on scenarios involving either entirely connected vehicles, platooning strategies, or have omitted the consideration of turning movements. In contrast, my research endeavors to encompass a broader spectrum by adopting a more comprehensive approach that accounts for mixed traffic conditions, including conventional vehicles and diverse turning movements. The intricacies of my investigation have brought to light that these distinct strategies can yield promising outcomes when individually applied. Hence, while recognizing the merits of prior work, the distinctive nature of my study's focus on co-optimization prompts a nuanced evaluation of their results within the context of a holistic framework.

Chapter 3

Functional Building Blocks

Before introducing the ECoTOp approach, it is important to establish functional building blocks that provide essential groundwork for its development and pave the way for future advancements, including the exploration of an adaptive optimization strategy. The development and implementation of functional building blocks are critical steps in advancing transportation systems towards improved efficiency, sustainability, and safety. These building blocks encompass a range of innovative technologies and methodologies that address key challenges in transportation, energy, and air quality. By establishing these functional building blocks, researchers and practitioners can create a solid foundation for the deployment and evaluation of novel strategies and approaches. This section provides an overview of the functional building blocks employed in this study, which include the establishment of an Innovation Corridor as a real-world testbed, the development of a speed advisory tablet app for in-vehicle use, the utilization of lane-level GNSS applications for assessing U.S. DOT MAP message creator tool, the implementation of a simple queue estimation application, and the refinement of the MOVES emission model through sub-binning. These building blocks serve as essential components in the broader research framework, paving the way for the subsequent development and evaluation of an adaptive optimization strategy for vehicle trajectories and traffic signal timing.

3.1 Development of an Innovation Corridor Testbed for Shared Electric Connected and Automated Transportation

The field of Intelligent Transportation Systems (ITS) is rapidly expanding and is at the forefront of four significant ongoing revolutions in transportation: shared mobility, vehicle

electrification, vehicle connectivity, and vehicle automation. While ITS has traditionally focused on enhancing safety and improving mobility, it also holds immense potential for increasing energy efficiency and reducing emissions. Recognizing the importance of these environmentally-focused benefits, particularly in California, we need to effectively manage the impact of shared mobility, vehicle electrification, vehicle connectivity, and vehicle automation on transportation. If these revolutions evolve independently, there is a risk of increased vehicle miles traveled, leading to higher emissions and greater fuel consumption. To explore how shared, electric, connected, and automated vehicle technologies can be harmoniously integrated to favor the environment, we propose the establishment of a comprehensive "testbed" in both simulated and real-world settings.

The City of Riverside has made significant strides towards becoming a "smart city," integrating new technologies for transportation, energy, and city management. As part of this initiative, UC Riverside and the City of Riverside are developing an "Innovation Corridor" along a six-mile stretch of University Avenue, connecting the UCR campus with downtown (refer to Figure 3.1). This corridor has been chosen due to its proximity to expanding transit and alternative transportation networks, research institutions affiliated with UC Riverside, and the growing entertainment hubs in downtown Riverside. Our plan involves updating all traffic signal controllers along the corridor to adhere to SAE connectivity standards. Dedicated Short-Range Communication (DSRC) roadside units will be installed at each traffic signal, facilitating the direct transmission of Signal Phase and Time (SPaT) messages to DSRC-equipped vehicles. Additionally, DSRC devices will broadcast Radio Technical Commission for Maritime Services (RTCM) and Map messages, supporting geofencing and precise positioning capabilities.

This proposed Innovation Corridor will serve as a vital testbed in Southern California for exploring Connected and Automated Vehicle (CAV) applications, including connected eco-approach and departure (EAD), eco-transit operations, smart intersection management, and other

applications aimed at improving safety, mobility, and environmental sustainability. Simultaneously, a "virtual" testbed was developed, simulating the same University Avenue corridor using the high-fidelity microscopic traffic simulation model, VISSIM. This simulation platform will enable us to vary traffic volumes and simulate different penetration rates of connected vehicles.

Figure 3.1. Innovation Corridor in Riverside, CA, *Google Maps*, 2018.

3.1.1 Simulation Setup

A microscopic simulation model of the traffic network at the real-world corridor was set up, and created using PTV VISSIM. The simulation will allow for the testing of different traffic scenarios and different traffic signalization algorithms. Traffic signalization in the simulation is actuated, as it is along the real-world corridor. Also, vehicle behavior in the simulation is calibrated to match real-world conditions there. Data such as traffic signal timing and vehicle position/speed is shared among vehicles and the infrastructure in the simulation, to represent the wireless exchange of Basic Safety Message (BSM) and Signal Phase and Timing (SPaT) information in the real world.

3.1.2 Innovation Corridor

This six-mile corridor has three consecutive intersections (Iowa Street, Cranford Avenue, and Chicago Avenue) where DSRC road-side units (RSU) that can transmit SPaT and MAP information were installed for this project, but will remain installed for future experiments. This corridor is located between the University of California, Riverside and downtown Riverside. The

corridor has proximity to expanding transit and alternative transportation network, research institutions associated with UCR, and the ever-expanding entertainment destinations in the downtown region, as shown in Figure 3.1. Along the corridor, all traffic signal controllers have been updated to be compatible with SAE connectivity standards. DSRC roadside-units are mounted along with each traffic signal. SPaT messages are directly transmitted to the DSRC units and forwarded to the vehicles equipped with onboard units. Meanwhile, RTCM and MAP messages are broadcasted via DSRC devices to support geofencing and accurate positioning. This Innovation Corridor serves as a critical testbed in southern California for Connected and Automated Vehicles (CAVs) applications, such as connected eco-approach and departure, eco-transit operation, smart Intersection management, and other applications to improve safety, mobility and environmental sustainability.

There are many state-of-the-art elements to the Innovation Corridor that address not only transportation but also energy and air quality. New generation air quality sensors are planned to be deployed at buses stops intersections and downwind/upwind of the freeways to evaluate the air quality and health impact of the traffic. A variety of other futuristic elements will also be integrated into the corridor, such as user-focused shared zero-emissions mobility services, renewable energy generation, and vehicle-to-grid interaction. More information on this project can be found in [42].

3.2 Speed Advisory Tablet App

The development of the speed advisory tablet app has revolutionized the way drivers receive real-time information and guidance during their travel. This innovative application harnesses the power of connected vehicle technologies and advanced data analytics to provide drivers with personalized speed recommendations. By leveraging information from GNSS sensors and vehicle-to-cloud communication, the app delivers dynamic and context-aware speed advisories to drivers, enabling them to optimize their driving behavior.

The successful implementation of the speed advisory tablet app has paved the way for the realization of cooperative ramp merging field experiments. By integrating the app's functionality with advanced vehicle-to-cloud communication systems, researchers have been able to establish a cooperative environment where merging vehicles receive real-time speed advisories based on the prevailing traffic conditions and the behavior of other vehicles. This cooperative ramp merging approach enhances the merging process by facilitating smoother and more efficient maneuvers, reducing delays and improving overall traffic flow. Figure 3.2 shows an image of the speed advisory tablet app [43].

The cooperative ramp merging field experiments made possible by the speed advisory tablet app have provided valuable insights into the potential benefits of cooperative driving strategies. Through rigorous data collection and analysis, researchers have been able to assess the impacts of the app's speed recommendations on traffic performance, safety, and driver behavior. The findings from these experiments have demonstrated the effectiveness of the cooperative ramp merging approach in reducing congestion, improving travel times, and enhancing the overall efficiency of highway operations.

The successful combination of the speed advisory tablet app and cooperative ramp merging field experiments marks a significant advancement in intelligent transportation systems. The integration of real-time guidance and cooperative driving principles holds immense potential for enhancing the safety, efficiency, and sustainability of our transportation networks. The insights gained from these experiments can inform the development of future mobility solutions, such as adaptive traffic control systems, connected vehicle technologies, and cooperative vehicle-infrastructure systems, with the aim of improving overall traffic operations and delivering a seamless and enjoyable travel experience.

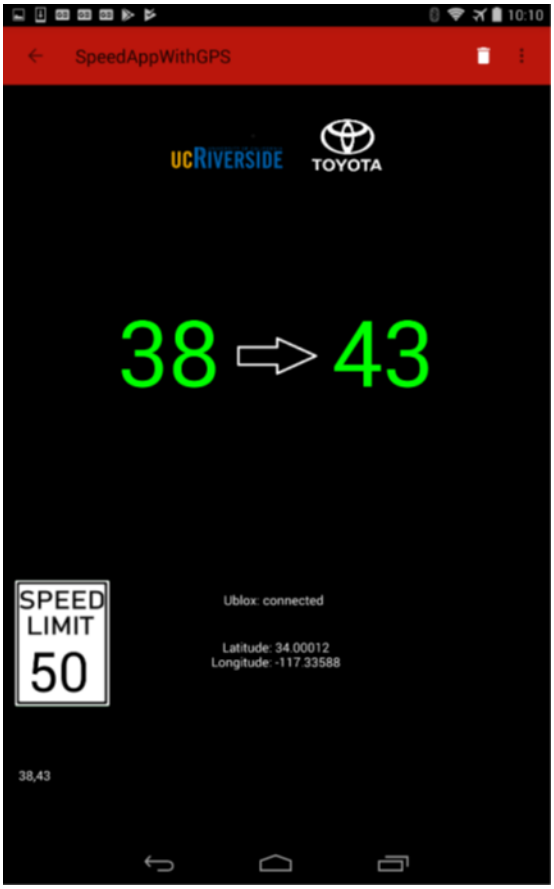

Figure 3.2. Speed advisory tablet app user interface.

In addition to its significant impact on traffic operations and cooperative ramp merging, the speed advisory tablet app has also played a crucial role in driver behavior modeling and understanding the dynamics of human-vehicle interaction. By collecting and analyzing data on driver responses to the speed recommendations provided by the app, researchers have gained valuable insights into driver decision-making processes, behavioral patterns, and adaptation mechanisms.

The app's integration with driver behavior modeling studies has enabled researchers to examine the influence of real-time information and guidance on driver behavior. Through data analysis techniques such as trajectory analysis, driving simulation experiments, and statistical modeling, researchers have been able to characterize the effects of the app's speed

recommendations on various aspects of driver behavior, including speed selection, lane changing, and merging patterns. These findings contribute to a deeper understanding of how drivers perceive and respond to real-time guidance, and they provide valuable inputs for the design and refinement of future advanced driver assistance systems (ADAS) and connected vehicle applications.

Moreover, the availability of comprehensive data collected through the speed advisory tablet app has facilitated the development and validation of driver behavior models. By leveraging advanced modeling techniques such as agent-based modeling, machine learning, and statistical analysis, researchers have been able to capture the complex interactions between drivers, vehicles, and the environment. These models serve as valuable tools for predicting driver responses, simulating traffic scenarios, and evaluating the potential impacts of new technologies and interventions on driver behavior and traffic performance.

More information about the cooperative ramp merging field experiments can be found in [43]. More information about the driver behavior modeling can be found in [44].

3.3 Lane-Level Localization and Map Matching for Advanced Connected and Automated Vehicle (CAV) Applications

The utilization of lane-level Global Navigation Satellite System (GNSS) applications has revolutionized the way we assess and evaluate transportation systems, particularly in terms of their efficiency, safety, and overall performance. This section focuses on two key applications: the assessment of the U.S. Department of Transportation (DOT) MAP message creator tool and the implementation of a simple queue estimation application.

3.3.1 Assessment of U.S. Department of Transportation Lane-Level Map for Connected Vehicle Applications

Lane-level GNSS applications have provided an invaluable tool for assessing the U.S. DOT MAP message creator tool, which is designed to facilitate the exchange of dynamic roadway information between vehicles and infrastructure. By leveraging the precise positioning capabilities of GNSS technology, researchers have been able to collect highly accurate and detailed data on vehicle trajectories, lane occupancy, and other relevant parameters. These data have enabled a comprehensive evaluation of the effectiveness and performance of the MAP message creator tool in terms of its ability to provide accurate and timely information to connected vehicles, support situational awareness, and enhance overall traffic management.

3.3.1.1 USDOT Connected Vehicles Tool

The USDOT J2735 MAP tool provides a web application user interface that uses satellite imagery to enable users to manually select and map lanes and features to create J2735 MAP messages. J2735 MAP messages describe an intersection's physical layout, such as lanes, stop bars, allowed maneuvers, etc., in a digital form standardized by the Society of Automotive Engineers (SAE) [45]. The USDOT MAP tool can generate binary output as specified for Dedicated Short-Range Communications (DSRC) roadside units or usable through cellular Infrastructure-to-Vehicle (I2V) communications. At present, the literature does not include any assessment of the accuracy of the maps produced by the USDOT map tool. In addition, the establishment of MAP or SPaT message in this map tool requires a verified point for each intersection. The assessment of the effective range of one verified point is conducive to decrease the demand of the number of verified points for dense MAP messages.

The USDOT Connected Vehicles Tool offers free on-line access at https://webapp2.connectedvcs.com/. It offers tools for creating maps to support various Connected

and Automated Vehicle (CAV) message types. The ISD Message Creator constructs lane-level intersection maps to support MAP and SPaT messages. The detailed instructions under the "Help" button make the site self-explanatory. Our interest herein is assessing the position accuracy of the J2735 MapData message, which is one output type provided by the tool.

3.3.1.2 Accuracy Assessment Method

Accuracy will be assessed by comparing the coordinates of feature points determined by two different methods: the USDOT Map Tool and GNSS Real-time Kinematic Positioning (RTK) survey. These feature points are selected to satisfy the following specifications:

- Each point should be easily and uniquely identifiable both to the surveyor and within the US-DOT tool. This is typically achieved by defining the points to be at the intersection of two nearly orthogonal lines.
- Each point should have a clear view of the sky.
- Each point should be near, but not on the road. This constraint is added to ensure the safety of the person performing the survey without needing to interrupt normal traffic operation.
- The features in the US DOT imagery and the real environment should be at the same locations. The US DOT imagery is based on georectification of historic photos that may have been taken months in the past; therefore, recent changes in the real environment may not be accurately represented in that imagery.

Figures 3.3 and 3.4 use imagery from the US-DOT tool to show the geographic distribution of the feature points. Each orange dot in Figure 3.3 shows the location of each of $N_1 = 39$ feature points near University of California-Riverside (UCR) College of Engineering Center for Environmental Research and Technology (CE-CERT). One of these points is defined

as the verified point (denoted $\mathbf{P}_v^e$) for the US-DOT tool. The feature points in Figure. 3.3 are each within about 200 meters of the verified point. The solid red box displays the region within the dashed red line at the maximum zoom level allowed by the tool. Figure 3.4 uses orange dots to indicate the location of 11 survey areas. Each survey area, labeled from S_1 to S_{11}, includes 5 feature points. These $N_2 = 55$ feature points allow accuracy to be assessed over longer distances from the verified point. The red box in Figure 3.4 indicates the region portrayed in Figure 3.3.

To assess accuracy, we compare GNSS survey and USDOT mapping tool locations for each feature point. The symbol $\mathbf{P}^e$ denotes the feature position determined by GNSS survey. The symbol $\widehat{\mathbf{P}}^e$ denotes the position of the feature point determined by the US DOT mapping tool. The superscript on the vector $\mathbf{P}$ denotes the frame-of-reference, such as e for Earth-Centered Earth-Fixed (ECEF) and g for the North, East and Down (NED) frame. The NED frame feature location of a point $\mathbf{P}^g$ is computed by

$$\mathbf{P}^g = \boldsymbol{R}_e^g(\mathbf{P}^e - \mathbf{P}_v^e) \tag{3.1}$$

Where P_v^e is the origin of the NED frame and R_e^g is the rotation matrix from the ECEF frame to the NED frame [45]. Eqn. (3.1) is valid both for GNSS survey and USDOT mapping tool locations.

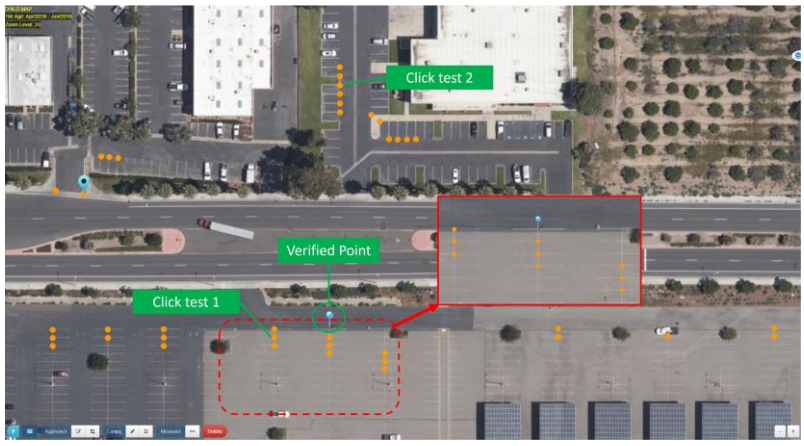

Figure 3.3. USDOT map accuracy test points near UCR CE-CERT.

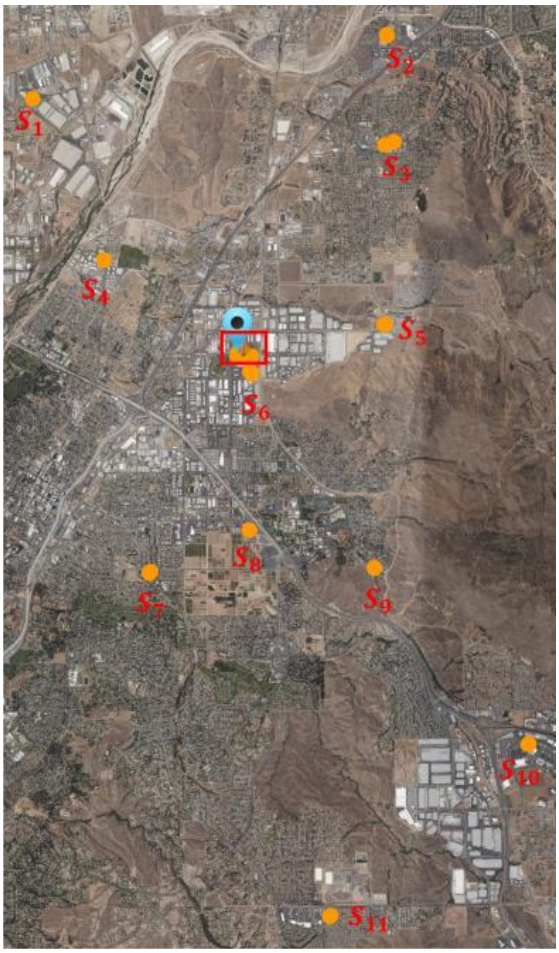

Figure 3.4. Expanded test area for accuracy analysis.

Section 3.3.1.3 discusses the GNSS survey and assesses its sources of error when determining the coordinates of each point. Section 3.3.1.4 discusses the US-DOT tool and assesses its sources of error when determining the coordinates of each point. Section 3.3.2 combines the US-DOT and GNSS data to assess the overall map accuracy.

3.3.1.3 Data Acquisition: GNSS Survey

This section presents the procedure for determining the real-world position of the verified point and of each feature point (denoted $\mathbf{P}_k^e$ for $k = 1, \ldots, N$) by use of GNSS RTK survey, using a dual-frequency u-blox ZED-F9P receiver connected to a dual-band u-blox antenna. The antenna

is placed on the ground above the corresponding feature point. The receiver communicates with the UCR base station to obtain Radio Technical Commission for Maritime Services (RTCM) corrections and reports RTK fixed position solution in WGS84 ECEF frame.

During the survey process for each point, the ZED-F9P in RTK fixed mode was used to record the position for at least 20 seconds. The mean of these measurements is used in Sec. 3.3.2 as the surveyed position. The standard deviation of each coordinate in each surveyed position is less than 0.005m. The RTK GNSS surveyed position Mean Square Error (MSE), denoted herein as σ_G at the centimeter level (see e.g., Table 21.7 in [46]).

In addition to the RTK GNSS survey position error characterized by σ_G, there is also antenna placement error due to the fact that the human operator cannot perfectly place the antenna over the feature and account for the antenna phase offset. This error is accounted for by the symbol σ_S with MSE $\sigma_S = 0.01m$.

3.3.1.4 Data Acquisition: USDOT Map Tool

The goal of this section is two-fold: (1) to describe the process by which this tool was used to obtain the geodetic coordinates for the selected locations; and (2) to define and assess the related sources of error.

Process. Starting from the URL for the US-DOT tool given in Section II, the steps are as follows:

1) In the ISD Message Creator,
   a) Click ‘View Tool’, then under ‘File’ button click ‘New Parent Map’.
   b) Center the map imagery over the region of interest at the ‘Zoom Level 21’, which is the highest resolution, as shown in the inset of Figure 3.3.
   c) Click ‘Builder’ from the left bottom corner.

d) Drag the ‘Verified Point Marker’ to the feature point defined in Section III and shown in Figure 3.3. A ‘Verified Point Configuration’ window will automatically open. Input the GNSS survey coordinates for the verified Latitude/Longitude/Elevation.

e) Drag the ‘Reference Point Marker’ near the verified point in the map. The reference point is required for the tool. It determines the relative position of all feature locations in the J2735 map message, but does not affect the results of the experiments.

2) Under the ‘File’ button from the top menu, select ‘New Child Map’. Click ‘Cancel’ for the popup questions. Use the pencil in the ‘Lanes’ button located near the left bottom corner. Double-click each desired feature location. An orange dot will be displayed as shown Figure 3.3.

3) Click the pencil in the ‘Lanes’ button to turn it off. Then, select (i.e., mouse click) each feature point in the tool imagery (e.g., orange points in Figure 3.3) and note their coordinates as $\widehat{\mathbf{P}}_k^e$.

Note that all positions acquired from the US-DOT tool are WGS84 ECEF geodetic coordinates.

Error Sources. The above process allows measurement error to occur in at least two ways. First, the user will have error in the clicking of points. For example, Steps 1d and 2 involve mouse clicks to select points. At best, the accuracy of such mouse clicks will be the size of the pixel in meters; however, the screen resolution may result in lower accuracy. The click error will be denoted by σ_C. Second, the geodetic coordinates assigned to the clicked points will be imperfect due to georectification errors. This mapping error will be denoted by σ_M.

Error Assessment. The goal of this subsection is to characterize the click accuracy σ_C in meters. Point-click experiments are performed for two feature points, which are marked as 'Click test' in Figure 3.3. For each experiment, using 'Zoom level 21', the targeted feature point is manually clicked 15 times (moving the cursor away and returning it between clicks) and their position $\widehat{\mathbf{P}}_{C_i}^{g}$ is recorded for $i = 1, \ldots, 15$.

The accuracy analysis is performed in a locally-level NED tangent frame with its origin point at the verified position $\widehat{\mathbf{P}}_{v}^{e}$. The NED feature location $\widehat{\mathbf{P}}_{C_i}^{g}$ is computed from $\widehat{\mathbf{P}}_{C_i}^{g}$ using Eqn. (1).

Herein, click test error is characterized by the Standard Deviation (STD) of each component of $\widehat{\mathbf{P}}_{C_i}^{g} = \left[P_{N_i}^{g}, P_{E_i}^{g}, P_{D_i}^{g}\right]^T$. The STD of North σ_N and East σ_E are listed in Table 1. The vertical STD σ_V is 0 since there are no changes in the Down coordinates in each click of each experiment. The horizontal STD, which defines the click accuracy σ_C, is calculated by

$$\sigma_C = \sqrt{\sigma_N^2 + \sigma_E^2}. \tag{3.2}$$

The values of σ_C summarized in Table 1, will be used in section 3.3.2 to estimate a value for σ_M.

Table 3.1. Standard deviation for click test.

	σ_N	σ_E	σ_C	σ_V
Click test 1	0.053 m	0.028 m	0.060 m	0.0 m
Click test 2	0.042 m	0.032 m	0.053 m	0.0 m

3.3.2 Accuracy Assessment

This section uses the USDOT data in comparison with the GNSS survey data to assess the accuracy of the feature locations provided by the USDOT mapping tool.

3.3.2.1 Bias Analysis on USDOT Tool: Verified Point

Figure 3.5 displays the north and east components of the error between the USDOT feature points from each click test $\widehat{\mathbf{P}}_{C_i}^{g}$ and the GNSS surveyed positions $\mathbf{P}_{C}^{g}$ for the same features. For each click test, the NED frame positions $\widehat{\mathbf{P}}_{C_i}^{g}$ and P_{C}^{g} are computed using Eqn. (3.1). The position error is calculated by

$$\delta \mathrm{P}_{C_i}^{g} = \mathrm{P}_{C_i}^{g} - \mathrm{P}_{C}^{g} \tag{3.3}$$

Where $\delta \mathbf{P}_{C_i}^{g} = \left[\delta P_{N_i}^{g}, \delta P_{E_i}^{g}, \delta P_{D_i}^{g}\right]^{T}$ are the NED components of mapping error for click test C_i.

Note that both the north and east components of the position error vector are biased by -0.13 m and 0.21 m, respectively. Due to the fact that the bias is statistically the same for both feature points (i.e., click tests) and all clicks, this bias is attributed to the error in the placement on the verified point within the USDOT tool. See also the discussion of Figures 3.6b and 3.75b.

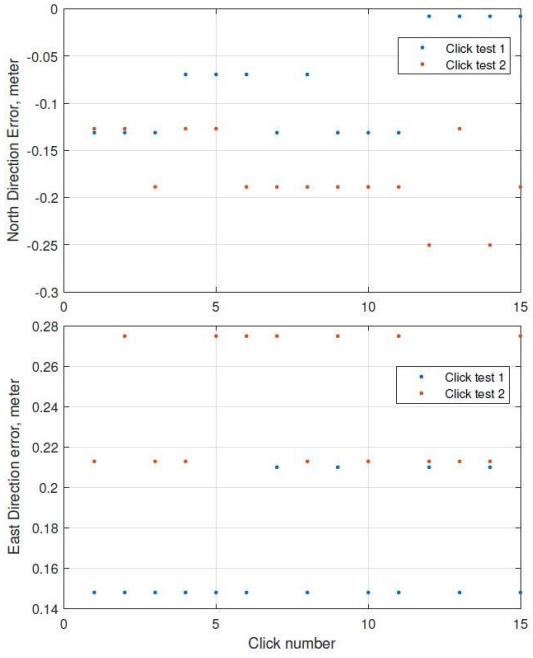

Figure 3.5. North and east errors between USDOT tool and GNSS survey using the two feature points for the click test.

3.3.2.2 Feature Mapping Accuracy Analysis

The USDOT map tool provides geographic coordinates (i.e., Longitude, Latitude, and Altitude) for feature points. The geographic coordinates are transferred to ECEF coordinates using the method described in Eqns. (2.9-2.11) of [47], then to local tangent plane using Eqn. (3.1). The USDOT location of feature k is denoted as $\widehat{\mathbf{P}}_k^e$ and $\widehat{\mathbf{P}}_k^g$. The GNSS surveyed location of feature k is denoted as $\mathbf{P}_k^e$ and $\mathbf{P}_k^g$. The position error for feature k is computed as

$$\delta\mathbf{P}_k^g = \widehat{\mathbf{P}}_k^g - \mathbf{P}_k^g = \boldsymbol{R}_e^g\left(\widehat{\mathbf{P}}_k^e - \mathbf{P}_k^e\right) \tag{3.4}$$

Where $\delta\mathbf{P}_k^g = \left[\delta P_{N_k}^g, \delta P_{E_k}^g, \delta P_{D_k}^g\right]^T$ defines the north, east, and down components of the error vector. The metrics for analyzing the accuracy of the k-th feature are the horizontal error norm:

$$\delta P_{H_k}^g = \sqrt{\delta P_{N_k}^{g\ 2} + \left(\delta P_{E_k}^g\right)^2}; \tag{3.5}$$

And, the vertical error: $\delta P_{D_k}^g$. The Horizontal Distance (HD) between the k-th test point and verified point $\left(\mathbf{P}_v^g = \mathbf{0}\right)$ is

$$D_{H_k} = \sqrt{\left(\mathrm{P}_{N_k}^g\right)^2 + \left(\mathrm{P}_{E_k}^g\right)^2}. \tag{3.6}$$

Figure 3.6 displays data for assessing accuracy for the features shown in Figure 3.2 that are near CE-CERT. Figure 3.6a displays the horizontal error norm and vertical error for the feature points near the UCR CE-CERT. Figure 3.7a presents data for the expanded area shown in Figure 3.3. The expanded area includes 11 clusters. Data for each cluster is depicted in a different color in Figure 3.7. In each figure the x-axis is the horizontal distance D_{H_k} from the verified point. Figure 3.6a shows 0.17 m mean and 0.30 m maximum horizontal error. Figure 3.7a shows the horizontal error norm and vertical errors over longer horizontal distances from the verified

point. Figure 3.7a shows 0.18 m mean and 0.31 m maximum horizontal error. There are no discernible trends in the horizontal error as a function of the distance from the verified point.

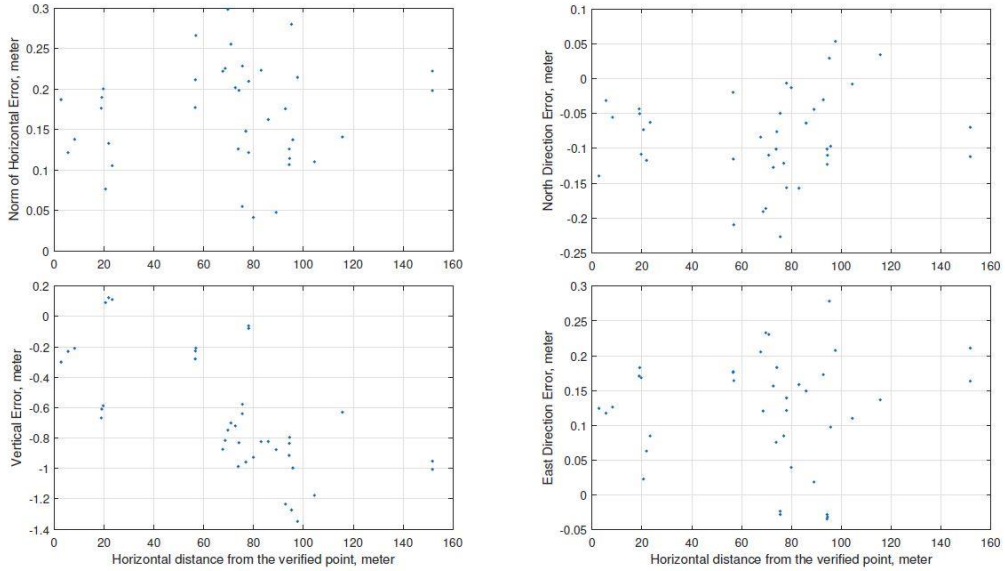

(a) Horizontal error norm $\delta P^g_{H_k}$ and vertical error $\delta P^g_{D_k}$ versus HD to the verified point (i.e., D_{H_k}).

(b) North and East error components versus HD to the verified point (i.e., D_{H_k}).

Figure 3.6. USDOT map accuracy assessment near UCR CE-CERT.

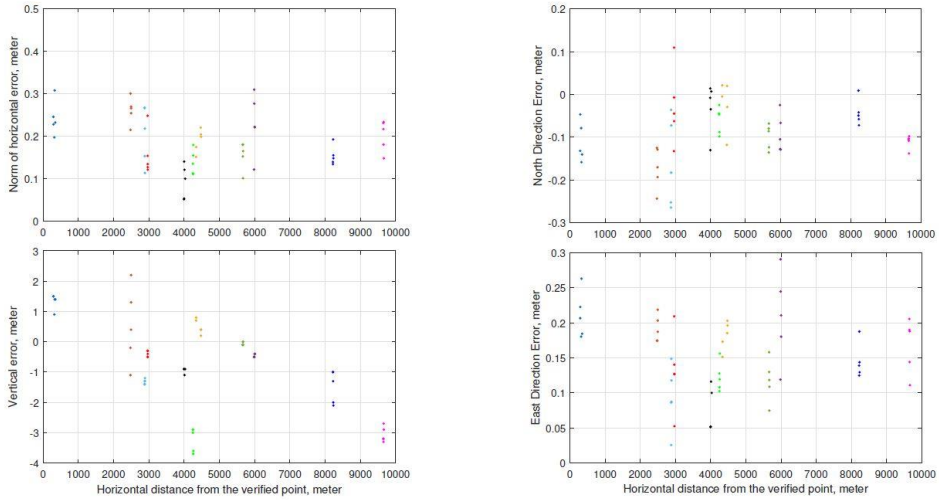

(a) Horizontal error norms and Vertical error

(b) North and East error components

Figure 3.7. Graphs of USDOT map accuracy assessment for expanded area.

Figure 3.7a also shows that the vertical error does change as a function of the distance from the verified point. The tool geo-rectifies remote sensing satellite imagery to achieve its accuracy in the horizontal directions. Satellite imagery does not provide depth information; therefore, the underlying vertical accuracy is limited. In Figure 3.7, In Figure 3.7, S_1 in green with HD near 5.7 km, S_2 in dark purple with HD near 6 km, S_3 in amber with HD near 4.4 km, S_4 in light blue with HD near 2.9 km, S_5 in orange with HD near 2.4 km, S_6 in blue with HD near 0.3 km, S_7 in black with HD near 4 km, S_8 in red with HD near 3 km, S_9 in green with HD near 4.2 km, S_{10} in deep blue with HD near 8.2 km, and S_{11} in magenta with HD near 9.7 km.

Figures 3.6b and 3.7b show the individual components of the horizontal error. In Figure 3.6b the mean north and east errors are -0.08 m and 0.12 m, respectively. In Figure 3.7b the mean north and east errors are -0.08 m and 0.15 m, respectively. These biases are consistent with each other and with those in Figure 3.5. This verifies the conclusion that the verified point selected within the USDOT tool is biased by this amount relative to the desired feature point, due to the limited resolution of the imagery in that tool.

The symbol σ_H represents the MSE of the experimental horizontal position error $\delta P_{H_k}^g$. The MSE of $\delta P_{H_k}^g$ is 0.18 m for N1 points and 0.20 m for N2 points. The MSE σ_H over all 94 feature points is 0.19 m.

Figure 3.8 plots the horizontal and vertical errors versus vertical difference relative to the verified point. The horizontal accuracy remains constant as elevation changes. The vertical error is an order of magnitude larger than the horizontal error and does change with both the horizontal and vertical separation from the reference point.

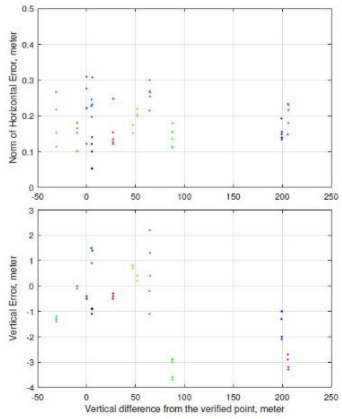

Figure 3.8. Horizontal error norms and Vertical error of expanded area.

3.3.3 Map Accuracy Assessment

The experimental horizontal position error σ_H is the result of the four specific errors discussed in Sections 3.3.1.3 and 3.3.1.4, specifically:

$$\sigma_H^2 = 2\sigma_C^2 + \sigma_M^2 + \sigma_G^2 + \sigma_S^2. \tag{3.7}$$

The US-DOT click accuracy σ_C is multiplied by 2 since it is applied to the clicks for both the feature point and the verified point. Since we have experimentally determined values for $\sigma_H, \sigma_C, \sigma_G$, and σ_S, we can compute $\sigma_M = \sqrt{\sigma_H^2 - (2\sigma_C^2 + \sigma_C^2 + \sigma_S^2)}$. Using either value of σ_C from the two click tests, the resulting value of σ_M is 0.17 m.

3.3.4 Conclusions

Hi-Def digital maps are an indispensable automated driving technology for CAV applications. The USDOT map tool allows users to create MAP and SPaT messages with free access, but an assessment of its accuracy does not exist in the current literature. This document assessed the accuracy of the US-DOT map tool using a set of 94 feature points with a 10 km area. The assessed accuracy is 17 centimeters. The assessment also demonstrated that this horizontal map accuracy was maintained within the 10 km distance of the USDOT map tool verified point that was used in this study.

3.4 Lane-Queue Estimation

In addition to assessing the MAP message creator tool, the implementation of a simple queue estimation application has further demonstrated the power of lane-level GNSS applications in capturing and quantifying traffic congestion and queue dynamics. By combining GNSS data with advanced algorithms and mathematical models, researchers have been able to estimate queue lengths, queue speeds, and other critical queue-related metrics with a high degree of accuracy. This information is vital for traffic management agencies and transportation planners to effectively identify congestion hotspots, optimize traffic signal timing, and implement proactive measures to mitigate congestion and improve overall traffic flow.

The lane-level queue estimation study conducted in simulation using VISSIM has been instrumental in advancing our understanding of traffic congestion and providing valuable insights for traffic management and control strategies. To accomplish this study, three key modules were developed: a GNSS error model, a lane-level map-matching module, and a lane-level queue length estimation module.

The first module, the GNSS error model, aimed to replicate the inherent inaccuracies and limitations associated with GNSS measurements. By incorporating realistic error distributions and considering factors such as satellite geometry, signal obstructions, and atmospheric conditions, the model introduced a level of uncertainty into the simulated GNSS data, mirroring the real-world variability of GPS measurements. This enabled a more accurate representation of the GNSS positioning data, closely resembling the error-prone nature of GNSS measurements in actual field conditions.

The second module, the lane-level map-matching module, played a critical role in linking the simulated vehicle trajectories with the underlying road network. By leveraging high-resolution lane-level maps and advanced map-matching algorithms, this module accurately associated each

vehicle's simulated position with the corresponding lane on the road network. This precise lane-level information was vital for subsequent analysis, as it enabled the estimation of queue lengths on a lane-by-lane basis, providing a more detailed and accurate representation of traffic congestion within the simulation environment.

The third module, the lane-level queue length estimation module, was the centerpiece of the study. Building upon the GNSS error model and the lane-level map-matching module, this module employed advanced algorithms and techniques to estimate the queue lengths in each lane of the simulated network. By analyzing vehicle trajectories, speeds, and spatial distributions, the module could identify stationary or slow-moving vehicles and accurately determine the extent and magnitude of queues in real-time. This lane-level queue length estimation provided valuable insights into congestion patterns, bottlenecks, and the overall performance of the simulated transportation system.

The combination of these three key modules facilitated a comprehensive analysis of traffic congestion and queue dynamics at a lane-level resolution. The lane-level queue estimation study not only enhanced our understanding of traffic flow characteristics but also provided valuable inputs for developing efficient traffic management strategies, optimizing traffic signal timings, and evaluating the impact of various interventions and control measures. The results obtained from this study offer valuable guidance for transportation practitioners and decision-makers in their efforts to alleviate congestion, enhance traffic operations, and improve overall mobility in urban environments.

3.4.1 Simulation Study

This simulation study focuses on the accuracy of lane-level intersection queue estimation as a function of two variables: probe vehicle penetration density and GNSS position accuracy.

3.4.2 Simulation Network

The simulations are done using the PTV VISSIM [48] microscopic traffic simulation software. The network in VISSIM is modelled after the Innovation Corridor in Riverside, California [42]. The simulated network is about 1.3 km of the Riverside Innovation Corridor and includes 3 intersections along University Ave.: Chicago Ave., Cranford Ave., and Iowa Ave. The majority of this corridor consists of 2 lanes in the Westbound direction and 2 lanes in the Eastbound direction, and a speed limit of 50 km/h. Fixed-time signal control is coded for all three intersections. According to the signal timing tables provided by the City of Riverside, the cycle lengths of the Chicago, Cranford and Iowa avenue intersections are 96, 78 and 96 seconds, respectively. Green and yellow intervals of all three intersections' East-West through phase are 30 and 5 seconds. Traffic demands have been calibrated based on the turning movement count survey on June 2nd, 2016 by the City. Figure 3.9 shows the study corridor in both Google Map and VISSIM.

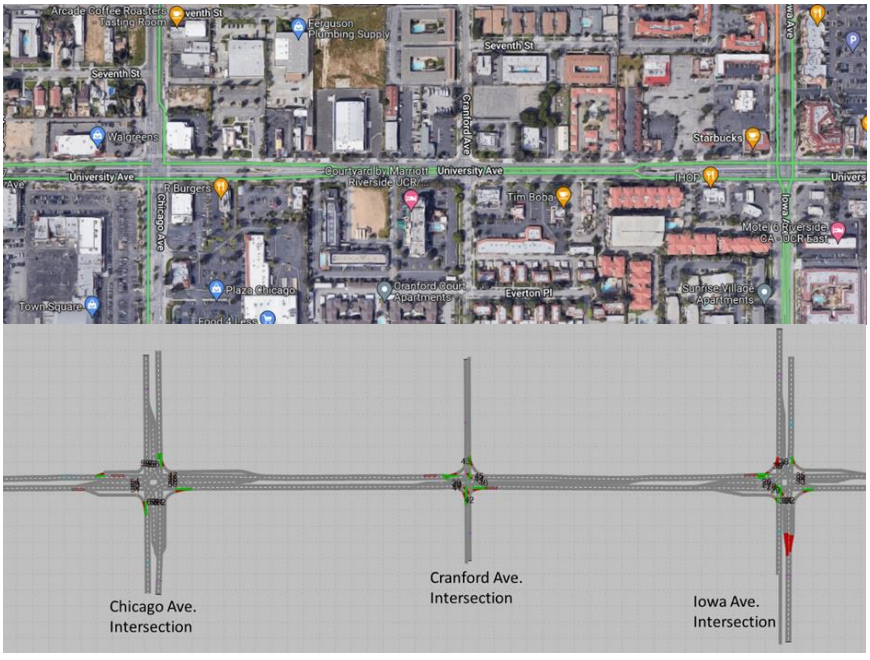

Figure 3.9. Portion of the Innovation Corridor in Riverside, CA that is studied in the simulation and demonstration. (a) Top – Google map view. (b) Bottom – VISSIM view.

3.4.3 Simulation Scenario

The simulation time is 1 hour, representing a typical morning peak hour (8 am – 9 am) traffic conditions along the corridor. There are 30 different scenarios simulated with each being run 10 times. These scenarios cover 5 different penetration rates of 20%, 40%, 60%, 80% and 100%; and, 6 different GNSS error levels with position error standard deviations of 0, 0.5, 1, 1.5, 2, and 2.5 m.

3.4.3.1 Key Modules

At signalized intersections, lane-level queue length is a critical traffic state that is monitored for efficient traffic signal control. To evaluate the impact of GNSS errors and probe vehicles density on real-time lane-level queue length estimation accuracy, we develop three key modules: GNSS error model, lane-level map-matching, and lane-level queue length estimation. All three are implemented in the simulation environment via application programming inter-faces (APIs).

PTV VISSIM allows for an external dynamic link library (DLL) to interface with its vehicle models. The DLL is written in C/C++, and is called for each vehicle at each time step of the simulation run. VISSIM passes the current state of the target vehicle to the DLL. The standard VISSIM computation engine provides the perfect location (i.e., the ground truth location) of the target vehicle. The simulation structure is shown in Figure 3.10. Using the API, the GNSS error model outputs a measured position by perturbing the ground truth position with a time-correlated random error process computed based on a user-specified position error standard deviation. The measured position is then fed into the lane-level map-matching algorithm to determine which lanes on which the target vehicles are traveling.

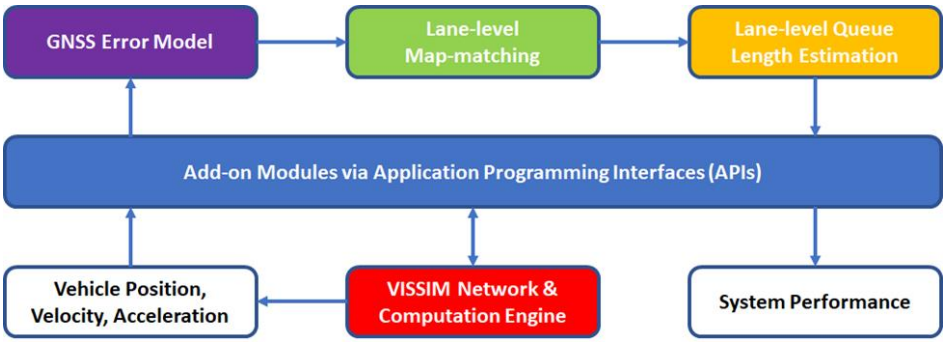

Figure 3.10. Key modules and flow diagram for the VISSIM lane-level queue length estimation.

Based on the lane indices and other state information (e.g., velocity), the queue length along each approaching lane of each intersection can be estimated online and compared with ground truth to determine the queue estimation error. The statistics of lane index errors and lane-level queue length errors are output and processed to evaluate the system performance.

3.4.3.1.1 GNSS Error Module

The standard PTV VISSIM implementation supplies user algorithms with the ground truth vehicle location at each time step. To study the effects of GNSS position estimation error on lane queue estimation accuracy, this project required a module that would additively corrupt the ground truth location with measurement error to produce a measured position.

This project designed, implemented, and used a GNSS error module. The theory underlying the implementation is described in Appendix B of [49]. That appendix also points to the GitHub URL for the software that implements the approach.

3.4.3.1.2 Lane-level Map-matching Module

Before incorporating the lane-level queue length estimation algorithm, a lane-level map-matching algorithm is required to determine the lane index (i.e., lane ID) of each probe vehicle at each simulation time step.

This lane determination algorithm used herein is a point-to-curve algorithm discussed under Task 3. Note that the default driver behavior in VISSIM moves vehicles along the centerline of its lane. The GNSS measurement of the vehicle position will not be on the lane center.

The lane determination accuracy A will be quantified as

$$P_c = \frac{S_c}{S_T}, A = 100 * P_c, \text{and } P_e = 1 - P_c \tag{3.8}$$

where S_c is the number of correct samples, S_T is the total number of samples, P_c is the probability of a correct determination, A is the percentage of determinations, and $P_e$is the probability of an incorrect determination.

3.4.3.1.3 Lane-level Queue Length Estimation Module

The lane-level queue length estimation method is presented in the Appendix C of [49]. Within the VISSIM evaluation code, the values of the algorithm parameters were: Ld = 100 (meters), Vf = 13.89 (meters/second); λ_0= 0.05555 for Westbound traffic (average number of arriving vehicles/ second), λ_0= 0.076389 for Eastbound traffic (average number of arriving vehicles/ second), h = 0.4 (seconds/vehicle), and k = 0.1429 (vehicles/ meter).

This algorithm aims to predict the maximum queue length in a cycle when some vehicles are still on their ways to approach the intersection. The algorithm was written by Dr. Peng Hao, Dr. Guoyuan Wu, and Dr. J.A. Farrell, from University of California, Riverside. Algorithm implemented in VISSIM by the author of this dissertation, David Oswald, University of California, Riverside.

Definitions:

The following is a list of parameters and variables used in this document. Various of the parameters and variables are illustrated in Figure 3.11.

- Length of the detection zone (Ld): The distance between an upstream location (defined as the boundary of the detection zone) and the stop-bar along an ingress approach.
- The set of vehicles in the intersection detection zone has two subsets, those that are detected and those that are not detected.
    - The detected vehicles are also referred to as probe vehicles or probes. Probe vehicles have an estimate of their position and velocity, which they communicate to the infrastructure and to other vehicles. All CVs are assumed to be detected.
    - Undetected vehicles do not communicate with the infrastructure or with other vehicles.
- The set of vehicles will be divided into the following three categories.
    - Queued Vehicles: Detected or not detected vehicles that are stopped in front of the last detected queued vehicle at the current time. The last detected queued vehicle is included.
    - Arrival Flow Vehicles: Vehicles that have arrived in the detection zone following the last detected queued vehicle and before the current time t.
    - Future Flow Vehicles: Vehicles that may arrive after the current time. Arrival and future flow vehicles are currently in free flow, but may transition to queued in the future.
- Future Deceleration rate (a): rate at which detected vehicles decelerate in the detection zone.
- Average departure headway (h): The time gap between each vehicle passing the stop line (seconds per vehicle).
- Jam density (k): The average number of vehicles per unit of distance per lane in the queue.
- Penetration Rate (p): Expected ratio of probe vehicles to the total number of vehicles.

- Stop location (Ls): The stop position relative to the stop-bar for the last detected vehicle in the queue. This is positive for vehicles approaching the stop-bar and negative for vehicles that have passed the stop-bar.
- M: The maximum number of vehicles that can fit in a lane of length Ld at the assumed jam density k (i.e., M = Ld k).
- Free-flow speed (Vf): Assumed velocity of vehicles that are not decelerating.
- Current time (t): The time at which the queue length is computed.
- T' is the time at which the free flow line of the last detected queued vehicle would intersect the stop line. The free flow line is extended from before the time that the vehicle became queued (see Vehicle A in Figure 3.11). If there is no detected arriving or queued vehicle, then T' is the time that the signal becomes red TR.
- Time at which a free-flow vehicle will pass the stop bar if it enters the detection zone at time t (T=t+Ld/Vf)
- Estimated discharge time of the last queued vehicle ($TQ1$).
- Time the lane signal turns green (TG).
- Time the lane signal turns red (TR).
- Vehicle arrival rate ($\lambda 0$): The average number of arriving vehicles per unit of time per lane.
- Queue index: The queue position (in number) of a queued vehicle of a specific lane
- $Q1$: Total number of queued vehicles at time t, i.e., the index of the last queued vehicle (see Part 1).
- $E[Q2]$: The expected number of arrival flow vehicles that will become queued vehicles (see Part 2).
- $E[Q3]$: The expected number of vehicles outside Part 1 and Part 2 that will be queued within the current cycle.

The parameters that affect the performance of the algorithm are: h, p, k, and $\lambda 0$. The variables $Q1$, $E[Q2]$, and $E[Q3]$ are computed by the algorithm.

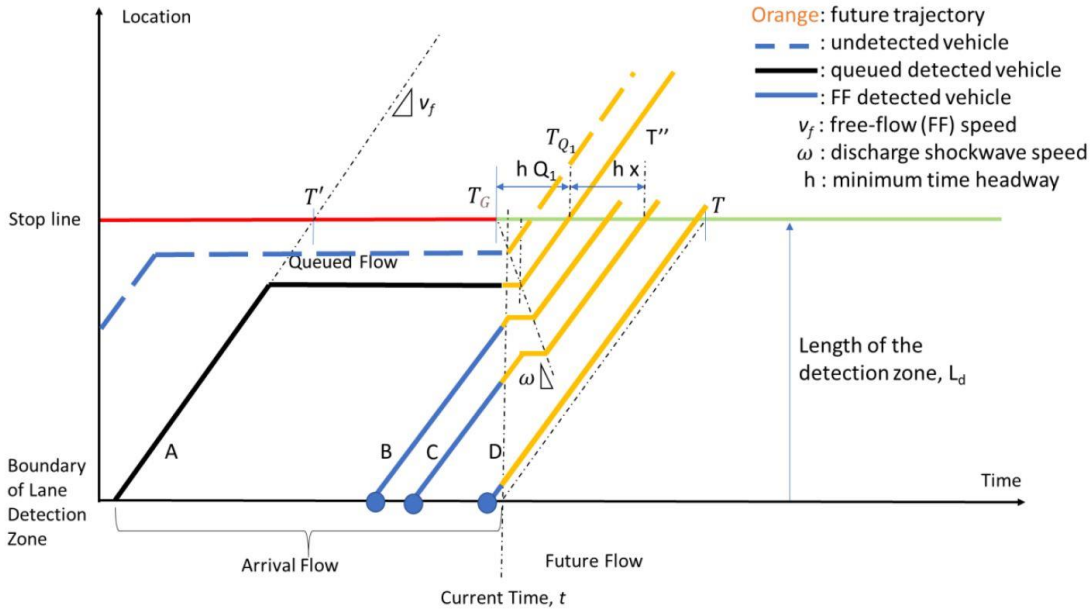

Figure 3.11. Illustration of variables and parameters for one lane of an intersection approach.

For Figure 3.11, Vehicle A is stopped at time t. Vehicles B, C, D are detected, but not queued and not decelerating. Q1 is computed only using the position of A and is at least 1. For the value of x this figure, n(x) = 2.

Assumptions:

This algorithm uses the following assumptions:

1. All lanes in an intersection approach have the same value of Ld.
2. All vehicles have the same type, size and shape, which is known.
3. Vehicle position means the center of the vehicle.
4. The position of the GNSS antenna from the vehicle center is known, so that the vehicle position can be computed from the GNSS position and heading.

5. The average headway (h), jam density (k), penetration rate (p), free-flow speed (Vf), and deceleration (a) are known and the same for all vehicles.
6. Vehicle arrivals at the boundary of the detection zone are described by a Poisson process with average rate λ_0 (# of vehicles per unit time). The arrival rate parameter (λ_0) is known.
7. No lane changes occur within the observation zone.

Later these assumptions can be relaxed.

Part 1: Queued Detected Vehicles Flow

This section focuses on detected vehicles that are either already stopped or that are decelerating with the expectation that they will be stopped. In Figure 3.11, vehicle A is the last detected vehicle in the lane queue.

In Figure 3.11, the black solid line shows the stop location as a function of time for the last detected vehicle (vehicle A).

The goal of this section is to compute $Q1(t)$. The formula is

$$Q_1(t) = \lfloor k \cdot L_s \rfloor + 1, \tag{3.9}$$

where k is the jam density, L_s is the stop position relative to the stop bar for the last detected vehicle in the queue, and $\lfloor \cdot \rfloor$ represents the floor function. Note that Q_1 is an integer. The computation needs to consider two possible situations.

Stopped Vehicles (Vehicle A at time t in Figure): This case only applies if there are no detected decelerating probe vehicles and there is at least one queued probe (i.e., stopped). In this case, the calculation applies only to the last detected vehicle. (i.e., vehicle A in Figure 3.11). From the stop location of the last detected vehicle, $Q_1(t)$ can be directly computed:

$$L_s = L_c, \tag{3.10}$$

where L_c is the current distance of the last stopped vehicle in the lane queue to the stop-bar. Therefore, Q_1 can be computed using eqn. (3.9).

Decelerated vehicles: If there is at least one Decelerating Probe vehicle (a<0), then the one with the most positive value of L_s will be the last one (i.e., furthest from the stop bar), coming to a stop behind vehicle A. The predicted stop location L_s of the decelerating vehicle is

$$L_s = L_c - \frac{v^2}{2a}, \tag{3.11}$$

which can be used in eqn. (3.9). In this equation, L_c is the current location, v is the current speed, and a is the deceleration rate.

Part 2: Arriving Flow

This section accounts for the contribution to the queue from arrival flow vehicles, whether detected or undetected. In Figure 3.11, at the current time t vehicles A, B, C, D are detected, and B, C, D are in the arrival flow. There may be additional undetected arrival flow vehicles.

The additional queue length, denoted as $E[Q2]$, that is computed in this section is the number of vehicles expected to arrive at the stop line between $\max(T', T_R)$ and $\min(T_{Q_1}, T)$. All symbols are defined in the Definitions section. This includes detected free flow vehicles and undetected vehicles.

If $Q_1(t) = 0$ (there is no Decelerating/Queued Probe), then $T'(t) = T_R$ and $T_{Q_1}(t) = T_G$.

If $Q_1(t)$ is greater than zero, then T' is as defined in the Definitions Section. The last detected queued vehicle's departure time (i.e., the time to clear the known queue) is predicted as

$$T_{Q_1}(t) = T_G + hQ_1(t), \tag{3.12}$$

where the queue discharges at the stop line, h is the average headway, and T_G is the time of the start of the green.

If the penetration rate was 100%, then all vehicles would be detected. When the penetration rate is less than 100%, then there may be undetected vehicles in the queue and additional undetected vehicles may arrive. The theory to accommodate vehicles that are expected to arrive is as follows.

Let x denote the number of undetected vehicles in the queue after the last detected vehicle in the queue (i.e., vehicle A). The time to clear the queue is

$$T(x)'' = \min(T_G = h(Q_1 + x), T), \tag{3.13}$$

In this expression, $T_G + h(Q_1 + x)$ is the expected departure time of the last queued vehicle in the Arrival Flow, and T is defined in the Definitions Section.

For each value of x from 0, …, M:

1. Compute T(x)'' using eqn. (3.13).
2. Compute the number of known probe vehicles (e.g., B, C, D) predicted to pass the stop bar between T' and T''. This number is n for this x (i.e., n(x)).

The probability mass function for $Q_2 = x$ is

$$P(Q_2 = x) = \beta P_{P_0}(x; \lambda) P_B(n|x; p), \tag{3.14}$$

Where β is a normalization factor, $P_{P_0}(x; \lambda)$ is the Poisson distribution for x given rate $\lambda = \lambda_0(T'' - T')$.

$$P_{P_0}(x, \lambda) = \frac{\lambda^x e^{-\lambda}}{k!}; \tag{3.15}$$

$P_B(x, n)$ is the probability of n probes out of x given penetration rate p (Binomial distribution),

$$P_B(n|x; p) = \begin{cases} \binom{x}{n} p^n (1-p)^{x-n}, for\ x \geq n \\ 0, otherwise \end{cases}. \tag{3.16}$$

Therefore, the expectation of Q_2 is

$$E[Q_2] = \frac{\sum_{x=0}^{M} x P(Q_2 = x)}{\sum_{x=0}^{M} P(Q_2 = x)}. \tag{3.17}$$

In this expression, M is the maximum number of vehicles that can fit in the lane of length Ld at the assumed jam density k (i.e., M = Ld k).

Part 3: Future Flow

Based on the results from Part 2, if $T_G + h(Q_1 + Q_2)$ is later than the T defined in the Definitions Section, then traffic may arrive after the current time and may also contribute to the queue. As there is no detected vehicle information here from which to infer the queue length, the algorithm uses the expected value of the vehicles in this time interval to approximate the additional expected queue length Q_3 in this part:

$$E[Q_3] = \max(0, \lambda_0[T_G + h(Q_1 + Q_2) - T]). \quad (3.18)$$

The complete answer

The queue length is then $Q_1 + E[Q_2] + E[Q_3]$.

3.4.3.2 Lane-level Queue Length Estimation Simulation Results

This section assesses the impact of GNSS position error and CAV penetration rate on the accuracy of queue length estimation.

The queue length estimation error is defined as

$$E = Q_a - Q_e, \quad (3.19)$$

where Q_a represents the actual queue length computed by VISSIM using ground truth and Q_e represents the queue length estimated by the intersection controller using the measured position data from the CAV's.

Figure 3.12 shows one of the normalized grouped histograms of lane-level queue length estimation errors for each penetration rate as a function of the GNSS error standard deviation in meters. In each figure, the GNSS error standard deviations take the values: 0 m, 0.5m, 1m, 1.5m, 2m, and 2.5m. Figure 3.12 shows the error statistics for a CAV penetration rate of 100%; figures for other CAV penetration rates can be found in [49]. The penetration rate for each figure is stated in the figure title. The horizontal axis in each figure represents the number of vehicles by which

the estimated queue length differs from the actual queue length. For instance, “0” means that the queue estimation is correct; an error of “1” means that the queue estimation is under-estimated by 1 vehicle; an error of “-1” means that the queue estimation is over-estimated by 1.

Figure 3.13 shows one of the normalized grouped histograms of lane-level queue length estimation error for each GNSS error level as a function of penetration rate. Figure 3.13 shows the queue estimation error statistics for a GNSS error of 0 for each CAV penetration rate, i.e., 20%, 40%, 60%, 80% and 100%, respectively. Figures for more GNSS errors can be found in [49].

Figures 3.12 and 3.13 (and further figures in [49]) show that queue length estimation errors increase as the GNSS error increases and as the penetration rate decreases from 100%. This decline in performance is especially strong with respect to the decreasing penetration rate. This is because the algorithms performance is heavily dependent on the probability that a CAV is sufficiently near the end of the queue.

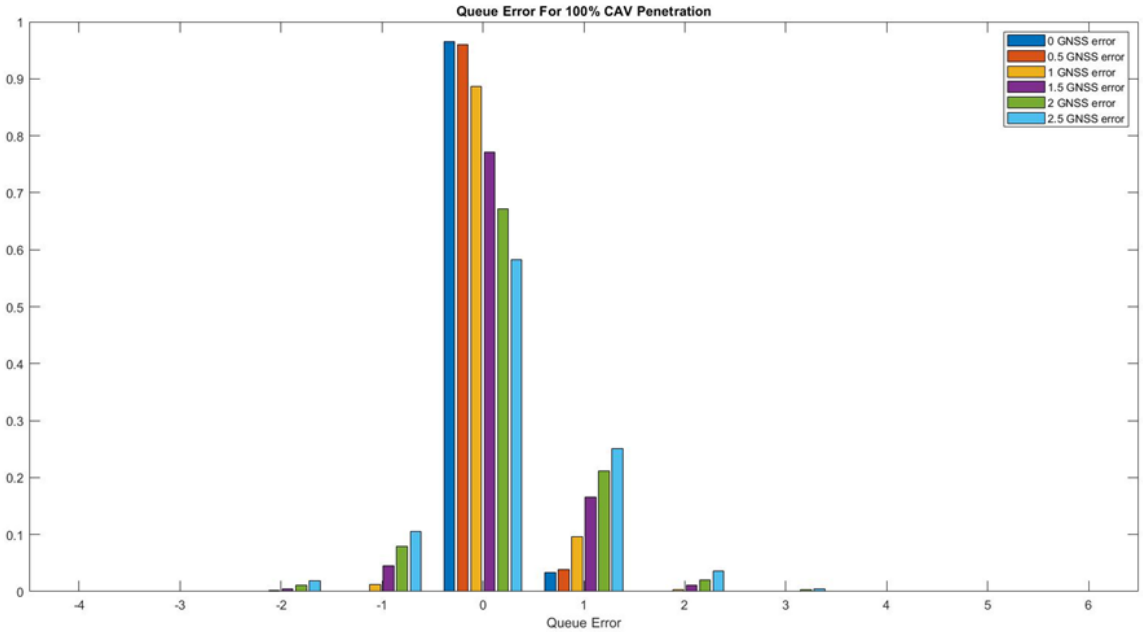

Figure 3.12. Grouped histograms of lane-level queue length estimation error for different GNSS error levels at 100% CAV penetration rate.

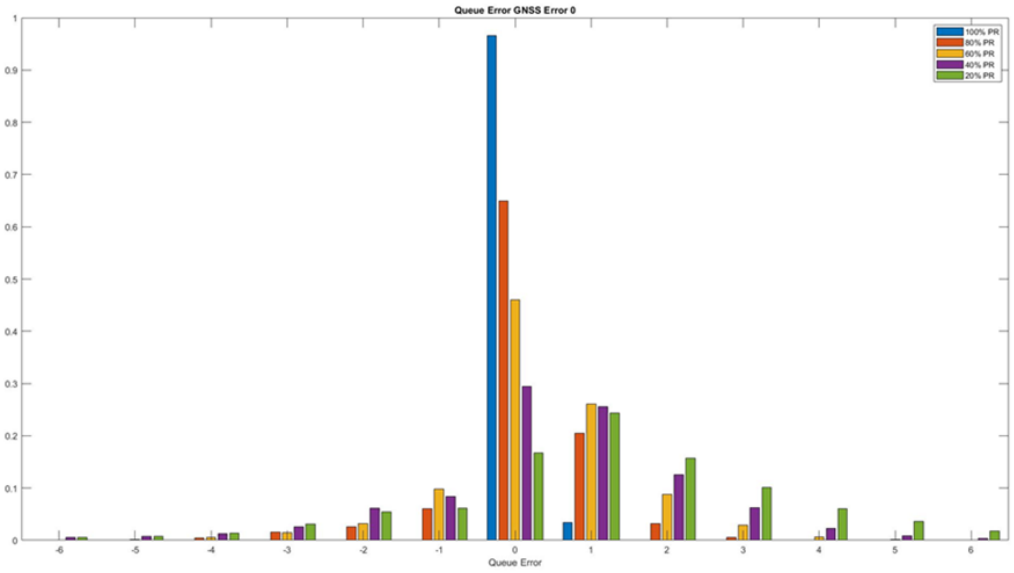

Figure 3.13. Grouped histogram of lane-level queue length estimation error for different penetration rates of technology.

It is clear that the lane-level queue estimation accuracy using only the position measurements from the CAV's is strongly affected by the penetration rate. CAV's do have additional information from the safety sensors that can be useful, such as distance to adjacent vehicles in front, behind, and in adjacent lanes. New queue determination methods that include this additional information could significantly improve performance at lower penetration rates.

3.5 MOVES Emission Model Refinement

The refinement of the MOVES emission model through sub-binning has been a significant endeavor in improving the accuracy and reliability of emission estimates in transportation systems. This section focuses on the advancements made in refining the MOVES emission model and its application in two field studies: one comparing a binning-style emission model to the Comprehensive Modal Emissions Model (CMEM) using data from EAD (Eco-approach and Departure) field experiments, and the other analyzing data from a project with Honda testing a Reactive Force Pedal (RFP) to compare MOVES against the refined MOVES model and actual CO_2 measurements.

The refinement of the MOVES emission model involved the development and implementation of sub-binning techniques, which allowed for a more granular representation of vehicle characteristics and driving patterns. By dividing vehicle operations into finer subcategories, such as specific vehicle types, engine sizes, driving conditions, and operating modes, the refined MOVES model was able to capture the subtle variations in emissions that were previously not adequately accounted for in the original model.

In the first field study, the comparison between a binning-style emission model and CMEM using data from EAD field experiments provided valuable insights into the performance and accuracy of the refined MOVES model. By analyzing emissions data collected from real-world driving scenarios, the study evaluated the ability of the refined MOVES model to better predict emission levels and capture the variations across different driving conditions and vehicle characteristics. More information can be found in [50].

The second field study focused on analyzing data from a project with Honda, specifically testing a Reactive Force Pedal (RFP) that aimed to promote more fuel-efficient driving behavior. In this study, the MOVES emission model was compared to the refined MOVES model and actual CO_2 measurements obtained from the RFP-equipped vehicles. The goal was to assess the effectiveness of the refined MOVES model in accurately estimating CO_2 emissions and its compatibility with real-world measurements. More information can be found in [51].

By conducting these field studies and comparing the refined MOVES model with alternative models and actual measurements, valuable insights were gained regarding the performance, accuracy, and applicability of the refined MOVES model. These findings provide a solid foundation for further refinement and improvement of emission estimation models, paving the way for more accurate assessments of transportation-related emissions and the development of effective emission reduction strategies.

3.5.1 Evaluating the Environmental Impacts of Connected and Automated Vehicles: Potential Shortcomings of a Binned-Based Emissions Model

The primary goal of this study is to compare different energy and emissions modeling approaches for analyzing connected and automated vehicles. Actual energy and emissions are measured on a set of vehicles, which are then later compared to the U.S. Environmental Protection Agency's MOVES model and also to the Comprehensive Modal Emissions Model (CMEM). These measurements and model predictions are shown for the Eco-Approach and Departure (EAD) application, where two vehicles are compared: one that has the EAD technology and one that does not. In this study, we first provide a brief background on the two energy and emission models, as well as the EAD application. The experimental methodology is then described, followed by the results and conclusions.

3.5.1.1 Background

3.5.1.1.1 Motor Vehicles Emission Simulator

The EPA developed the Motor Vehicles Emission Simulator (MOVES) energy and emissions model originally in the year 2000 and has periodically updated it ever since. MOVES is used for a variety of applications, including a number of regulatory processes (see https://www.epa.gov/moves for details). MOVES can operate as either a macroscopic or microscopic model, depending on how it is used. MOVES is very data intensive, requiring estimates of vehicle activity, energy and emissions rates, and a number of other inputs. MOVES can assess the emissions of all vehicles on a road segment, based on aggregated data. The model represents the relationship between vehicle characteristics, operating conditions and the emission/fuel consumption rates from large datasets collected in both the laboratory and on the road using on-board portable emissions measurement systems. [52].

MOVES categorizes all vehicles into source types and estimates the emission rates of the vehicles in one source type under specific operation mode (opmode). Consequently, when an individual vehicle is evaluated with MOVES, the average behavior of all vehicles of the same source type is given. Therefore, when evaluating the emission and fuel consumption of one specific vehicle, MOVES is not able to distinguish this vehicle from the average vehicle of the same source type [52]. It also uses a binning technique for its operation modes, using bins that generated for different levels of vehicle specific power (VSP) and average speed.

For MOVES, the user defines vehicle types, speed data, traffic activities, geographical areas, pollutants, vehicle operating attributes, and meteorology parameters as the inputs of the model; then the model provides estimates of total emission inventories or emission factors [52][53].

3.5.1.1.2 Comprehensive Modal Emissions Model

The Comprehensive Modal Emission Model (CMEM) is a microscopic, physical emissions model that estimates the emissions of individual vehicles [54]. CMEM was developed to capture the physical relationships between vehicle characteristics, operating conditions, and the emission/fuel consumption rates [52]. One prominent advantage of this approach is that it is possible tailor many of the physical parameters to fit a very specific type of vehicle (i.e., down to make and model) [54].

Both MOVES and CMEM takes the attributes of an individual vehicle, and its second-by-second speed profile as input, and predicts second-by-second fuel consumption and tailpipe emissions of carbon monoxide (CO), carbon dioxide (CO_2), hydrocarbons (HC), and oxides of nitrogen (NOx). Like MOVES, CMEM can predict energy and emissions from individual vehicles and an entire fleet of vehicles [54].

3.5.1.1.3 Relevant Work

In 2002, Cappiello et al. [55] presented a statistical emissions model called EMIT (EMIssions from Traffic), where CMEM and EMIT were compared to measured data. For fuel consumption rate, CMEM had a -2.2% error, while EMIT had a 5.3% error. However, the data used by Cappiello et al. came from the same database that was used to develop CMEM, so the results are somewhat biased.

In 2003, Rakha et al. [56] compared CMEM, MOBILE5a, and MOBILE6, which are the EPA's predecessors to MOVES, and VT-Micro. In this comparison, VT-Micro and MOBILE6 were shown to be more accurate than CMEM, but the database used in the study was the same database used to develop VT-Micro and MOBILE6.

Chamberlin et al. [57] developed a microsimulation of a 3-leg intersection and used MOVES and CMEM to evaluate the different intersection control strategies. In the study, only NOx and CO were considered; MOVES and CMEM showed similar results for NOx but had disparities for CO outputs.

Zhang et al. [52] used MOVES and CMEM to evaluate the fuel consumption and emissions for a variable speed limit. In the study, the I-710 freeway in California was built in VISSIM and used historical data from the California Department of Transportation. The study showed that CMEM and MOVES were qualitatively similar, but there were discrepancies in the actual values output from the two models.

Many CAV applications use MOVES to evaluate simulations or estimate emission outputs. Abou-Senna et al. [58] used MOVES to estimate emissions for a limited access highway simulation built in VISSIM. Liu et al. [59] used smoothing techniques on EPA eco-autonomous driving cycles. The emission results were estimated using MOVES. Xu et al. [60] simulated transit eco-driving

methods using an algorithm that limits vehicle specific power while preserving the average speed, and the MOVES was used for the analysis.

3.5.1.2 Results

The methodology and experiment for this study will be presented and analyzed in Chapter 4. Briefly, the experiments were conducted on the Innovation Corridor, implementing a modified version of the Eco-driving strategy for actuated signals described in [29]. The evaluation focused on the Eco-Approach and Departure (EAD) application, involving simultaneous testing of two light-duty vehicles. One vehicle utilized the EAD application for actuated signals, while the other vehicle followed regular driving patterns in traffic. The tests were conducted during weekdays between 10:00 am to 12:00 pm and 1:30 pm to 3:30 pm.

MOVES uses vehicle specific power (VSP) and vehicle speed data to select emission values from an operation mode (opmode) bin. The MOVES-based binning model utilized in this experiment uses the same approach as MOVES, but the data the values are chosen from were calibrated specifically for the test vehicle.

For CMEM, the model was calibrated specifically for the test vehicle. This means that the readily available parameters, such as mass, engine displacement, the idle speed of the engine, were obtained, and the calibration parameters were derived, as described in [60].

The fuel consumption estimates given from the emission models CMEM and MOVES were compared to the measured fuel consumption. The measured fuel consumption (FC), in grams, is obtained from using the mass airflow (MAF) and air/fuel ratio (AFR), which are read from the vehicle via the OBD-II cable.

As an example, Figure 3.14 shows the comparison of CO_2 outputs from the binning model and CMEM, to the measured value along with the velocity profile for a portion of the test data. In Figure 3.14, the overestimation of emission output from the binning model can be observed.

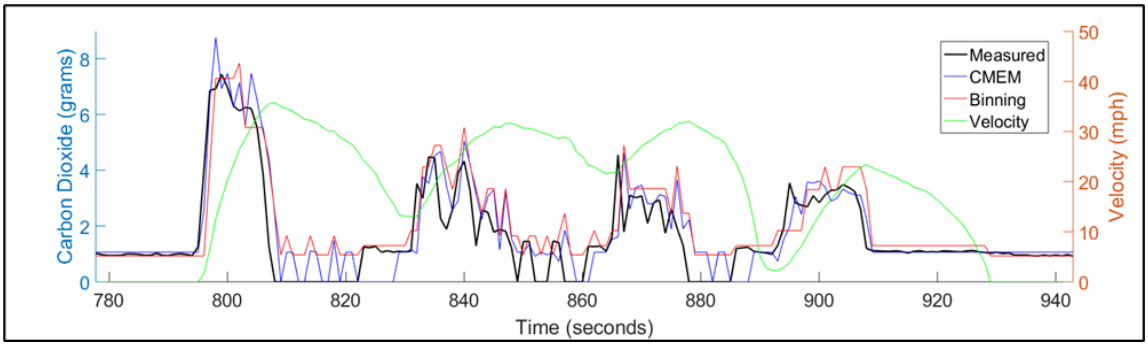

Figure 3.14. Emissions model comparison with velocity for an example experimental run.

Table 3.2 summarizes the results of the MOVES-based binning model and CMEM compared to the measured data. It can be seen that the MOVES-based binning model overestimates the fuel consumption and CO_2 emissions. This is most likely due to the fact that the MOVES-based binning approach does not take into account the vehicle's fuel shutoff effects during decelerations. In this case, CMEM also over predicts emissions, but to a lesser extent than the MOVES-based binning approach.

Table 3.2. Emissions model comparison

Method	Fuel Consumption Avg. g/mile	CO_2 Avg. g/mile
Measured	144.66	457.84
CMEM	152.29	481.99
	+5.27%	+5.27%
MOVES-based Binning Model	163.58	517.72
	+13.08%	+13.08%

One of the reasons why the binning model misrepresents emission savings is presented in Figure 3.15. Figure 3.15 shows how the MOVES opmode bins are defined by several VSP ranges and three vehicle speed ranges. One opmode bin can be used for a wide range of VSP or vehicle speeds, and each data point will generate the emissions rate associated with the bin in which the

data point falls. If a CAV application, such as EAD, is implemented and the VSP goes down slightly, but the data point is in the same bin, the benefit of the CAV application will not be captured.

Table 3.3 shows the results of the EAD application with the CMEM and the binning model estimates compared to the measured values. As previously mentioned, the measured values were recorded at the same time with two vehicles, one implementing EAD technology and one driving normally. Each time the corridor was entered, both vehicles entered at the same time and stayed in different lanes to not influence the other driver. The CO_2 and fuel consumption used in Table 3.3 are the average grams per mile where the total grams from the measured values and the outputs from both models are individually summed, and then divided by the total miles travelled. The improvement column from Table 3.3 is the percentage decrease from no EAD to EAD. The MOVES-based binning model underestimated the benefits of EAD by about half, whereas the CMEM estimate was closer to the actual measured improvement.

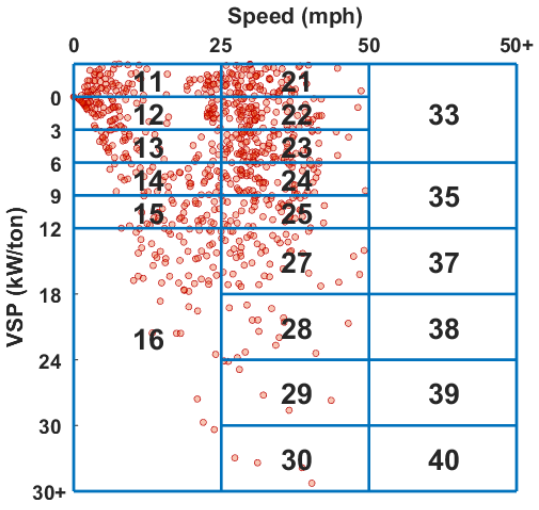

Figure 3.15. MOVES binning method showing MOVES opmode bins with measured test data presented in red.

Table 3.3. Eco-Approach and departure evaluation

		No EAD	EAD	Improvement
Actual	CO_2 (g/mi)	430.7	402.3	6.6%
	Fuel (g/mi)	137.63	128.5	6.63%
CMEM	CO_2 (g/mi)	439.9	419.83	4.5%
	Fuel (g/mi)	138.97	132.5	4.65%
MOVES-based binning	CO_2 (g/mi)	475.4	462.69	2.67%
	Fuel (g/mi)	151.87	147.8	2.7%

3.5.1.3 Conclusion

In this study, the fuel consumption and emissions of a light-duty vehicle recorded during real-world tests are compared to the fuel consumption estimates given from the Comprehensive Modal Emissions Model (CMEM) and a binning model based on the binning method of the Motor Vehicles Emission Simulator (MOVES) emission model.

CMEM overestimated fuel consumption by 5.3%, and the binning model overestimated it by 13.1%. Therefore, this experiment suggests that CMEM is a more accurate emissions model. MOVES is a data-driven model and is less sensitive to transient processes because it describes the average behavior of a general vehicle type (e.g., passenger car, pickup truck) [54].

To demonstrate binning models' underestimation of the fuel saving from CAV applications, an Eco-Approach and Departure application was performed on the Innovation Corridor with real-world traffic. When comparing two vehicles with and without the technology, the CMEM-based method gave a more accurate estimate of the energy and emissions differences than the MOVES-based model. The results of these tests demonstrate the importance of using a physical model for connected vehicle applications.

3.5.2 Real-world Efficacy of a Haptic Accelerator Pedal-based Eco-driving System

It is well known that vehicle acceleration is one component of driver behavior that can have a major impact on fuel consumption and GHG emissions. Vehicle acceleration requires a certain amount of energy based on vehicle weight, vehicle speed, and road grade. Acceleration events requires more energy than cruising at a steady-state speed, resulting in increased fuel consumption. Over a fixed distance of travel, aggressive acceleration events result in higher fuel consumption and GHG emissions, and smoother driving (consisting of mild acceleration events) result in lower overall emissions [61]. Therefore, there have been a number of eco-driving technologies that have been developed, with the intent of reducing hard accelerations down to mild accelerations.

One of these technologies is an accelerator pedal-based eco-driving tool that provides a reactive force to the driver to encourage gentle acceleration events. This Reactive Force Pedal (RFP) provides force feedback through the accelerator pedal, and can be in one of three modes: OFF, LOW, or HIGH. Each mode refers to the amount of force feedback from the pedal to the driver.

In this study, 40 drivers were recruited to evaluate the RFP technology following a predetermined route, use all of the different RFP modes. Each driver followed the route three times, each time using a different mode, and the sequence of modes was randomized. For example, one driver would have the RFP OFF for the first trip, then on LOW for the second trip, and HIGH for the final trip. Then the next driver might have the RFP LOW for the first trip, OFF for the second, and HIGH for the final trip. The sequence would not always be the same in case there was an impact on driving. The velocity trajectories for each trip were used as input to the U.S. EPA's emission model Motor Vehicle Emission Simulator (MOVES, see [16]) to estimate fuel consumption. The MOVES fuel consumption estimates are also compared to an "Acceleration Energy Equivalent (AEE)" method, described later in section 3.4.5 (change to correct section).

3.5.2.1 Background

Over the years, there have been several eco-driving systems that have been developed that provide feedback to the drivers through the accelerator pedal. For example, in 2006, Nissan Motor Corporation began developing a driver support system that included accelerator pedal reaction force control [62], which later became the Nissan "ECO-Pedal" system [63]. Initially the support system was being designed to improve drivers' awareness of a changing situation ahead in hopes of reducing rear-end collisions. The reactive force on the accelerator pedal would increase as the vehicle approaches another vehicle ahead. The system works in an anticipatory fashion, with a pedal pushback when the driver exerts excessive pressure on the accelerator pedal. According to Nissan's internal research data, the ECO-Pedal improves fuel efficiency by 5-10% in most driving conditions [64].

In 2007, Ford Motor Company developed a real-time advisory system for hybrid electric vehicles (HEV) [65]. The advisory system used force feedback on the accelerator pedal, using two fuzzy logic controllers to determine the maximal driver demand corresponding to the desired fuel economy level, engine operating conditions, and vehicle speed. Testing was done on isolated test tracks, resulting in HEV fuel economy improvements by up to 3.5%. By 2009 the system was improved and achieved a 22% energy consumption savings for aggressive drivers in an HEV [66].

In Sweden, an acceleration advisory tool was installed in four postal delivery vehicles [67]. The advice was supplied to the drivers through resistance in the accelerator pedal. Data were collected for six weeks without the advisory tool and six weeks with the advisory tool. The study found that heavy acceleration was significantly reduced; however, no significant reduction in fuel consumption or emissions was recorded.

In 2010, an experiment was conducted at Renault's Technical Centre for Simulation using the CARDS driving simulator [68]. The simulator has a modular cockpit that is completely

instrumented to resemble a real car. The study was done to evaluate the efficiency of basic eco-driving instructions, and to compare visual, haptic and coupled visual-haptic eco-driving assistances. Visual assistance was given on a 7-inch display on the mid-console, and the haptic assistance was given using a force feedback system on the accelerator pedal. The study showed no significant difference between assistance feedback type, meaning the visual feedback provided the same eco-performance as a haptic pedal. But drivers relied on the haptic pedal more when using both visual and haptic assistance. It was found that tailpipe emissions were decreased by 5 to 7% in the experiments [68].

In 2015, a comparison of twelve eco-driving interfaces was carried out using a high-fidelity driving simulator [69]. This study was done specifically for feedback on accelerator pedal usage. The twelve interfaces included six haptic, three visual, and three visual-auditory systems. Each eco-driving interface advised the driver on the most fuel-efficient accelerator pedal angle in real-time. The haptic systems tested were force feedback, stiffness feedback, and adaptive stiffness feedback. Each haptic system consisted of two profiles: one to advise of the 7% angle at constant speed, and one to advise of the 23% angle during acceleration. Of the six haptic systems, a strong force feedback system was the most preferred by an array of drivers.

Finally, in 2014, Honda Motor Company developed and produced a reactive force pedal for their Acura RLX vehicle, and in 2019 Honda teamed with UC Riverside for evaluating this technology. This research addresses the efficacy of this reactive force pedal.

3.5.2.2 Methodology

3.5.2.2.1 Experiment

The purpose of these experiments was to assess the impact the force feedback pedal would have on an average driver in the United States. In total, 40 drivers were recruited to drive an Acura RLX equipped with the RFP technology. This vehicle was outfitted with a datalogger which logged

speed and other data from the engine control unit (ECU), as well as front and rear cameras for recording the driving scene. The force feedback pedal was capable of three modes: 'Off', 'Low', and 'High'. In the 'Off' mode there is no pedal force, so the driving behavior reflects baseline driving conditions. In the 'Low' mode, the driver feels some mild pedal feedback with sustained resistance. In the 'High' mode, the driver feels an instantaneous burst of reactive pedal force at certain pedal stroke positions and a similar sustained resistance as the 'Low' mode.

The 40 drivers were all required to be at least 21 years of age, hold a valid driver's license, and have no prior experience driving an Acura RLX. For the participant pool to match the U.S. driving population closely, a target was set for different age/gender groups (see Table 3.4). These targets are based on the 2017 count of licensed drivers in the U.S. from the Federal Highway Administration [70].

The driving route is the blue loop in the Riverside California, shown in Figure 3.16 (the driving direction is clockwise). The route is roughly equally split between highway and arterial roadway driving, and takes approximately 40 minutes to complete a single loop. A human navigator sat with the driver to ensure that the driver remained on the route. Each driver drove the route three times, using a different setting for the pedal force each time. However, the drivers were not told the pedal force setting at the time of driving. Since drivers would become more familiar with the car as they continued to drive it, the order of pedal force settings was randomized for each driver. For example, for one driver it could be {OFF, LOW, HIGH} and for the next it could be {LOW, OFF, HIGH}. The entire test sequence was usually completed within a three-hour period.

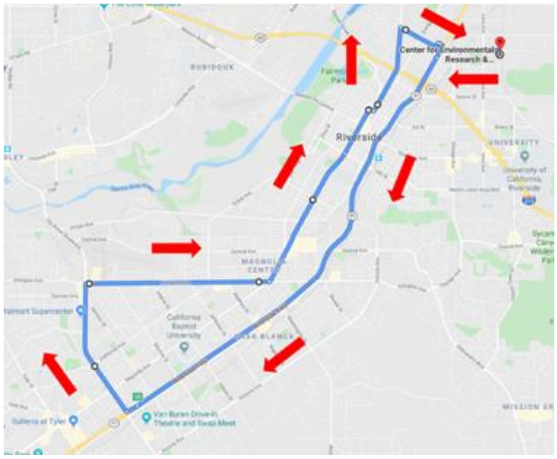

Figure 3.16. Driving route for experiment in Southern California, *Google Maps*, 2019.

Table 3.4. Number of driver participants in different age-gender groups.

Age Group	Male		Female	
	Target	Actual	Target	Actual
under 30	5	7	4	4
30-44	5	5	5	5
45-64	7	7	7	7
65+	4	3	3	2
Total	21	22	19	18

3.5.2.2.2 Data Analysis

The velocity trajectories for each trip were used as input to the US EPA's MOVES model to estimate fuel consumption. MOVES relies on Vehicle Specific Power (VSP) and velocity to estimate emission rates, including fuel consumption. It takes in second-by-second velocity trajectories, then calculates VSP (3.20) and uses this data to determine from which operation mode (OpMode) to assign an emission factor. For our data analysis, we have calculated VSP distributions for each driver, along with their acceleration-vs.-speed profiles, as shown in Figure 3.17.

$$VSP = v * \left(a * (1 + \epsilon) + G * \theta + 4.448222 * \frac{A + B * v_2 + C * v_2^2}{M} \right) \qquad (3.20)$$

$$A = 36.39, B = 0.3156, C = 0.01918$$

VSP = vehicle specific power $\left(\frac{kW}{Ton} = \frac{m^2}{s^3}\right)$

v = velocity $\left(\frac{m}{s}\right)$

a = acceleration $\left(\frac{m}{s^2}\right)$

ϵ =Mass factor (0.1 in this case)

G = acceleration of gravity $\left(\frac{m}{s^2}\right)$

θ = road grade (0 in this case)

v_2 = velocity (MPH)

M = vehicle test weight (kg)

A is rolling resistance $\left(\frac{KW}{mps}\right)$, B is friction term $\left(\frac{KW}{mps^2}\right)$, C is aerodynamic drag $\left(\frac{KW}{mps^3}\right)$

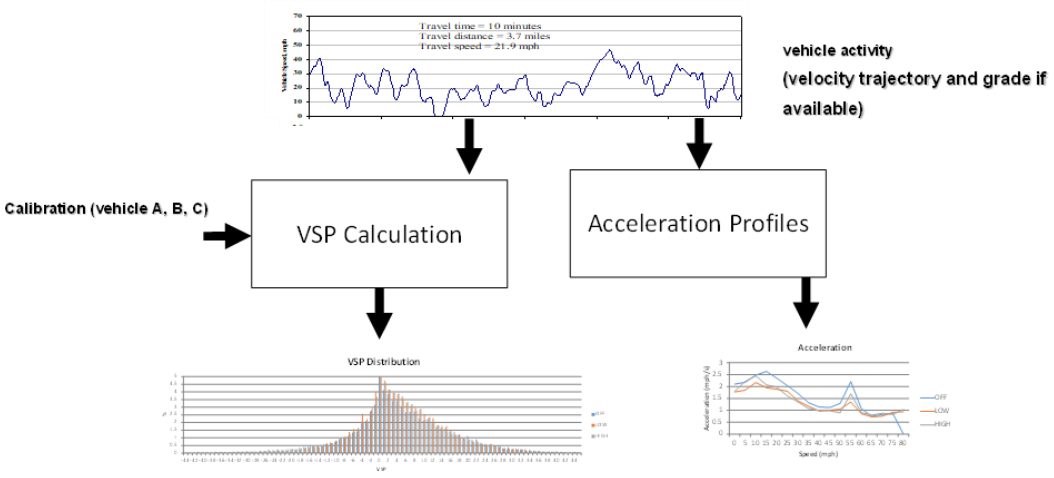

Figure 3.17. VSP distribution and acceleration profile generation methodology.

This methodology was applied to all of the drivers, and the resulting VSP distributions and acceleration profiles allow us to best understand how the RFP technology changes the driving micro-behaviors. In addition, we were able to calculate the OpMode bins in the MOVES model (Figure 3.15) for each second of driving.

The procedure for the MOVES model is as follows: First, the second-by-second velocity profile is used to calculate a VSP profile. The instantaneous VSP and speed values are then used to determine which OpMode bin the activity falls in to. In our first method, we calculate an emissions and energy value using the default MOVES emission factors for a 2017 generic light-duty vehicle. As a second method, we used energy and emission factors that was calibrated for the specific test vehicle (2018 Acura RLX).

The three versions of MOVES analysis were also compared to an Acceleration Energy Equivalent (AEE) methodology. The AEE method calculates positive energy utilization as shown in (3.22) [71].

$$AEE = \sum_{k=1}^{K} \sigma_k \left(v_k^2 - v_{k-1}^2\right), \tag{3.22}$$

AEE units are $\left(\frac{mile^2}{s^2}\right)$.

v is velocity $\left(\frac{mile}{s}\right)$.

$\sigma_k = 1$ if $v_k > v_{k-1}$ otherwise $\sigma_k = 0$.

3.5.2.3 Results

3.5.2.3.1 Overall Comparison

For this analysis, we compared several different methodologies for determining the fuel consumption impacts from the RFP technology. Specifically, we compared:

- Measured Fuel Consumption (baseline)
- Honda AEE method
- MOVES Generic Vehicle Methodology
- MOVES Calibrated for target vehicle
- MOVES Calibrated for target vehicle, with enhanced sub-binning

Measured Fuel Consumption: The test vehicle was equipped with a Honda's proprietary data logger that is able to very accurately measure fuel consumption at 10Hz. These data were subsampling to 1 Hz. so that they are compatible with the MOVES model.

Acceleration Energy Equivalent method: This method is a specific energy-based calculation that focuses on cumulative positive acceleration events.

MOVES Generic Vehicle Methodology: The fuel consumption is predicted from MOVES for a generic 2019 Light Duty Vehicle (LDV), using MOVES default OpMode energy and emission rates. These fuel consumption rates are shown in Figure 3.18.

MOVES Calibrated for Target Vehicle: The measured fuel consumption data for the target vehicle was used to calibrate the specific values of the MOVES OpMode bins. A similar model to that used in [50]. These fuel consumption rates are shown in Figure 3.19.

MOVES Calibrated for target vehicle with enhanced sub-binning: The default range of the MOVES OpMode bins were selected to cover a large number of vehicle types over a wide range of activity patterns. Simultaneously, the number of bins were selected so that the overall calculations were computationally tractable. However, because of the bin size, MOVES is sometimes insensitive to small changes in VSP and speed, because many activity points fall within the same bin. As a result, we have enhanced the MOVES model by splitting the bins that have wide VSP ranges into sub-bins, providing a more accurate estimation method. The method of creating sub-bins is shown in Figure 3.20. The fuel consumption rate for these new sub-bins is shown in Figure 3.21.

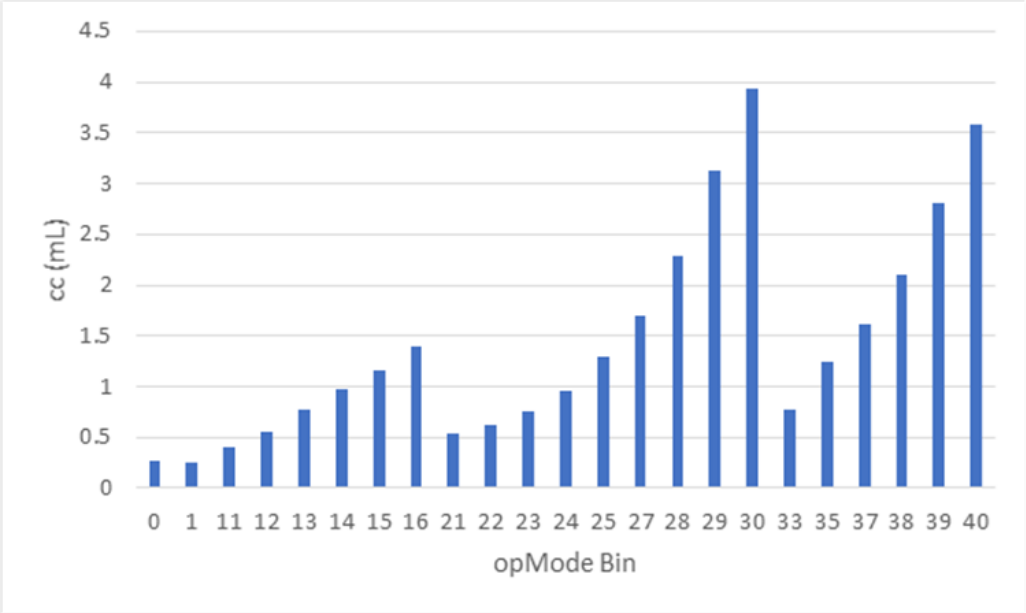

Figure 3.18. EPA MOVES OpMode fuel consumption values for a 2019 default light-duty vehicle.

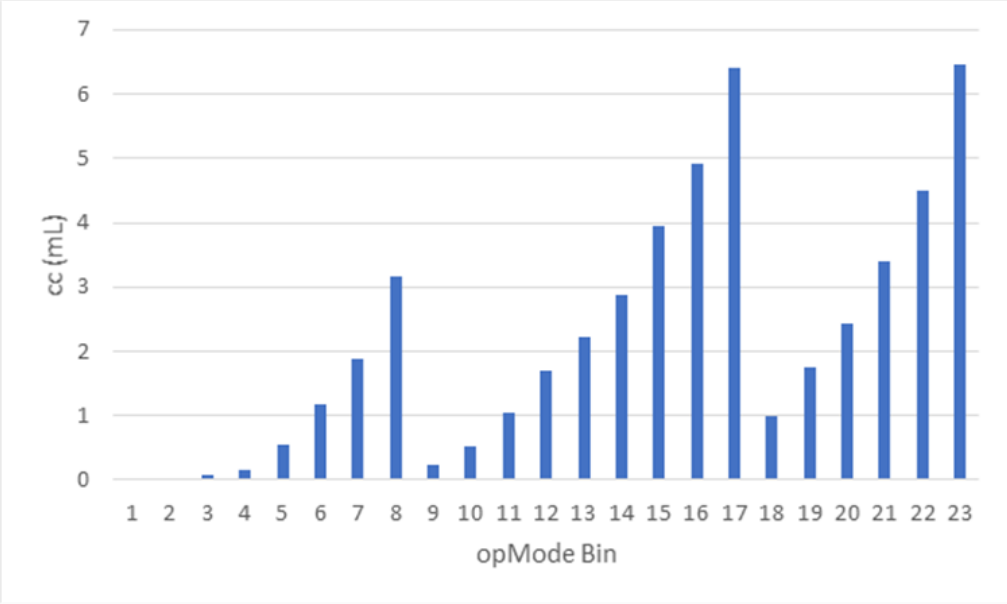

Figure 3.19. MOVES OpMode fuel consumption values calibrated for the Acura test vehicle.

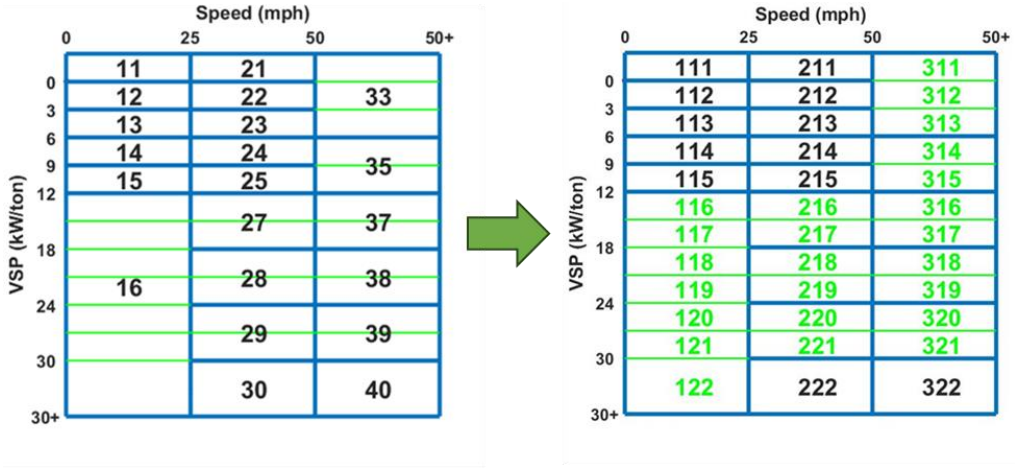

Figure 3.20. MOVES OpMode sub-binning methodology.

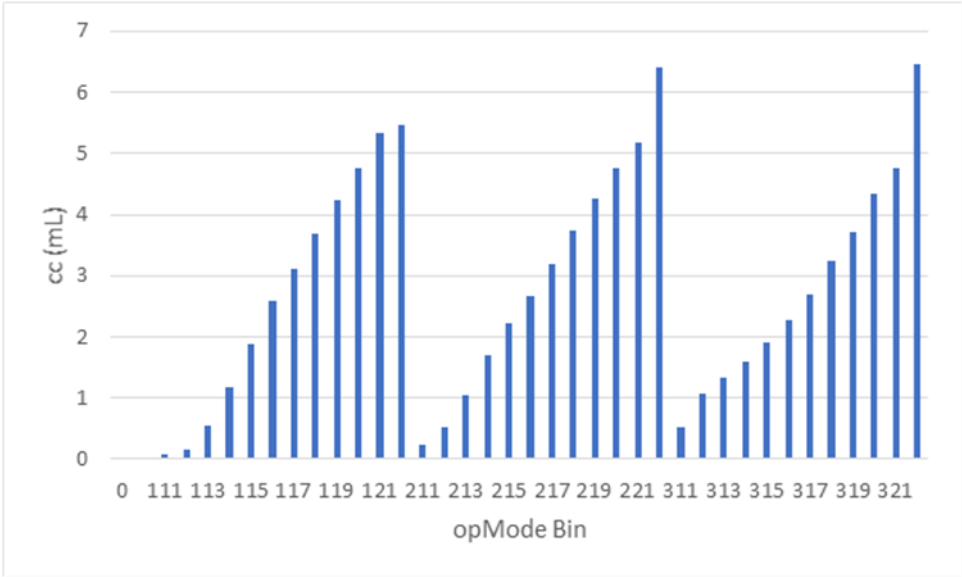

Figure 3.21. MOVES OpMode sub-bin fuel consumption values calibrated for the Acura test vehicle.

Each run had slightly different distance so fuel consumption calculations are normalized by distance traveled in order to be fairly compared. When considering the average response of the methodologies, we can compare the results as illustrated in Figures 3.22. Figure 3.22 illustrates the average savings with error bars when RFP setting is on LOW and HIGH compared to when the RFP is set to OFF during acceleration events. It can be seen that all four methods were able to estimate fuel consumption close to the measured value when RFP setting is on LOW.

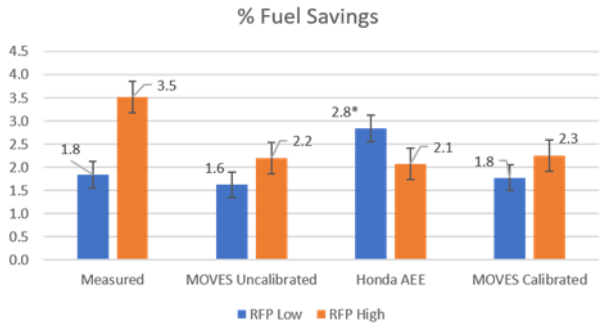

Figure 3.22. RFP average fuel consumption savings.

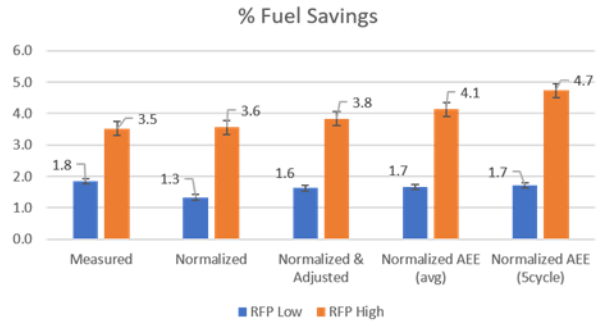

Figure 3.23. RFP average fuel consumption savings after normalization.

The average savings during acceleration events given the measured fuel consumption turned out to be 1.8% for the RFP on the LOW setting, and 3.5% for the RFP on the HIGH setting. The uncalibrated MOVES using the generic 2019 LDV fuel consumption seems to follow the trend of the measured fuel consumption. For individual drivers, the uncalibrated MOVES results could be off by a significant margin. Table 3.5 shows a select group of drivers and MOVES is notably different from the measured results; however, when data from all drivers is taken into account, the MOVES results are comparable to the measured results. Lastly, the MOVES sub-binning method results are closer to the measured than the MOVES original bin as expected since it provided more sensitivity to the change in vehicle specific power.

Next, we normalized the modeling results due to the differences in traffic conditions during the driving experiments without and with the RFP technology in order to reduce potential biases

due to those differences. Figure 3.23 shows the results after this normalization process. In Figure 3.23, "Normalized" means that the calibrated MOVES results were corrected for unnecessarily long idling. "Normalized & Adjusted" means that the calibrated MOVES was corrected based on the effect of change in the amount of speeding beyond the speed limit on top of the unnecessary idling. Figure 3.23 also shows normalizing for the AEE method. The "Normalized AEE (avg)" means that the AEE was adjusted by distance rate to average. The "Normalized AEE (5cycle)" means that AEE was adjusted based on the accumulated distance per total driven distance of combined 5-cycle City/Highway cycle; based on EPA's 5-cycle driving pattern. After this normalization process, the results are more similar to the measured fuel consumption savings.

Table 3.5. Selected drivers' data fuel estimation method comparison.

SubjectID	Measured		MOVES Uncalibrated		Honda AEE		MOVES Calibrated		MOVES Sub-bins	
	RFP low % savings	RFP high % savings	RFP low % savings	RFP high % savings	RFP low % savings	RFP high % savings	RFP low % savings	RFP high % savings	RFP low % savings	RFP high % savings
1	-7.58	0.63	4.10	2.47	0.50	-0.84	0.39	-1.94	0.10	-2.33
8	-4.33	-5.41	3.96	2.83	4.91	9.36	-1.30	-1.96	-1.57	-2.63
10	-7.38	-0.73	-11.69	-6.15	-16.86	-3.30	-7.61	-2.75	-7.65	-1.20
16	3.55	0.32	0.46	2.26	9.04	4.19	3.59	-1.22	3.16	-1.81
24	1.76	-1.48	7.03	1.20	8.22	3.54	1.85	1.02	1.81	1.85
33	-4.15	-0.13	-1.64	2.44	-6.61	-5.42	-4.24	-1.14	-3.97	-1.07

3.5.2.3.2 Specific Driver Examples

The results for all 40 drivers were processed (see appendix), but for this report we have selected drivers 6, 12, and 39 as examples to highlight the insights of the different methodologies. These three driver results are good representations out of the full data set. In these examples, the acceleration and VSP distributions are first shown. Next, the MOVES OpMode distributions for the three drivers are shown. Then, a comparison of the MOVES estimated fuel consumption and the measured fuel consumption is discussed.

Figures 3.24, 3.28, and 3.32 show the acceleration and deceleration profile graphs of each example driver. The acceleration graphs illustrate that the RFP technology reduces the acceleration rates for all drivers. The acceleration rate (by speed) is an important indicator since it plays a large role in the VSP calculation.

Since VSP is the main component for the MOVES model, we illustrate the VSP distributions for each driver in Figures 3.25, 3.29, and 3.33. The VSP distribution plots are useful in observing how we can perform sub-binning to provide greater model sensitivity.

Figures 3.26, 3.30, and 3.34 illustrate the data for each driver plotted on top of the MOVES OpMode bins, while Figures 3.27, 3.31, and 3.35 “OpMode bin distribution” charts show a bar graph distribution of the actual numbers for each OpMode bin (normal MOVES on right, MOVES sub-bins on left). Figures 3.26, 3.30, 3.34, and the “OpMode bin distribution” charts show the same information but illustrate the data in a different insightful way.

Figures 3.27, 3.31, and 3.35 “OpMode bin distribution” charts show that the higher VSP valued bins have less data points than the lower VSP valued bins, however the “Fuel used” charts show the fuel consumption by OpMode bin. The bins for higher VSP values actually account for a big portion of fuel consumption.

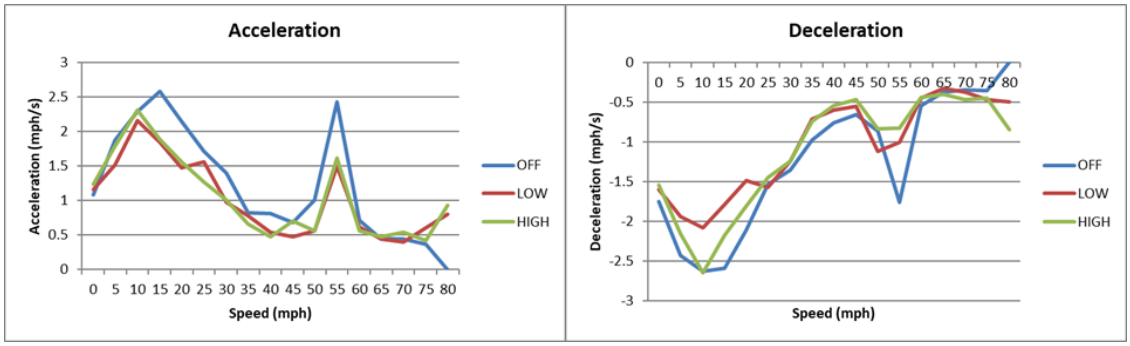

Figure 3.24. Acceleration and deceleration profiles for Driver 6.

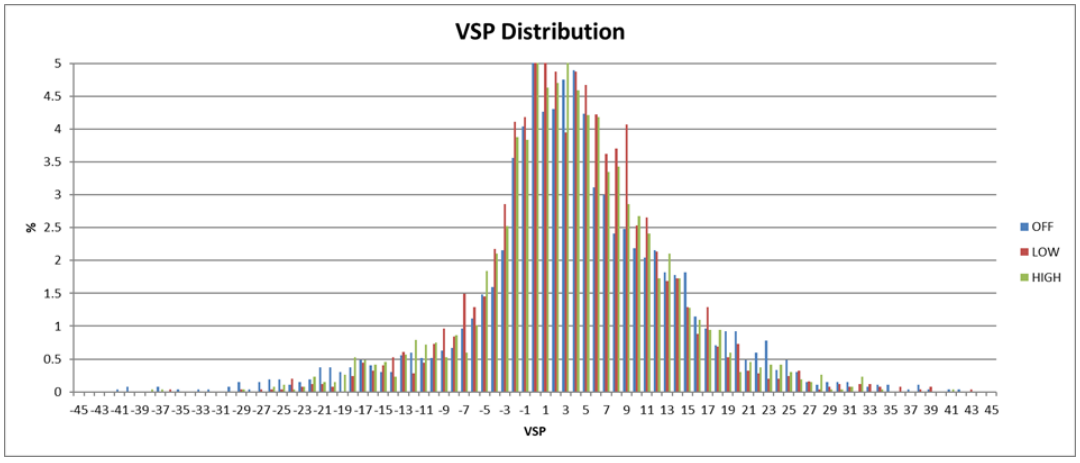

Figure 3.25. VSP distribution chart for Driver 6.

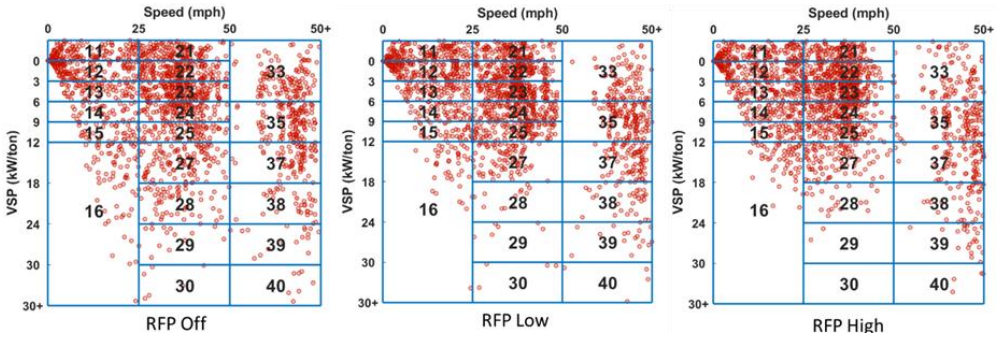

Figure 3.26. Driver 6 data plotted onto MOVES OpMode bins.

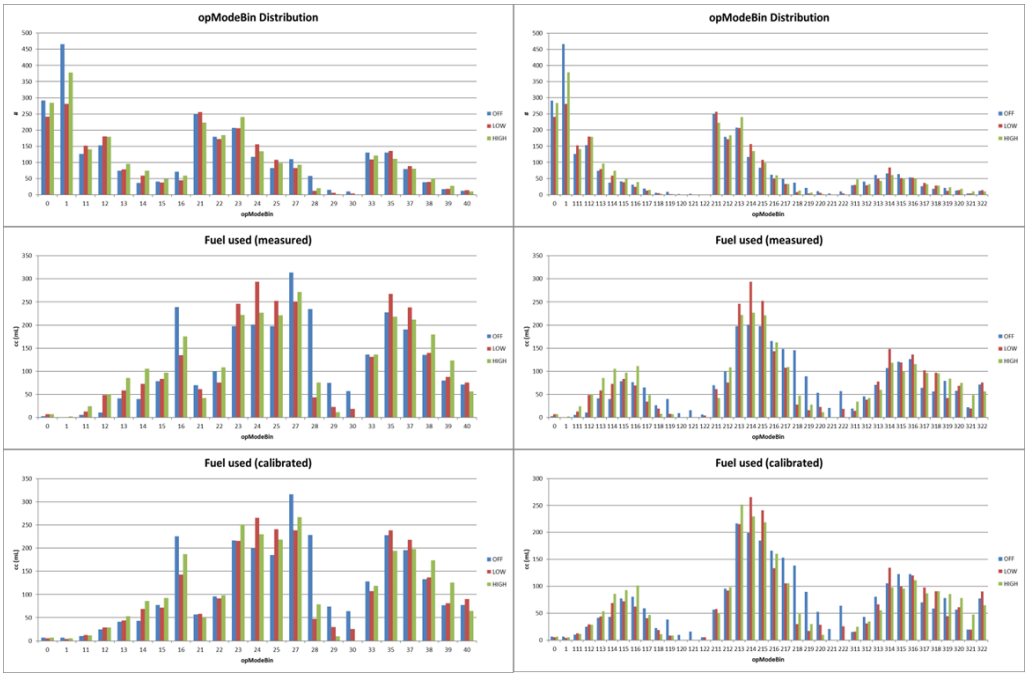

Figure 3.27. Driver 6 data separated into MOVES OpMode bins.

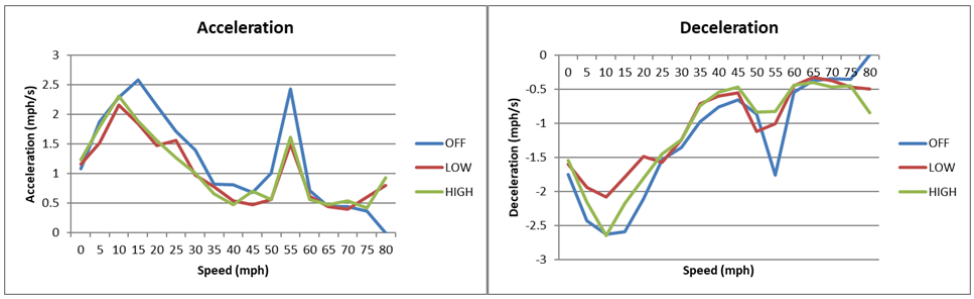

Figure 3.28. Acceleration and deceleration profiles for Driver 12.

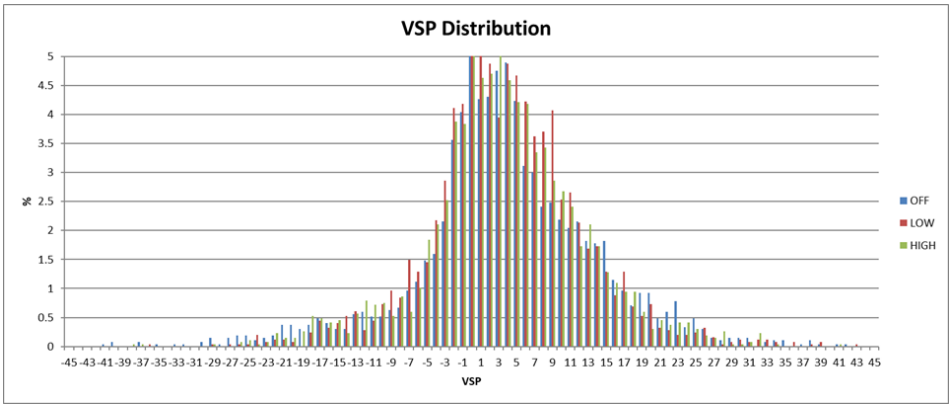

Figure 3.29. VSP distribution chart for Driver 12.

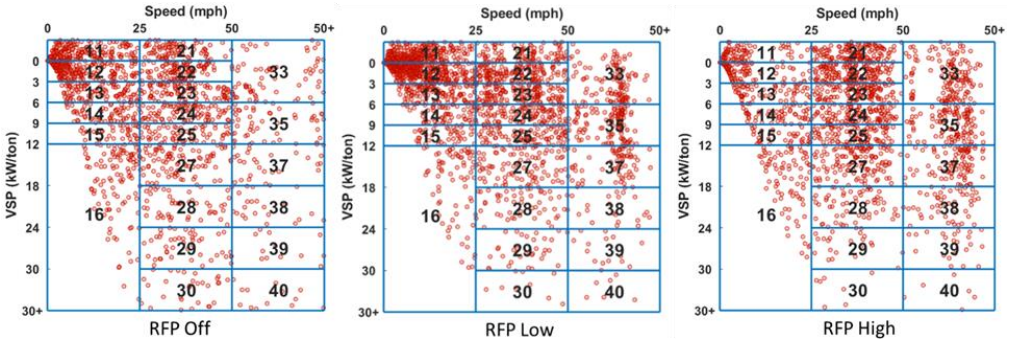

Figure 3.30. Driver 12 data plotted onto MOVES OpMode bins.

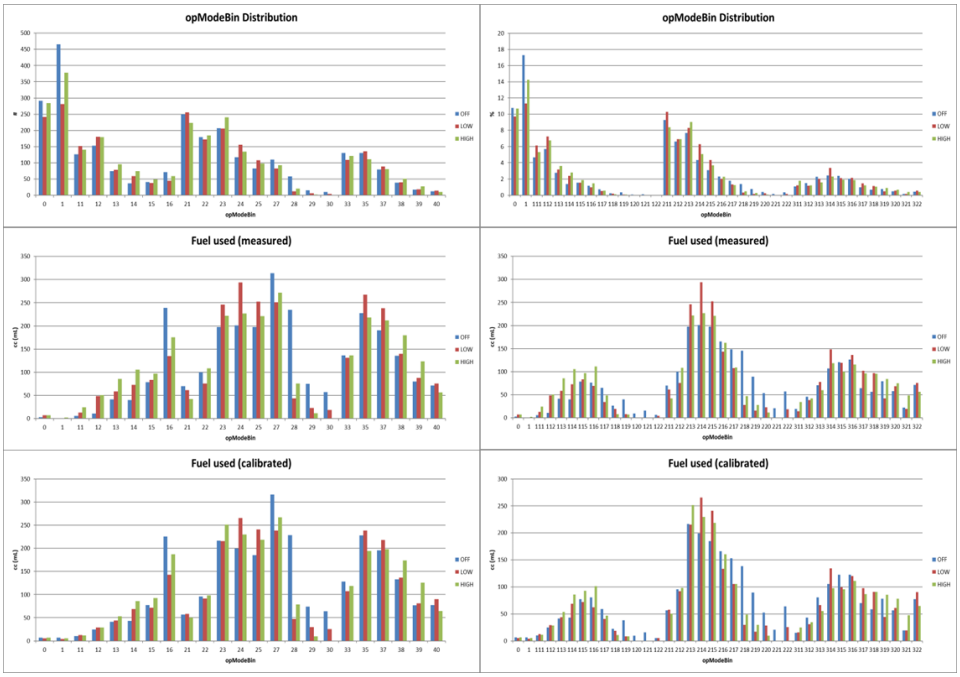

Figure 3.31. Driver 12 data separated into MOVES OpMode bins.

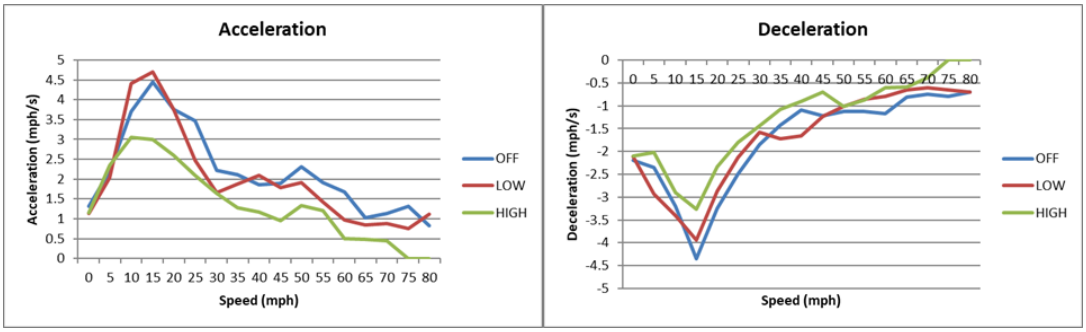

Figure 3.32. Acceleration and deceleration profiles for Driver 39.

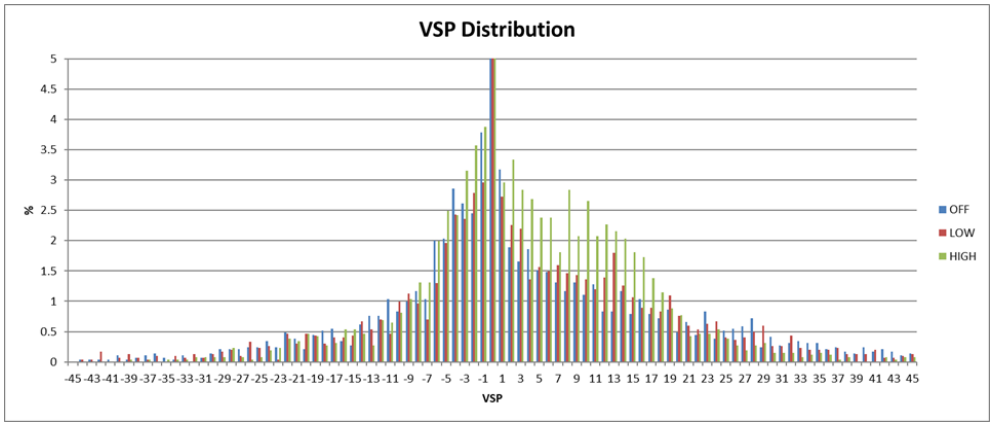

Figure 3.33. VSP distribution chart for Driver 39.

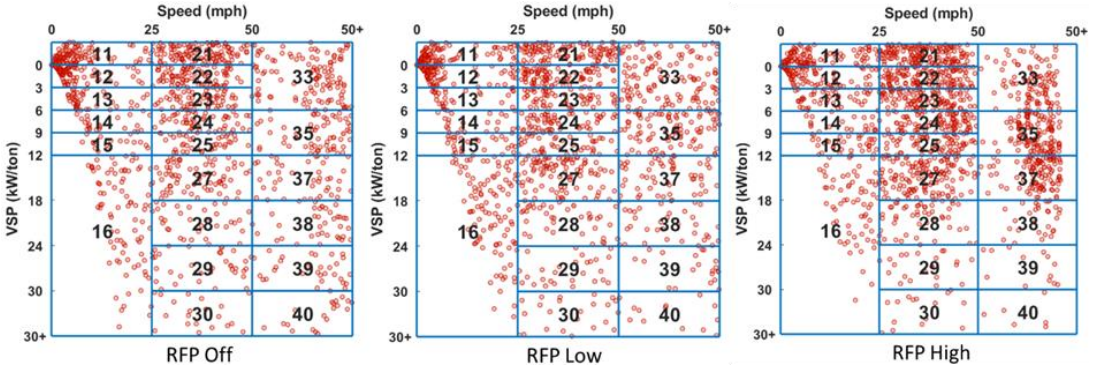

Figure 3.34. Driver 39 data plotted onto MOVES OpMode bins.

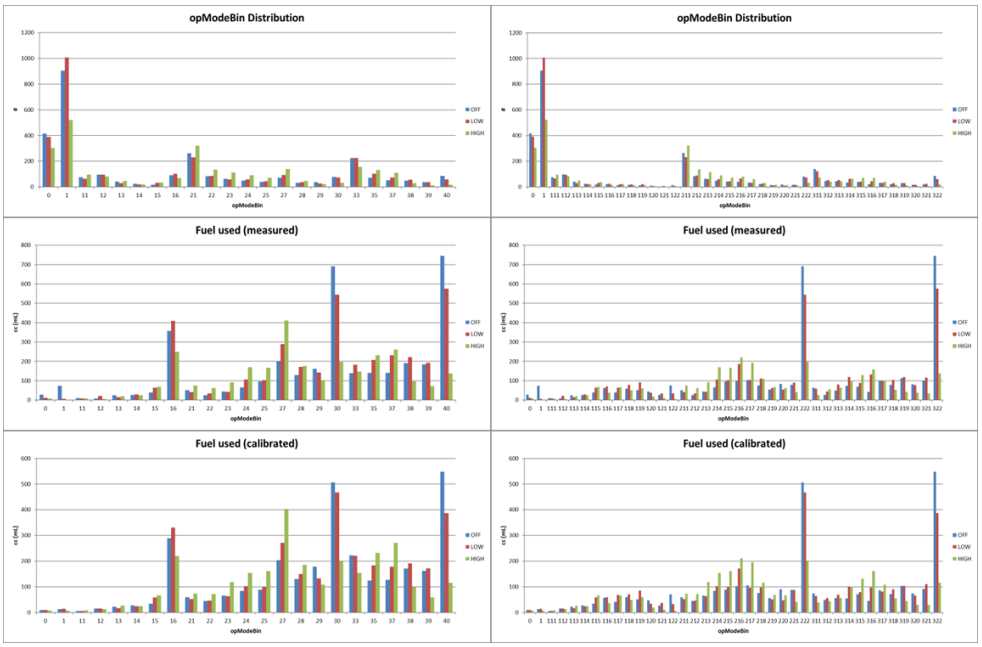

Figure 3.35. Driver 39 data separated into MOVES OpMode bins.

3.5.2.4 Conclusions and Future Work

By comparing several methodologies, we can gain a number of insights not only on the performance of the RFP technology, but also on the strengths and weaknesses of the estimation methodologies.

The RFP technology was designed to encourage drivers to accelerate in a gentler fashion. Section (show correct section) shows the acceleration profile for three drivers, but all drivers had similar results. On average, the drivers' accelerations were reduced when using the RFP technology, resulting in a fuel savings and GHG emissions reduction in the range of 1.5% - 3%

Three estimation methodologies were analyzed in this research: Uncalibrated MOVES, Calibrated MOVES, Calibrated MOVES with Sub-binning, and the AEE method. The direct comparison of the AEE method to the original MOVES results was not fair because the AEE method only considers positive acceleration. In order to make a fair comparison, only acceleration events were considered for both of the MOVES-based methods. During acceleration events, the RFP technology saved fuel consumption by 1.8% for LOW setting and 3.5% for HIGH setting.

On average, MOVES provides results that are similar to the actual fuel savings; however, Table 3.5 shows that for individual drivers MOVES can be off by a significant margin. Using the MOVES model with the default OpMode bins typically under-estimates high power events because OpMode bins can represent a vast range of VSP values, but have the same emission factor for all data points in that bin. Also, the MOVES default bins can under-estimate traffic smoothing effects, see Figure 3.36. A traffic smoothing effect can cause a large amount of data points to shift slightly, but in the MOVES model those data points would remain in the same OpMode bin. In reality, shifting enough data points could change the fuel consumption dramatically, but the MOVES model would not show any change.

Based on what we have seen to date, we have the follow conclusions:

- On average, the MOVES model provides average results that are similar to actual measured fuel savings; however, it is clear that MOVES performance greatly improves when the model is specifically calibrated for the test vehicle.
- It is unclear what is going on with Honda AEE method, particularly with the results of the RFP HIGH mode. We are having further discussions with Honda about their method.
- When the specific vehicle activity patterns are analyzed in detail (for example drivers 6, 12, and 39), we see that the MOVES predictions are sometimes quite a bit off, for a variety of reasons. The potential problems with the MOVES method include:
    - The bin sizes are too large for OpModes within the high emission rates;
    - MOVES typically underestimates energy and emissions of high VSP values, particularly at low speed.
- To address the bin size problem, we have developed a sub-binning method, which tends to increase the sensitivity of the model predictions.

For future work, we will explore further developing the sub-binning version of MOVES to make it more sensitive to small changes in VSP and speed.

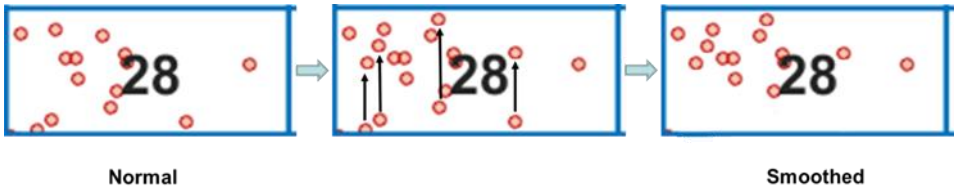

Figure 3.36. Traffic smoothing effect in MOVES OpMode bins.

Chapter 4

Eco-trajectory Planning

This chapter focuses on the eco-trajectory planning optimization component of the ECoTOp system, which plays a crucial role in achieving efficient and safe transportation operations. It encompasses the description and analysis of two field experiments conducted to gather real-world data and insights, followed by a detailed exploration of the eco-trajectory planning optimization methods used within the ECoTOp framework.

The first field experiment aimed to capture and analyze real-world vehicle trajectories and using the data to compare to a binning-based emission estimation model similar to the U.S. Environmental Protection Agency's MOVES model and also to the Comprehensive Modal Emissions Model (CMEM) described in section 3.5.1. Through the deployment of advanced sensing technologies, such as GPS devices and onboard data recorders, a wealth of trajectory data was collected from a set of vehicles in real-world traffic. This section will describe the experiment and eco-trajectory planning algorithm used for the study in section 3.4.3 (put correct section).

The second field experiment focused on comparing the performance of Dedicated Short-Range Communications (DSRC)-based and cellular-based Eco-Approach and Departure (EAD) systems along signalized corridors. The study was conducted in a real-world setting with a variety of vehicles and traffic conditions. The data obtained from this experiment provides valuable insights into the potential benefits and challenges associated with different eco-trajectory planning strategies and control approaches.

Building upon the knowledge gained from the field experiments, the chapter then delves into the eco-trajectory planning optimization methods employed within the ECoTOp algorithm. These methods incorporate a combination of mathematical modeling, optimization algorithms, and

data-driven approaches to determine the optimal vehicle trajectories in response to changing traffic conditions and signal timings.

The chapter concludes by discussing the integration of the vehicle trajectory optimization component within the broader co-optimization framework. It highlights the interactions and coordination between vehicle trajectories and traffic signal timings, emphasizing the need for a holistic approach that simultaneously considers both elements to achieve optimal system-wide performance. The findings and insights gained from this chapter contribute to the development of a comprehensive and effective co-optimization strategy, enabling improved transportation efficiency, reduced congestion, and enhanced mobility in urban environments.

4.1 Field Study for Emission Model Comparison

4.1.1 Experiment Setup

In our experiments, we utilized a test vehicle (2008 Nissan Altima with a 4-cylinder, 2.5-liter engine) that is equipped with EAD enabling hardware. The vehicle has a radar system in front to detect preceding vehicles; it is also equipped with a Savari MobiWAVE MW1000 as a DSRC on-board unit (OBU), a laptop computer with Linux operating system, and a built-in driver-vehicle display. The operating system used on this OBU is Linux.

Figure 4.1 shows the on-board devices and the interaction between them. In Figure 4.1, the radar sends information to the laptop through Kvaser CAN (Controller Area Network) Interface, the OBU receives the SPaT message from the RSU and then sends those to the laptop, and an ELM327 OBD-II to USB cable sends the vehicle operational data to the laptop, including fuel consumption.

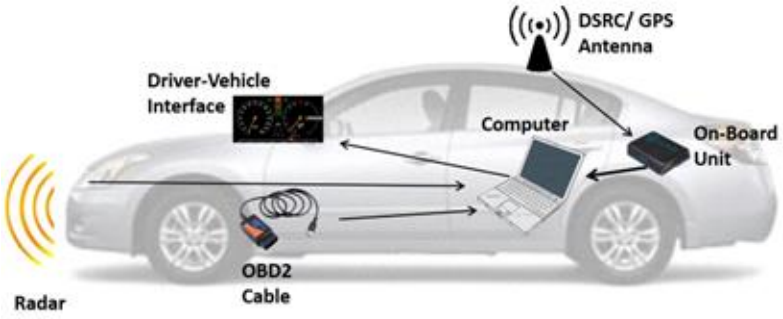

Figure 4.1. Experiment vehicle with on-board devices.

4.1.2 Eco-Approach and Departure for Actuated Signals

The aim of the EAD algorithm used for testing is to reduce the idling time at intersections, and avoid unnecessary accelerations, while also allowing for safe driving.

The signal controllers along the innovation corridor transmit SPaT information, providing a timestamp for the minimum time remaining and maximum time remaining. The traffic signals along the innovation corridor are actuated signals, making it difficult at times to predict the remaining time. For these reasons a variant of the Eco-driving strategy for actuated signals in [29] was employed. Note that in [29], due to the limited field of variables, only minimum time-to-change was provided for the green phase by the RSU, while maximum time-to-change was provided for the red phase. In our experiments, both maximum and minimum time-to-change are utilized.

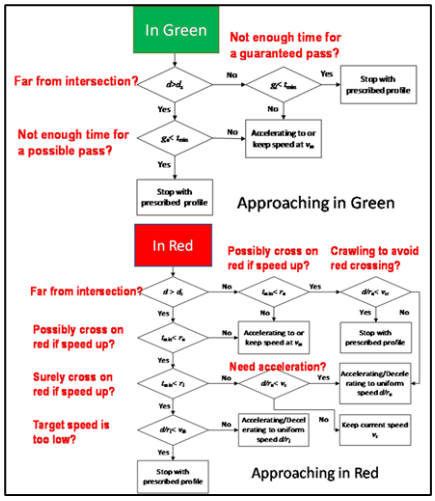

Figure 4.2. Flowchart for eco-approach to intersection.

The flowchart for this EAD algorithm is shown in Figure 4.2. Like other EAD algorithms, the objective is to provide a recommended trajectory that will have the vehicle pass the intersection as the signal turns green. The major difference of this EAD algorithm is that for the red-light case, the maximum time is used in order to check safety and determine if the vehicle needs to accelerate. For the other cases, the minimum time is used as the pivotal measure for planning.

4.1.3 Experiment

The experimental tests were performed along a section of the Innovation Corridor spanning three traffic intersections, indicated by the red box in Figure 3.1. Each test run started 100m east of Iowa Ave. to 100m west of Chicago Ave., then a U-turn was made and then return to 100m east of Iowa Ave. The entire length of each run was 1.38 miles.

For the EAD application, two light-duty vehicles were tested at the same time. One vehicle was employing the EAD application for actuated signals while the other driving normally with traffic. Tests were done between 10:00 am to 12:00 pm and 1:30 pm to 3:30 pm on weekdays.

MOVES uses vehicle specific power (VSP) and vehicle speed data to select emission values from an operation mode (opmode) bin. The MOVES-based binning model utilized in this experiment uses the same approach as MOVES, but the data the values are chosen from were calibrated specifically for the test vehicle.

For CMEM, the model was calibrated specifically for the test vehicle. This means that the readily available parameters, such as mass, engine displacement, the idle speed of the engine, were obtained, and the calibration parameters were derived, as described in [60].

4.2 Comparison of DSRC-based and Cellular-based Eco-Approach and Departure along Signalized Corridors: A Field Study

As part of a collaboration between the City of Riverside and University of California, Riverside, the traffic signal controllers along the Innovation Corridor were upgraded to adhere to SAE connectivity standards, in order to address the infrastructure connectivity issues. As part of this project, intersections were upgraded to support both dedicated short-range communications (DSRC) and cellular-based communications. The research team used resources already available, such as an equipped connected vehicle and their extensive knowledge of the development and deployment of CAV applications, and selected Connected Eco-Approach and Departure for Actuated Signalized Intersections [29] as the target application for a comparative (i.e., before and after) study in order to assess the potential benefits in terms of mobility and environmental sustainability. Environmental sustainability refers to the responsible use and management of natural resources in a way that meets the needs of the present generation without compromising the ability of future generations to meet their own needs.

In this study, field operational tests of various EAD ([72][73]) methods to evaluate the advantages of the infrastructure upgrades on the Riverside Innovation Corridor were conducted. By leveraging Signal Phase and Time (SPaT) data, EAD can optimize vehicle speed and trajectory to minimize stops and reduce travel time, while also improving safety by avoiding last-minute maneuvers.

Signal Phase and Time (SPaT) data [74] is a type of traffic signal information that provides details about the current and upcoming signal phases at an intersection. This data includes information such as the current signal phase (e.g., green, yellow, or red), the time remaining in the current phase, and the timing of the next phase transition. SPaT data is transmitted by connected infrastructure through Dedicated Short-Range Communication (DSRC) or cellular networks, and

can be used by CAVs to anticipate changes in traffic flow and adjust their driving behavior accordingly.

Dedicated Short-Range Communication (DSRC) [75] is a wireless communication technology that enables short-range communication between devices. DSRC is designed specifically for vehicular communication and is commonly used in Intelligent Transportation Systems (ITS). DSRC allows vehicles to communicate with each other and with the infrastructure around them, such as traffic lights, signs, and road sensors. This technology enables the exchange of important information, such as traffic conditions, road hazards, weather, and Signal Phase and Timing (SPaT), which can help drivers make more informed decisions and improve overall road safety. DSRC operates on a frequency band reserved for its use, and its short-range capabilities make it ideal for use in urban environments where there are high levels of congestion and frequent stops. Eco-Approach and Departure (EAD) uses the SPaT received through DSRC to optimize vehicle speeds through the intersection.

Cellular networks can play a crucial role in the deployment of connected and autonomous vehicles (CAVs). With their high bandwidth and low latency, cellular networks can provide the reliable and real-time communication required for CAV applications. CAVs generate massive amounts of data, which must be transmitted and processed quickly to enable safe and efficient driving. Cellular networks offer the capacity and speed needed to transmit this data, as well as the ability to support multiple connections simultaneously [76]. Additionally, cellular networks can enable CAVs to communicate with other vehicles [77], roadside infrastructure [77], and cloud-based services [78], providing greater situational awareness and coordination. As CAV technology continues to evolve, the use of cellular networks is likely to become increasingly important in supporting safe and efficient transportation systems. Cellular networks, like DSRC, can be used to send and receive SPaT data [79].

Connected Eco-Approach and Departure (EAD) application utilizes: 1) the SPaT data, either from DSRC or cellular communication, from the upcoming traffic signals; 2) map and route information (e.g., stop-bar location, road grade, road speed limit, turning movement); and 3) the states and powertrain limitations of the ego-vehicle (e.g., position via GNSS, instantaneous speed, acceleration/deceleration limit), to determine the optimal recommended speed profile that can minimize the target vehicle's energy consumption and tailpipe emissions when approaching to and departing from signalized intersections, without compromising the mobility performance [29]. The EAD program used in this project, in contrast to the majority of other EAD applications now in use, is capable of using the SPaT data from all downstream actuated signalized crossings to calculate the ideal vehicle trajectory for each corridor.

The remainder of this section is organized as follows: a short background of comparisons of DSRC and Cellular technologies. Next a description of the EAD methods tested in this research, including intersection-by-intersection and corridor-wise EAD. Then a description of the field test experiments conducted. Finally, the results are presented followed by a discussion of the results.

4.2.1 Background

DSRC (Dedicated Short-Range Communication) and 4G/LTE (Long-Term Evolution) are two wireless communication technologies that are commonly used for vehicular communication in Intelligent Transportation Systems (ITS). DSRC is a short-range wireless communication protocol that operates in the 5.9 GHz frequency band and is specifically designed for vehicular communication. On the other hand, 4G/LTE is a cellular-based communication technology that operates in the licensed frequency bands, typically in the 700 MHz to 2.6 GHz range.

In recent years, there have been numerous studies comparing the performance of direct I2V-based and cellular-based CAV applications [80],[81],[82]. These studies have investigated the reliability, latency, and throughput of the two technologies in various conditions and have provided

insights into the benefits and limitations of each technology. Understanding the strengths and weaknesses of DSRC and 4G/LTE technologies is crucial for designing effective EAD systems that can improve traffic efficiency and reduce emissions. The performance comparison between Dedicated Short-Range Communication (DSRC)-based and Cellular-based CAV applications has been studied extensively in the literature.

In a study by Xu et al. [80], a field experiment was conducted to compare the performance of DSRC and cellular-based CAV applications, which included Collision Avoidance, Traffic Text Message Broadcast, and Multimedia File Download. The experiment was conducted under different conditions. The results showed that the DSRC-based system had lower communication delay and higher packet delivery ratio, within communication range, compared to the cellular-based system. The authors concluded that a combination of DSRC and cellular-based systems depending on CAV application would work best.

Vinel [81] conducted a study in which analytical frameworks were developed to assess the performance of DSRC and cellular-based on the probability of delivering safety beacons before the deadline. The numerical results of the study indicate that when 50 vehicles are present, the probability of cellular communication is lower than that of DSRC. Specifically, the probability of DSRC was 83%, while the probability of cellular was even lower, which falls below the requirements for typical safety applications.

Similarly, a study by Rayamajhi et al. [82] conducted a field experiment to compare the performance of DSRC and cellular-based communication while driving. The study found that the DSRC-based system had larger average packet loss length and a larger mean burst length, which is the average length of burst packet loss, compared to the cellular-based system. Burst packet loss is when pack loss with more than one packet loss in the sequence occurs. With good line of sight (LOS) reliability for both technologies were similar.

Overall, the literature suggests that DSRC-based CV systems and cellular-based CV systems both have their upsides and downsides. The choice of communication technology may depend on factors such as data latency, packet loses, cost, infrastructure availability, and regulatory requirements.

4.2.2 Methodology

This study aims to evaluate and compare the effectiveness of corridor-wise Eco-Approach and Departure (EAD) and intersection-by-intersection EAD systems in reducing fuel consumption and emissions while improving traffic flow. Fuel consumption and emissions are the metrics being used to evaluate the impact on environmental sustainability. The study was conducted on the Riverside Innovation Corridor with multiple intersections equipped with DSRC and cellular communication.

4.2.2.1 Study Area and Data Collection

The infrastructure on the Riverside Innovation Corridor is continuously being instrumented with different emerging elements to facilitate research in Shared, Electric, Connected and Automated (SECA) transportation systems. In addition to the firmware upgrades of traffic signal controllers that are compatible with the latest version of SAE J2735 standard, three intersections along the Innovation Corridor are capable of broadcasting Signal Phase and Timing (SPaT), and Geographic Intersection Description (GID) or MAP messages via both direct I2V and cellular network communications. These three intersections include (from West to East) Chicago Avenue & University Avenue, Cranford Avenue & University Avenue, and Iowa Avenue & University Avenue, as indicated by red box in Figure 3.1.

4.2.2.2 Eco-Approach and Departure Deployment and Configuration

The EAD systems used in this study were deployed and configured based on their respective communication technologies, namely DSRC and cellular. The DSRC-based EAD system was installed using the V2I communication infrastructure, which included RSUs deployed at the signalized intersections along the study corridor. The cellular-based EAD system used a cellular Wi-Fi hotspot, which communicated with the cloud-based server for signal phase and timing information.

Both EAD systems were configured to provide the recommended speed to approaching vehicles, based on the signal timing and the position of the vehicle. The DSRC-based EAD system was configured to communicate with the on-board DSRC unit installed in the participating vehicles, which enabled vehicle-to-infrastructure (V2I) communication. The cellular-based EAD system was configured to use the cellular data communication for providing the recommended speed to the driver.

The DSRC-based EAD system was configured to operate in the 5.9 GHz frequency band, which is reserved for Intelligent Transportation Systems (ITS) applications. The cellular-based EAD system used the cellular network for communication, and thus had no frequency restrictions. Both systems were configured to operate in compliance with the applicable communication standards and protocols. The configuration parameters of the EAD systems, such as the recommended speed threshold and the distance to the stop bar, were kept consistent across both systems to ensure a fair comparison.

In this section, EAD methods using edge-computing were based on the EAD algorithm as in (3). EAD methods using cloud-computing were based on Hao et al. (12), in which a graph-based trajectory planning algorithm was developed to solve the optimal solution to EAD. In that work, the 3-D input states time-distance-speed (t-D-V) collected by the host vehicle and the vehicle

energy consumption dynamics are fed into the graph model. Using the derived energy model of the vehicle, the optimal speed could be derived using the Dijkstra's algorithm, i.e., $v_{(t+1)} = G(t, D_t, v_t)$. The input-output pairs are collected and used as input to train the random forest model, and the trained model is used as part of the on-line model for real-time computation. In the on-line system, once the vehicle enters the communication zone of the connected signalized intersection. Real-time vehicle states (t-D-V) are collected and fed into the system. First, the CV equipped radar will detect the front vehicle and check whether it is safe to start eco-driving. Then the kinematic equations are used to calculate whether the distance and time are enough to pass the intersection. If any of the two mentioned cases is not satisfied, the system will stop eco-driving and release control to human drivers. Finally, the vehicle states will be fed into the trained random forest model, the optimal speed at time t is calculated and the system will loop into the next timestamp t+1.

4.2.3 Experimental Design

With the infrastructure upgrades mentioned above, multiple EAD algorithms were able to be tested: 1.) DSRC-based communication EAD; and 2.) Cellular-based communication EAD. Compared with DSRC-based communication, the cellular-based communication allows for long communication range with a small sacrifice in communication delay, this would enable corridor-wise EAD algorithms which require long distance communication between the host vehicle and downstream intersection miles away. Then the EAD algorithms can be further classified in this case: 1.) intersection-by-intersection; and 2.) corridor-wise.

DSRC-based communication has to use edge-computing (i.e., EAD algorithms are running on-board) for EAD calculations whereas the cellular-based communication can either use cloud computing (i.e., EAD algorithms are running on the UCR server) or edge-computing by utilizing existing algorithms for DSRCs.

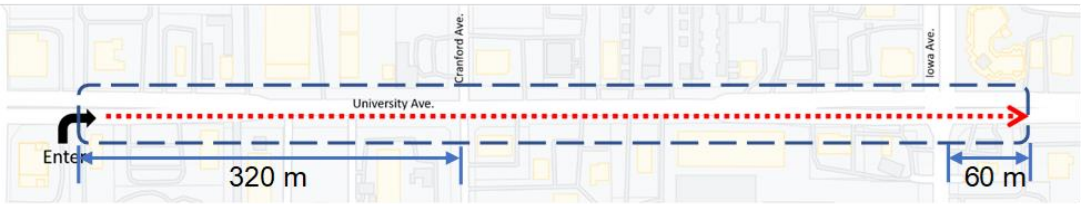

Figure 4.3. Upgraded Intersections along Riverside Innovation Corridor.

To evaluate the system performance under various algorithm/technology combinations, we focused on both mobility in terms of average travel time across the test area as shown in Figure 4.3, and environmental impacts including fuel consumption and emissions of CO_2, CO, HC and NOx which were estimated by the Comprehensive Modal Emission Model (CMEM) (25) previously developed by the research team.

CMEM (Comprehensive Modal Emissions Model) is an emissions and fuel consumption model that estimates the emissions and fuel consumption of vehicles based on their activity (speed and acceleration). The equations used in CMEM are complex and depend on various parameters such as vehicle weight, engine size, fuel type, and driving cycle. The model uses a series of sub-models to estimate the emissions and fuel consumption of different pollutants (such as CO_2, CO, NOx, and particulate matter) and fuel types (such as gasoline and diesel).

CMEM uses the following equations to estimate fuel consumption and emissions for a given vehicle:

$$FR \approx \left(k \cdot N \cdot V + \frac{P}{\eta}\right)\frac{1}{43.5} \cdot (1 + b_1 \cdot (N - N_0)^2) \tag{4.1}$$

$$K = K_0 \cdot \left(1 + C \cdot (N - N_0)\right) \tag{4.2}$$

$$N_0 \approx 30 \cdot \sqrt{\frac{3.0}{V}} \tag{4.3}$$

$$FR_{off} = FR \cdot (1 - f_{Red}) \tag{4.4}$$

$$ECO = a_{CO} \cdot FR + r_{CO} \quad (4.5)$$

$$EHC = a_{HC} \cdot FR + r_{HC} \quad (4.6)$$

$$NO_x = a_{NO} \cdot FR + r_{NO} \quad (4.7)$$

Where:

$FR =$ fuel rate in grams/second;

$P =$ engine power output in kW;

$K =$ engine friction factor;

$N =$ engine speed in revolutions per second;

$V =$ engine displacement in liters;

$\eta =$ measure of indicated efficiency for engine;

b_1 and $C =$ coefficients;

$fh =$ lower heating value of fuel;

$FR_{off} =$ off cycle fuel rate in grams/second;

$f_{Red} =$ fuel use reduction factor associated with off cycle fuel injection timing strategies;

$ECO =$ engine-out emission rate for Carbon Monoxide (CO) in grams/second;

a_{CO} and $r_{CO} =$ CO emission index coefficients;

$EHC =$ engine-out emission rate for Hydrocarbons (HC) in grams/second;

a_{HC} and $r_{HC} =$ HC emission index coefficients;

$NO_x =$ engine-out emission rate for Oxides of Nitrogen (NO_x) in grams/second;

a_{NO} and $r_{NO} = NO_x$ emission index coefficients;

4.2.4 Experiments

4.2.4.1 Eco-Approach and Departure Algorithm Comparison

Field tests were performed using a CAV test vehicle – a Nissan Altima equipped with different EAD algorithms, and a Toyota Corolla serving as the baseline vehicle. Testing was performed eastbound along University Avenue in Riverside, California. Figure 4.3 shows the route taken along University Avenue, mainly covering two intersections: Cranford Avenue & University Avenue, and Iowa Avenue & University Avenue, from 320 meters upstream of Cranford Avenue to 50 meters downstream Iowa Avenue. Two test vehicles enter the corridor at the same time, follow the dashed red line, and drive side-by-side, as shown in the figure. The system architecture for field operational tests is presented in Figure 4.4, where the blue vehicle represents Nissan Altima (i.e., connected vehicle) while the white vehicle represents Toyota Corolla (i.e., legacy vehicle).

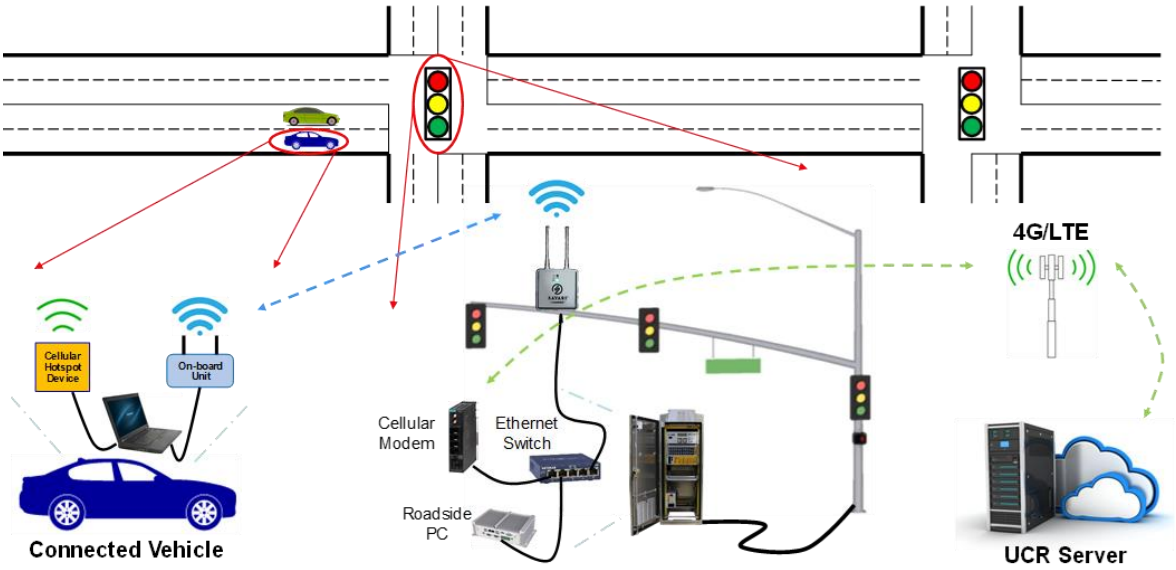

Figure 4.4. System architecture for EAD field operational tests.

Regarding test scenarios, to account for error introduced by the test drivers, two student drivers alternately drove two test vehicles along the inner through lane and outer through lane. The Nissan Altima was equipped with different communication technologies (i.e., DSRC on-board unit or cellular Wi-Fi hotspot) and enabled with different EAD algorithms (i.e., intersection-by-intersection or corridor-wise). In addition, to account for the communication latency, we further differentiated between edge computing and cloud computing.

4.2.4.2 Latency Comparison

In addition to the evaluation of system performance (in terms of mobility and environmental sustainability) of different EAD algorithms, and since the intersections are equipped with both DSRC and cellular communication, the research team was able to perform an experiment to estimate the disparity in communication latencies between DSRC and cellular communications. For the latency test, the test vehicle was driven along the testbed and ran the routine in the same on-board computer to simultaneously record the durations for both DSRC (one-way communication by listening the SPaT messages broadcast from RSUs) and cellular communication (two-way communication by requesting the SPaT messages and reckoning back from the UCR server).

4.2.5 Results

In summary, we tested four combinations of EAD algorithms and technologies:

- Combo 1: DSRC-based, intersection by intersection, edge computing;
- Combo 2: cellular-based, intersection by intersection, edge computing;
- Combo 3: cellular-based, intersection by intersection, cloud computing, but SPaT of the following intersection is masked;
- Combo 4: cellular-based, corridor-wise, cloud computing.

Therefore, the number of scenarios (considering drivers, lanes, and algorithm/technology combinations) are 2 (drivers) × 2 (through lanes) × 4 (combos) = 16 (scenarios). To mitigate the random effects, each scenario is repeated with 5 runs (both vehicles are driving in parallel). So, there are totally 80 runs in the field.

4.2.5.1 Mobility Performance

The mobility performance of the direct I2V and cellular-based EAD systems were evaluated in terms of travel time savings and speed variation.

The results show that both direct I2V and cellular-based EAD systems provided significant travel time savings and queue length reductions compared to the control scenario. However, the cellular-based EAD system outperformed the direct I2V-based EAD system in terms of mobility performance.

The travel time savings achieved by the cellular-based EAD system ranged from -12.8% to 10.7%, while the direct I2V-based EAD system achieved travel time savings ranging from -14% to 6.9%. A negative percentage would be an increase in travel time. The full summary of the statistics for the field tests are shown in Table 4.1.

Overall, the results demonstrate that both direct I2V and cellular-based EAD systems have the potential to significantly improve mobility performance at signalized intersections. However, the cellular-based EAD system outperformed the direct I2V-based EAD system in terms of travel time savings, particularly the corridor-wise EAD system (Combo 4).

4.2.5.2 Environment

The Eco-Approach and Departure (EAD) system aims to improve the environment by reducing fuel consumption and emissions. In this study, we evaluated the environmental impacts of DSRC-based and cellular-based EAD systems along signalized corridors.

Table 4.1. Summary of Key Statistics on Improvement for Field Operational Tests Using Different Combinations of Algorithm/Communication Technology

Combo	Lane	Statistics	Travel Time	Fuel	CO_2	CO	HC	NOx
1	Inner	Mean	6.9%	15.6%	15.5%	32.1%	-7.3%	29.0%
		STD	0.19	0.17	0.17	0.16	0.26	0.15
	Outer	Mean	-14.0%	9.5%	9.4%	26.7%	-33.6%	27.3%
		STD	0.27	0.25	0.25	0.41	0.29	0.30
	Overall	Mean	-3.5%	12.5%	12.5%	29.4%	-20.5%	28.1%
		STD	0.23	0.21	0.21	0.29	0.28	0.23
2	Inner	Mean	-4.6%	15.3%	15.2%	27.4%	-13.3%	23.8%
		STD	0.05	0.09	0.09	0.18	0.10	0.19
	Outer	Mean	-12.8%	13.0%	12.9%	24.6%	-12.9%	25.3%
		STD	0.33	0.22	0.22	0.46	0.30	0.36
	Overall	Mean	-8.7%	14.1%	14.1%	26.0%	-13.1%	24.5%
		STD	0.19	0.15	0.15	0.32	0.20	0.27
3	Inner	Mean	-5.4%	8.8%	8.8%	17.2%	-22.5%	17.2%
		STD	0.05	0.08	0.08	0.19	0.14	0.17
	Outer	Mean	2.4%	22.1%	22.0%	44.1%	-10.1%	40.2%
		STD	0.06	0.07	0.07	0.12	0.16	0.11
	Overall	Mean	-1.5%	15.5%	15.4%	***30.6%***	-16.3%	***28.7%***
		STD	***0.06***	***0.07***	***0.07***	***0.15***	***0.15***	***0.14***
4	Inner	Mean	10.7%	19.6%	19.6%	22.5%	4.0%	21.2%
		STD	0.29	0.19	0.19	0.18	0.34	0.15
	Outer	Mean	2.0%	11.6%	11.6%	16.0%	-7.8%	16.2%
		STD	0.03	0.10	0.10	0.25	0.11	0.21
	Overall	Mean	***6.3%***	***15.6%***	***15.6%***	19.3%	***-1.9%***	18.7%
		STD	0.16	0.15	0.14	0.22	0.23	0.18

The results showed that the cellular-based EAD system had lower fuel consumption and emissions compared to the DSRC-based EAD system. The average fuel consumption reduction was 12.5% for DSRC-based EAD compared to the baseline case without EAD, while it was 15.6% for cellular-based EAD. Similarly, the average reduction in CO_2, CO, HC, and NOx, emissions were 12.5%, 29.4%, -20.5%, and 28.1% for DSRC-based EAD, and up to 15.6%, 30.6%, -1.9%, and 28.7% for cellular-based EAD, respectively.

Table 4.1 summarizes the major results in terms of percentage improvement of different "Combos" over the baseline scenarios. As can be observed from the table, the developed EAD

algorithms for actuated signals can provide significant environmental benefits, with either DSRC or cellular networks. The corridor-wise EAD algorithm (i.e., "Combo 4") outperforms other combos in terms of mobility (travel time savings), fuel consumption, as well as CO_2 and HC emissions. The experiment results shows that the SPaT information from the downstream intersections along the corridor would provide additional travel speed and fuel consumption benefit as the vehicle can forecast the potential SPaT change from farside signals and make response according ahead of time. Especially for the intersections that are closely spaced, the SPaT information for the corridor is helpful in developing the optimal strategy.

These results suggest that Cellular-based EAD systems have a slightly better environmental performance than DSRC-based EAD systems. However, further research is needed to confirm these findings and to explore the potential of these technologies to reduce emissions and fuel consumption in different driving conditions and traffic scenarios.

4.2.5.3 Latency Comparison

In this study, we also evaluated the latency and communication range of the DSRC and cellular-based communication technologies. The latency of the communication system was measured as the time difference between the moment when the traffic signal controller sends the signal phase and timing information and the moment when the equipped vehicle receives this information.

Table 4.2 summarizes the key statistics of communication latencies for both DSRC and cellular communications. As can be observed from the table, the average latency of DSRC-enabled scenarios may well keep under 0.1 second while that of cellular-based communications may vary from 0.13 to 0.26 second on average. The standard deviation of communication latency for DSRC is much smaller (reduced by the range of 74.7% – 85.6%) than that of cellular network. However, based on the field operation test results, shown in Table 4.1, the latency of cellular network does

not result in negative effects on the target connected EAD application. A hypothesis is that the tested connected vehicle application (i.e., connected Eco-Approach and Departure) is intended for safety-critical scenarios (in the optimization), and a human driver may well tolerate such latency when following the driving guidance.

Table 4.2. Summary of key statistics on latency tests.

Test Run Index	No. of Samples	DSRC (μ sec[a])		Cellular[b] (μ sec)	
		Mean	STD[c]	Mean	STD
1	6	36,457	5,701	131,933	23,628
2	92	51,717	27,247	184,059	107,857
3	15	72,749	25,633	259,401	178,378
4	80	49,442	22,918	175,802	128,575

4.2.6 Conclusions and Future Work

The field study comparison of direct I2V-based and cellular-based Eco-Approach and Departure along signalized corridors contributed to the understanding of the effectiveness of each communication technology in terms of mobility, environment, and communication performance. The study demonstrated that both direct I2V and cellular-based technologies are capable of supporting Eco-Approach and Departure applications. direct I2V-based Eco-Approach and Departure demonstrated superior performance in terms of latency, while cellular-based Eco-Approach and Departure demonstrated superior performance in terms of mobility and fuel consumption.

The study also highlighted the importance of considering the trade-offs between communication range, latency, mobility, and environmental performance when selecting a communication technology for Eco-Approach and Departure applications. This research can help transportation agencies and researchers to make informed decisions about the selection of communication technologies for future Eco-Approach and Departure applications.

Further analysis demonstrates that from an environmental standpoint, cellular-based EAD applications perform better than the direct I2V-based method (e.g., Combo 2 vs. Combo 1). The direct I2V short communication range and the non-line-of-sight (NLOS) problem, caused by structures and trees that may affect the direct I2V wireless channel by causing radio signal reflections and diffraction, are some possible causes for direct I2V poor results. Another finding is that runs on the inner through lane tend to be more fluid than runs on the outside through lane. This discrepancy might be caused by the congestion level at the lane-level, where the outer lane is connected to the on-ramp of the I-215 South freeway and encounters significantly more frequent interruptions throughout the test duration

Regarding future work, the direct I2V and cellular-based communication technologies have their own advantages and limitations, and the study only compared their performances in a specific context. More research is needed to explore their performance in different traffic scenarios and road networks.

Secondly, the study did not consider the impact of weather conditions, road surface conditions, and vehicle speed on the performance of the Eco-Approach and Departure system. Future studies could investigate these factors to provide a more comprehensive understanding of the system's performance.

Lastly, the study only focused on the performance of the Eco-Approach and Departure system in terms of mobility, environmental impact, and communication latency. Future research could investigate other aspects such as the user experience, safety, and cost-effectiveness of the system.

4.3 ECoTOp: Eco-Trajectory Planning Module

The proposed ECoTOp system comprises of two major modules: the traffic signal optimization module and the eco-trajectory planning module. This section presents the mathematical formulations the eco-trajectory planning module.

4.3.1 Problem Formulation

The eco-trajectory planning module in our proposed system builds upon previous work on connected eco-driving strategies ([30],[31]). Specifically, time is discretized into fixed time steps (Δt) and denote T as the total number of time steps. The goal of the connected eco-trajectory planning problem is to minimize the total energy consumption of the vehicle across all time steps. By minimizing energy consumption while complying with various constraints, our proposed eco-trajectory planning module helps reduce fuel consumption and emissions, while improving overall vehicle efficiency.

We formulate the problem as:

$$\min_{a_0, a_1, \ldots a_T} \sum_{t=0}^{T} P(v_t, a_t)\, \Delta t \tag{4.8}$$

Subject to:

$$\sum_{t=0}^{T} v_t = X \tag{4.9}$$

$$v_t = v_{t-1} + a_{t-1}, \forall\, t \in [1, T] \tag{4.10}$$

$$a_{min} \leq a_t \leq a_{max} \tag{4.11}$$

$$0 \leq v_t \leq v_l \tag{4.12}$$

$$v_0 = v_s, v_T = v_d \tag{4.13}$$

Where:

v_t denotes the speed of the vehicle at time step t.

a_t denotes the acceleration rate of the vehicle at time step t.

$P(v_t, a_t)$ represents the energy cost associated with the vehicle's state at a given time step.

v_l denotes the speed limit.

X denotes the total travel distance.

v_d denotes the target speed.

We can transform the model presented in (4.8) into a graph-based model, where each node is represented by a unique 3-D coordinate (t, x, v) that describes the dynamic state of the vehicle. Solving this model for each time step provides the optimal speed (or acceleration) for the driver or vehicle controller to follow. By transforming the model into a graph-based representation, we can effectively capture the dynamic behavior of the vehicle and make informed decisions that optimize speed and energy efficiency, while adhering to various constraints. A machine learning-based trajectory planning algorithm (MLTPA) ([31]) then uses the graph-based model to create a pool of optimal trajectories and predicts the next target state of the vehicle.

4.3.2 Solution Algorithm

The eco-trajectory optimization problem is solved using dynamic programming approach, which is commonly used for solving optimal control problems. The dynamic programming algorithm generates an optimal control sequence by recursively solving a sequence of smaller sub-problems. The approach used in this research is based on the work of Hao et al. ([30]) and is known as a machine learning trajectory planning algorithm (MLTPA). Following offline training, MLTPA is implemented online to ensure optimal energy and computation efficiency.

The algorithm works as follows:

Offline:

1. Data Generation: Prior to starting simulations, MLTPA utilizes a graph-based trajectory planning algorithm (GBTPA) for EAD application to generate training data on a representative dataset of unique inputs.
2. Training: The training data is then used to train MLTPA to predict the next target state of the vehicle.

Online

3. Initialization: The algorithm is initialized at the start of each simulation episode. At the beginning of each time step, the algorithm generates a set of candidate control inputs for each vehicle, based on the vehicle's current state and the state of the traffic signal.
4. Target: A target state is set, which consists of the expected time, location (e.g., stop line), and speed so that the vehicle will safely pass the stop line.
5. Control Policy Determination: The algorithm generates the optimal control policy, which is the control input that corresponds to the minimum expected total cost at each time step.

The dynamic programming approach is well suited for vehicle trajectory optimization, as it allows for the consideration of complex driving scenarios, such as merging and lane changing, while still ensuring that the resulting trajectory is optimal ([39][83][84]).

4.3.3 Solution Method

The solution method for the eco-trajectory optimization problem is a key component of the ECoTOp framework. In this section, we present a description of the solution method used for solving the eco-trajectory optimization problem.

The input variables are scaled using the MinMaxScaler function, and the optimal vehicle acceleration is predicted using a Regressor function that employs the random forest algorithm, both created using MATLAB. These functions are then compiled into content-obscured, executable P-code files for use in the Python programming environment. Python is the programming language of choice for the simulation experiments conducted in the SUMO traffic simulation platform.

A Min-Max Scaler is a type of data preprocessing technique commonly used in machine learning to scale and normalize the input features in a dataset. The goal of normalization is to ensure that all input features are on the same scale, so that no feature dominates or biases the model training. This is important because many machine learning algorithms use distance measures between data points to identify patterns, and when features are on different scales, the distance measures may be dominated by features with larger values [85].

The Min-Max Scaler scales the features to a specified range, typically between 0 and 1, based on the minimum and maximum values of each feature in the dataset. This ensures that all features have the same range and preserves the shape of the original distribution.

Min-Max Scaler is preferred over other normalization techniques, such as StandardScaler, when the input features have a bounded minimum and maximum values or when there are outliers in the data that need to be preserved [86].

Random forest is an ensemble learning method that combines multiple decision trees to make predictions. In a regression context, a random forest model predicts a continuous dependent variable based on a set of input features [87].

During training, each decision tree in the random forest is constructed using a subset of the training data and a random subset of the input features. During prediction, the random forest algorithm aggregates the predictions of all the decision trees in the ensemble to produce the final prediction for a given input.

Overall, the MLTPA algorithm provides an efficient and effective solution method for the vehicle eco-trajectory planning optimization problem in the ECoTOp framework, which results in improved traffic efficiency and reduced travel time for vehicles in the network.

Chapter 5

Traffic Signal Optimization Module

This chapter focuses on the crucial aspect of traffic signal optimization within the ECoTOp framework for enhanced transportation efficiency. Traffic signal optimization plays a vital role in improving traffic flow, reducing congestion, and enhancing overall transportation performance. By strategically adjusting signal timings and coordination at signalized intersections, it aims to maximize throughput and optimize the progression of vehicles through the road network. By leveraging the findings and methodologies from the literature, we lay the groundwork for the seamless integration of traffic signal optimization with vehicle eco-trajectory planning, creating a synergistic approach that maximizes transportation efficiency and minimizes emission output.

5.1 Problem Formulation

The signal optimization module of the ECoTOp system is based on three basic assumptions that ensure a reliable level of trajectory planning for connected autonomous vehicles (CAVs) and align with common driving practices of human drivers. These assumptions include a constant cycle length (C), identical phase orders in every cycle, and equal phase durations for corresponding phases in the upper and lower rings of the phase diagram. Additionally, signal optimization is performed at the beginning of each cycle and remains unchanged throughout that cycle. Based on these assumptions, we propose a scenario for an isolated signalized intersection that can receive real-time locations from all proximate CAVs and detect the locations of non-connected vehicles through the use of roadside sensors. This approach provides a reliable solution for facilitating smooth and efficient traffic flow at signalized intersections (e.g., cameras similar to [40]).

We then formulate the optimization problem which aims to maximize the throughput from all phases in the cycle, while minimizing the variance of oversaturated vehicle number from all phases to ensure fairness, as follows:

$$\max_{G_i} z = w_1 * \frac{1}{k}\sum_{i=1}^{k} N_i - w_2 * \frac{1}{k}\sum_{i=1}^{k}(N_i - M_i)^2 \tag{5.1}$$

Subject to:

$$\sum_{i=1}^{k} G_i = C - \sum_{i=1}^{k} Y_{ii} \tag{5.2}$$

$$N_i \geq N_{i,j}, \qquad \forall i,j \tag{5.3}$$

$$M_i = G_i * \frac{1}{h}, \qquad \forall i \tag{5.4}$$

$$N_{i,j} = \text{count}_{i,j}(X_{i,j}), \qquad \forall i,j \tag{5.5}$$

$$X_{i,j} = v * \left(G_i + \sum_{ii=1}^{i-1} G_{ii} + Y_{ii} \right) \quad \forall i,j \tag{5.6}$$

Where:

$N_{i,j}$ denotes the total number of vehicles that need to be serviced in each lane within the detection zone for lane j in phase i.

N_i denotes the max of $N_{i,j}$ among all associated lanes in phase i.

M_i denotes the discharge capacity per lane in phase i, and calculated as $M_i = G_i * \frac{1}{h}$.

G_i denotes the green time of phase i.

h is the saturated time headway in the discharge process.

$N_i - M_i$ is the expected maximum number of oversaturated vehicles in phase i.

$\text{count}_{i,j}(X_{i,j})$ denotes a function defined as the current number of vehicles at lane j of phase i measured from the stop line to $X_{i,j}$ in the upstream.

5.2 Signal Model

The traffic signal model used in the traffic signal optimization for ECoTOp system is crucial in accurately representing the behavior and performance of the signal system in the simulation. In this section, we describe the traffic signal model used in our optimization problem.

We consider a fixed-time signal control system, where the signal phases and their durations are pre-determined for each cycle. The signal cycle length is denoted by C, and the durations of the green, yellow, and red phases of each signal phase are denoted by G_i, Y_i, and R_i, respectively, where i is the index of the signal phase. Figure 5.1a illustrates key variables in an example intersection. Figure 5.1b shows the direction for each signal phase.

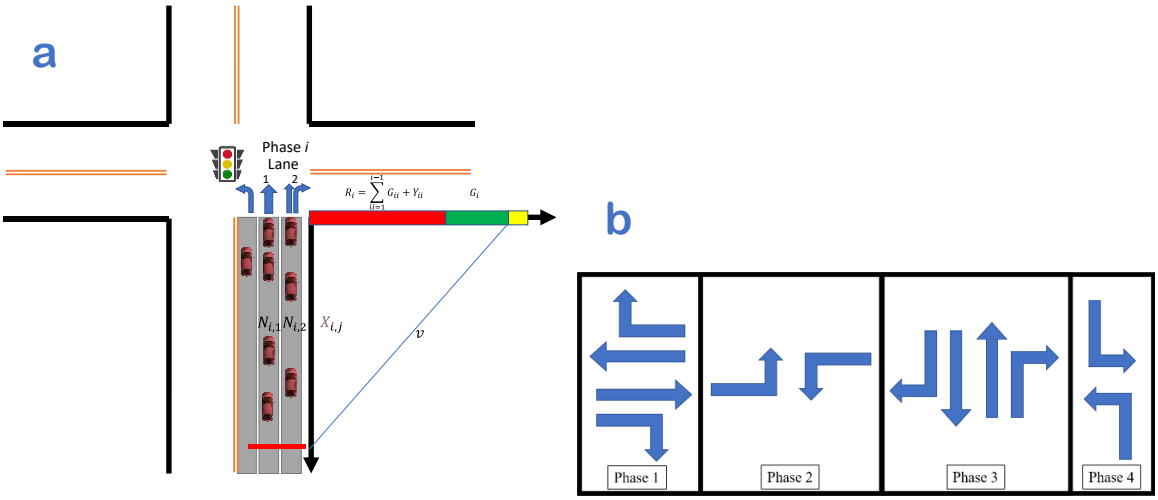

Figure 5.1. Key variables and phases for example intersection.

5.3 Solution Algorithm

At the start of each cycle, the proposed Traffic Signal Optimization module of the ECoTOp system obtains the total number of vehicles that need to be serviced in each lane within the detection zone, denoted by $N_{i,j}$ for lane j in phase i. We then calculate N_i as the maximum value of $N_{i,j}$ among all associated lanes in phase i. This value is used to represent the number of vehicles that need to be serviced in phase i during the optimization process. Note that only vehicles that reach the stop line before the end of phase i are included in the calculation of N_i. Assuming that the green time for phase i is G_i, and the yellow and all-red time after phase i is G_d, $N_{i,j}$ is determined based on the number of vehicles along the distance from the stop line of lane j of phase i to $X_{i,j}$ upstream.

To solve the optimization problem (5.1) for Traffic Signal Optimization module, the sequential least squares programming (SLSQP) algorithm [88] is employed. The SLSQP is a good choice for optimization in the traffic signal optimization due to several reasons. Firstly, SLSQP is well-suited for nonlinear optimization problems with inequality and equality constraints [89], which is exactly the case for this optimization problem. In this problem, the objective is to maximize throughput of the intersection and minimize the variance of oversaturated vehicles from all phases subject to constraints such as signal timing, lane capacity, and number of oversaturated vehicles.

Secondly, SLSQP is a gradient-based method that is efficient and robust for high-dimensional optimization problems [90][91][92]. This is beneficial for the overall ECoTOp problem as it involves optimizing the signal timing and vehicle trajectory simultaneously, resulting in a high-dimensional optimization problem.

Lastly, SLSQP is a well-established optimization algorithm, and many software packages provide SLSQP solvers, such as SciPy in Python [93], which makes it widely accessible. The SciPy Python package is used in this algorithm.

Chapter 6

Eco-friendly Cooperative Traffic Optimization (ECoTOp)

This chapter presents the core of the ECoTOp framework, which combines vehicle eco-trajectory planning optimization and traffic signal optimization to achieve enhanced transportation performance at isolated signalized intersections. Building upon the preceding chapters on vehicle eco-trajectory planning and traffic signal optimization, this chapter integrates the two components to develop a comprehensive co-optimization approach. The ECoTOp framework not only enhances transportation performance at isolated signalized intersections but also serves as a foundational approach for dynamically selecting the most suitable optimization strategy based on real-time traffic conditions and environmental considerations.

The primary objective of this chapter is to showcase the effectiveness and potential of the co-optimization approach in improving transportation efficiency, reducing congestion, and enhancing overall system performance. By combining vehicle trajectory optimization and traffic signal timing optimization, synergistic benefits can be achieved.

Throughout this chapter, we delve into the methodologies, algorithms, and models used in the co-optimization process. The solution algorithm is developed to iteratively optimize the trajectories and signal timings, aiming to achieve an optimal balance between individual vehicle performance and overall traffic flow efficiency.

A series of simulation experiments are conducted to evaluate the performance of the co-optimization approach in various scenarios, and compare the results to the individual modules. These experiments consider different penetration rates of connected and automated vehicles

(CAVs). Performance metrics such as throughput and emissions are analyzed to assess the effectiveness of the co-optimization approach.

Furthermore, the safety implications of the co-optimization approach are evaluated using advanced models and simulation techniques. By leveraging the Surrogate Safety Assessment Model (SSAM), potential crash risks and safety improvements associated with the co-optimization strategy are assessed, providing valuable insights into its safety performance.

By introducing the co-optimization approach, evaluating its results, and comparing them to the outcomes of the individual modules, this chapter not only contributes to the advancement of transportation research and practice but also establishes the foundation for future development of an adaptive optimization strategy. The findings highlight the potential of integrating vehicle eco-trajectory planning and traffic signal timing optimization and serve as a stepping stone towards the development of a dynamic optimization framework capable of adapting to real-time traffic conditions and environmental factors. These insights will guide transportation professionals, policymakers, and researchers in designing future strategies and policies for the efficient co-optimization of eco-trajectory planning and traffic signals.

6.1 Eco-friendly Cooperative Traffic Optimization (ECoTOp) at Signalized Intersections: Paving the Way for an Adaptive Optimization Strategy

Traffic congestion at signalized intersections is a major problem in urban areas, leading to increased travel time, fuel consumption, and emissions, as well as decreased safety and mobility [18]. Traffic signals are one of the most common methods used to control the flow of vehicles at intersections, but they are typically designed based on fixed time or actuated control strategies that do not consider the dynamic interactions between vehicles and traffic signals [94]. As a result, the timing and sequencing of signal phases may not be optimized for the prevailing traffic conditions, leading to inefficiencies, delays, and congestion.

Co-optimization of vehicle trajectories and traffic signal timing has emerged as a promising approach to address these issues, by jointly optimizing the timing and sequencing of signal phases and the trajectories of vehicles passing through the intersection. This approach leverages advances in connected and automated vehicle (CAV) technologies, which enable vehicles to communicate with each other and with the traffic signal system in real-time, and to adjust their speed and trajectory to optimize their performance under the prevailing traffic conditions [95][96][77].

The motivation for co-optimization lies in its potential to significantly improve the efficiency, safety, and sustainability of traffic operations at signalized intersections. By coordinating the timing and sequencing of signal phases with the trajectories of vehicles, the co-optimization approach can reduce fuel consumption, and emissions, while also improving safety and mobility. Moreover, the co-optimization approach can adapt to changing traffic conditions, such as fluctuations in traffic demand, non-recurrent incidents, and weather events, to ensure optimal performance at all times.

Despite the potential benefits of co-optimization, there are still several challenges that need to be addressed, such as the development of efficient and effective optimization algorithms, the integration of CAV technologies with the traffic signal system, and the evaluation of the safety and effectiveness of the co-optimization approach under different traffic scenarios. In this chapter, we address these challenges by presenting the ECoTOp approach, and by evaluating its performance through simulations using the SUMO traffic simulation platform [97].

6.1.1 Research Objectives

The main objective of this section is to propose a co-optimization approach for vehicle trajectories and traffic signal timing at isolated signalized intersections, and to evaluate its effectiveness compared to vehicle trajectory and traffic signal timing optimization methods. Specifically, we aim to achieve the following research objectives:

1. To develop a hybrid co-optimization approach that combines model-based and data-driven methods, and that uses connected and automated vehicle (CAV) technologies to improve the accuracy and efficiency of the optimization process.
2. To evaluate the effectiveness of the proposed approach against vehicle trajectory optimization alone and traffic signal timing optimization alone, in terms of travel time, fuel consumption, emissions, and other performance measures, using simulations in the SUMO traffic simulation platform.
3. To evaluate the safety of the proposed approach using the Surrogate Safety Assessment Model (SSAM) [98], which is a widely-used tool for predicting crash risk at signalized intersections.
4. To perform sensitivity analyses to examine the effects of various factors, such as CAV penetration rates, and traffic volumes, on the performance and safety of the proposed approach in order to show that dynamically changing approaches may be a needed based on varying traffic conditions.

The contributions of this section are twofold. First, we propose a novel hybrid co-optimization approach that combines the strengths of both model-based and data-driven methods, and that leverages CAV technologies to improve the accuracy and efficiency of the optimization process. Second, we evaluate the performance and safety of the proposed approach compared to baseline scenarios of vehicle trajectory optimization and traffic signal timing optimization alone, using simulations and the SSAM model, providing insights into its potential for improving transportation efficiency and sustainability. These contributions can help inform the development of more efficient and sustainable transportation systems, and can also provide a basis for further research in this area.

6.1.2 Methodology

6.1.2.1 Combined Optimization Problem

The proposed ECoTOp system comprises of two major modules: the traffic signal optimization module and the eco-trajectory planning module. These modules are designed to interact with each other but often have inherent conflicts when pursuing their own optimization goals. The traffic signal optimization module seeks reliable information from incoming vehicles, including current dynamic state and future movement, as early as possible. It also requires the flexibility to adjust the signal timing plan at any time to adapt to the dynamic traffic conditions. On the other hand, the eco-trajectory planning module requires reliable signal timing information ahead of time to plan trajectories that can save fuels and reduce emissions. However, vehicles operating under the eco-trajectory plan still require some flexibility in operation to improve safety, mobility, and energy performance in certain situations, such as emergency braking and lane changing. It is not feasible to create an ideal co-optimized system in an isolated intersection with mixed traffic due to two main reasons. Firstly, unconnected vehicles with human drivers have diverse and personalized driving styles, which can be an unpredictable factor in the system. Secondly, the limitations in sensing, communication, and control make it impossible to predict the time and state when each vehicle enters the system, even for connected autonomous vehicles (CAVs). Figure 6.1 shows the conflict between the signal optimization module and the eco-trajectory planning module. In a mixed traffic environment, each module must make trade-offs to achieve an integrated optimization. This section presents the method for interaction between the two modules.

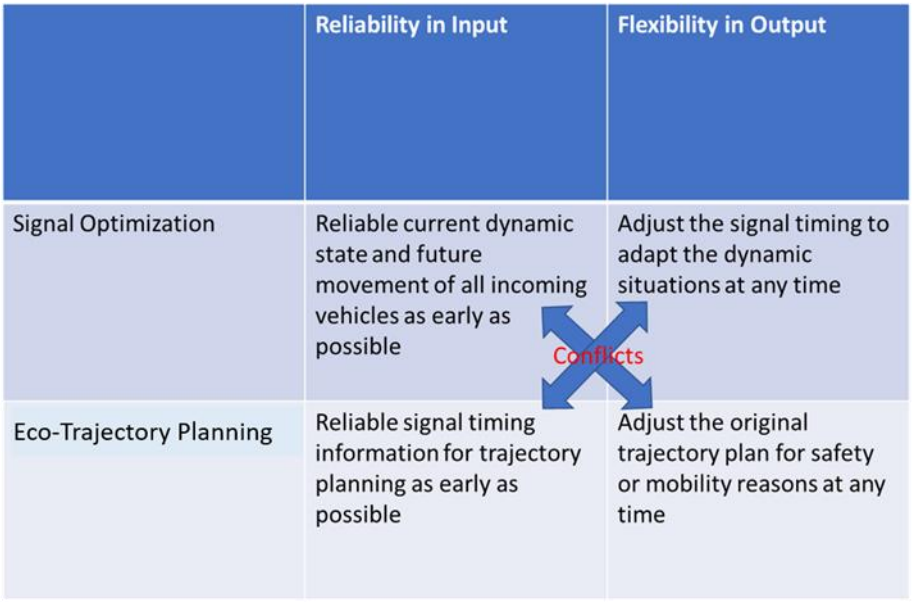

Figure 6.1. Conflict between signal optimization and eco-trajectory planning.

6.1.2.2 Solution Algorithm

The ECoTOp system achieves the co-optimization of signal control and vehicle trajectory by following the flowchart depicted in Figure 6.2. The ECoTOp system works as follows for the co-optimization of signal control and vehicle trajectory:

1. Count the number of vehicles for each lane in the network within the communication range.
2. Count the number of vehicles that can be served within the current green time for each lane.
3. Use the counts to get the time required for the delayed vehicles controlled by the phase for that lane to pass through the intersection and also the time required for maximum throughput.
4. Put this information into a Sequential Least Squares Programming (SLSQP) optimizer to obtain the new phase times.
5. Each connected and autonomous vehicle (CAV) receives the Signal Phase and Timing (SPaT) information and queue information.

6. Use the queue information to possibly change lanes and add a queue buffer to timing.
7. Send the new time and the current vehicle velocity to a Random Forest-based trajectory optimizer to obtain the new trajectory.
8. Finally, update the signal controller for real-time control with the optimal phase timing obtained from the SLSQP optimizer.

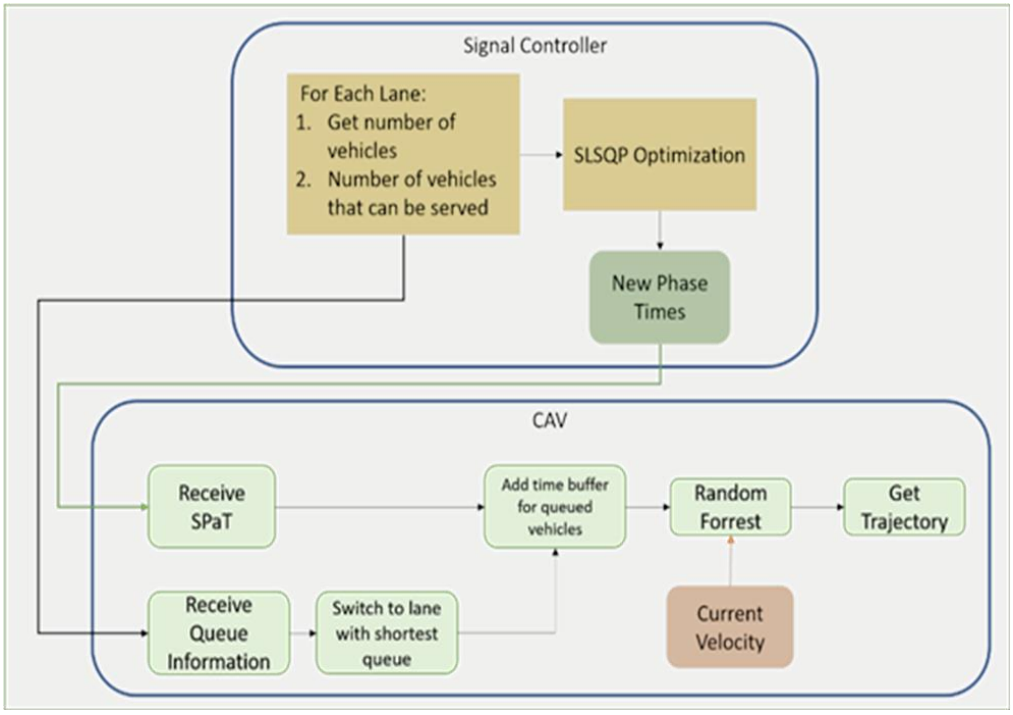

Figure 6.2. ECoTOp algorithm flowchart for traffic simulation.

In the intricacies of the ECoTOp algorithm, it's imperative to highlight the dynamic nature of our approach. The Eco-Trajectory Planning module operates at a high frequency, precisely at every time step, which for the simulations presented here is at a rate of 10 Hz. This rapid calculation ensures that the trajectory adjustments align seamlessly with real-time traffic conditions, thereby enhancing vehicle movement and energy efficiency. In contrast, the Traffic Signal Optimization module is executed at a distinct phase, occurring at the culmination of the previous cycle during a

dedicated 2-second all-red phase. This deliberate timing allows for the assimilation of the latest trajectory data and optimal signal timing strategies, culminating in a harmonious orchestration that bolsters the overall efficacy of our ECoTOp framework.

6.1.3 Case Study

The Case Study section presents a comprehensive analysis of the ECoTOp system. In this section, we describe the simulation setup used to model the intersection and the vehicles' behavior. We also present the results of simulation-based experiments that evaluate the performance of our proposed ECoTOp system, and compare it with three baseline scenarios: a fixed-timed traffic signal with no optimization, the eco-trajectory planning module, and traffic signal optimization module. The experimental results section provides a preview of the key findings, which demonstrate significant improvements in intersection performance through the proposed approach. The insights gained from this study have the potential to inform policy and decision-making in the transportation sector and contribute to the development of smarter and more efficient transportation systems.

6.1.3.1 Simulation Setup

To evaluate the effectiveness of the proposed ECoTOp approach, a simulation study was conducted using the SUMO traffic simulation software. The simulation was set up to replicate a typical isolated signalized intersection, with four approaches controlled by fixed-time traffic signals. The intersection layout consisted of two through lanes and one or two left-turn lanes in each approach, with a shared left-turn lane for opposing directions. The signal cycle length was set to 66 seconds, with a 4-second yellow interval and 2-second all-red interval after phases 1 and 2, and a 2-second all-red interval after phases 3 and 4. The traffic signal optimization is done during the second all-red interval.

In the simulation setup, the car following model used is the Intelligent Driver Model (IDM) developed by Treiber et al. [99]. The IDM model is widely used in traffic simulation studies and is based on the principle of maintaining a safe distance between vehicles while accounting for acceleration and deceleration. IDM uses equations (6.1) and (6.2) to model car following behavior.

$$\dot{v}_\alpha = a\left[1 - \left(\frac{v_\alpha}{v_0}\right)^\delta - \left(\frac{s^*(v_\alpha, \Delta v_\alpha)}{s_\alpha}\right)^2\right] \tag{6.1}$$

$$s^*(v, \Delta v) = {s_0}^\alpha + T^\alpha v_\alpha + \frac{v_\alpha \Delta v_\alpha}{2\sqrt{a^\alpha b^\alpha}} \tag{6.2}$$

Where:

α is the vehicle.

v_a is velocity.

$a = 0.73\frac{m}{s^2}$ is maximum acceleration. $b = 1.67\frac{m}{s^2}$ is the desired deceleration.

$v_0 = 16\frac{m}{s}$ is desired velocity.

$\delta = 4$ is the acceleration exponent.

$s_\alpha = \Delta x_\alpha - L$ is the actual gap. L=5m is the length of the vehicle. $\Delta x_\alpha = x_{\alpha-1} - x_\alpha$ is the position difference.

s^* is the desired gap.

$s_0 = 2m$ is jam distance.

$T = 1.6s$ is the safe time headway.

$\Delta v_\alpha = v_{\alpha-1} - v_\alpha$ is the velocity difference.

CAVs out of range for the ECo-TOp algorithm also use the IDM model for car following. This ensures that the simulation accurately represents real-world traffic scenarios where not all vehicles are equipped with CAV technology. The traffic demand is taken from real-world data from an intersection camera system on a similar real-world intersection.

To evaluate the safety performance of the different optimization strategies, the Safety Summation Analysis Method (SSAM) was employed. SSAM is a widely used safety evaluation tool that takes into account the frequency and severity of conflicts between vehicles ([100][101][102] [103][104]). In this study, the number of conflicts between vehicles was counted and analyzed for each simulation run.

The simulation was run for a total of 60 minutes for each optimization strategy, with a warm-up period of 5 minutes to allow for stabilization of traffic flow. Each simulation run was repeated ten times to ensure statistical accuracy. The simulation results were then analyzed to compare the safety and traffic performance of the different optimization strategies.

The performance metrics used in this study include the intersection throughput, Carbon Dioxide (CO_2) output, and safety performance, mentioned above. Throughput is defined here as the number of vehicles that traverse the intersection from entry to exit within the time period; measured in vehicles per hour. Total delay is defined as the time a vehicle spends waiting at an intersection plus the time spent in queue before the intersection, and measured in seconds. Total stops refer to the number of times a vehicle comes to a complete stop at the intersection. Fuel consumption and CO_2 are measured in terms of grams per mile.

To obtain the values of these metrics, SUMO provides detailed output files containing the necessary data to calculate these performance metrics. In the simulation setup, we implemented the ECoTOp approach for vehicle trajectories and traffic signal timing, and measured the performance of this approach in terms of the aforementioned metrics. The Comprehensive Modal Emissions Model (CMEM) [54] is used to estimate fuel consumption and CO_2 output. The results of this evaluation are presented in the following section.

6.1.3.2 Experimental Results

In this section, we present the results of the simulations for each experimental scenario. We evaluate the performance of the ECoTOp approach in comparison to the baseline, traffic signal optimization module alone, and eco-trajectory module alone scenarios, at CAV penetration rates of 20%, 40%, 60%, 80%, and 100%, and a V/C ratio of 0.82. The key findings for each performance metric are summarized below. Graphs, tables, and figures are included to help illustrate the results.

Throughput: Table 6.1 provides a summary of the throughput, also called vehicle flow, for each CAV penetration percentage. As expected, the signal optimization module alone provided the most improvement with 17.5% increase, and the eco-trajectory module alone causing a decrease. Also, the ECoTOp approach being in-between the two modules at each CAV penetration percentage. Interestingly, the eco-trajectory module alone approaches the baseline scenario as the CAV penetration percentage goes down, and the ECoTOp system approaches the signal optimization module alone as the CAV penetration percentage decreases. This is illustrated in Figure 6.3.

Table 6.1. Vehicle flow results for signal optimization module, eco-trajectory module, and ECoTOp compared to baseline.

CAV %	**Baseline Flow**	**Signal Opt. Flow**		**Eco-Traj. Flow**		**ECoTOp Flow**	
	Veh/hr	Veh/hr	Improvement %	Veh/hr	Improvement %	Veh/hr	Improvement %
20	1120.4	1316.6	17.5	1109.1	-1.01	1307.4	16.7
40	1120.4	1316.6	17.5	1099.9	-1.8	1284.8	14.7
60	1120.4	1316.6	17.5	1067.5	-4.7	1277.7	14.1
80	1120.4	1316.6	17.5	1045.3	-6.7	1242.8	10.9
100	1120.4	1316.6	17.5	1039.5	-7.2	1217.4	8.6

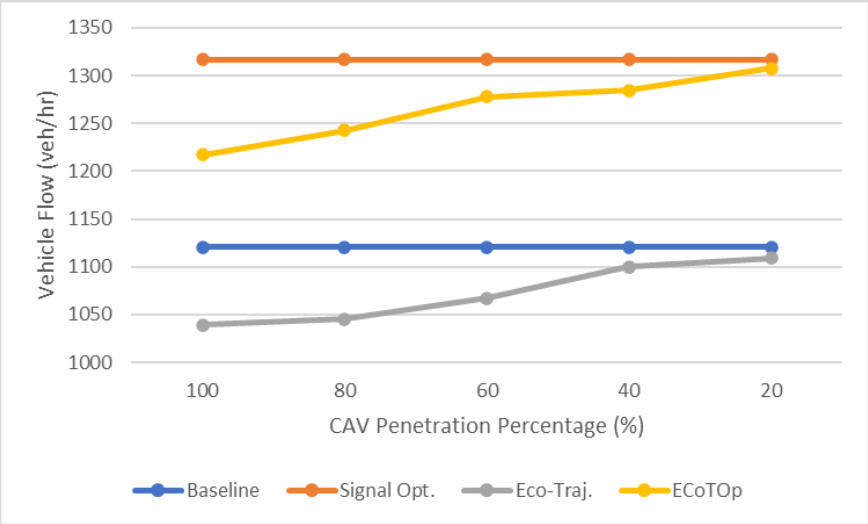

Figure 6.3. Plot of vehicle flow across different CAV penetration percentages.

CO_2 output: As expected, the eco-trajectory module alone provided the best performance, with up to 11.7% reduction in CO_2 output. The signal optimization module alone had a slight increase in CO_2 output, 1.04%, but the ECoTOp approach was often in-between the baseline scenario and the eco-trajectory module alone. Table 6.2 provides a summary of the CO_2 output for each CAV penetration percentage.

The CO_2 output can be further analyzed between CAVs and legacy vehicles. Figure 6.4 shows the plots of average CO_2 output for CAVs (6.4a) and for legacy vehicles (6.4b). Interestingly, for CAVs, even as the penetration percentage decreases, the average CO_2 output is similar. For legacy vehicle, however, there is a reduction in CO_2 output when the CAV penetration percentage is higher, but then approaches that of baseline for eco-trajectory module alone and that of signal optimization module alone for ECoTOp. It should be noted that for Figure 6.4a, CAVs CO_2 output, the Baseline and Signal Opt. vehicles plotted are the equivalent vehicles in the eco-trajectory module alone and ECoTOp scenarios. In other words, the legacy vehicles from baseline and signal optimization that became CAVs in eco-trajectory planning and ECoTOp are plotted against each other, and the legacy vehicles that stayed legacy vehicles are plotted against each other.

Table 6.2. Emissions results for signal optimization module, eco-trajectory module, and ECoTOp compared to baseline.

CAV %	Baseline CO_2	Signal Opt. CO_2		Eco-Traj. CO_2		ECoTOp CO_2	
	g/mile	g/mile	Improvement %	g/mile	Improvement %	g/mile	Improvement %
20	443.3	447.9	-1.04	431.1	2.7	443.4	-0.02
40	443.3	447.9	-1.04	402.9	9.1	428.6	3.3
60	443.3	447.9	-1.04	393.4	11.3	419.0	5.5
80	443.3	447.9	-1.04	392.6	11.4	416.5	6.1
100	443.3	447.9	-1.04	391.3	11.7	412.4	6.97

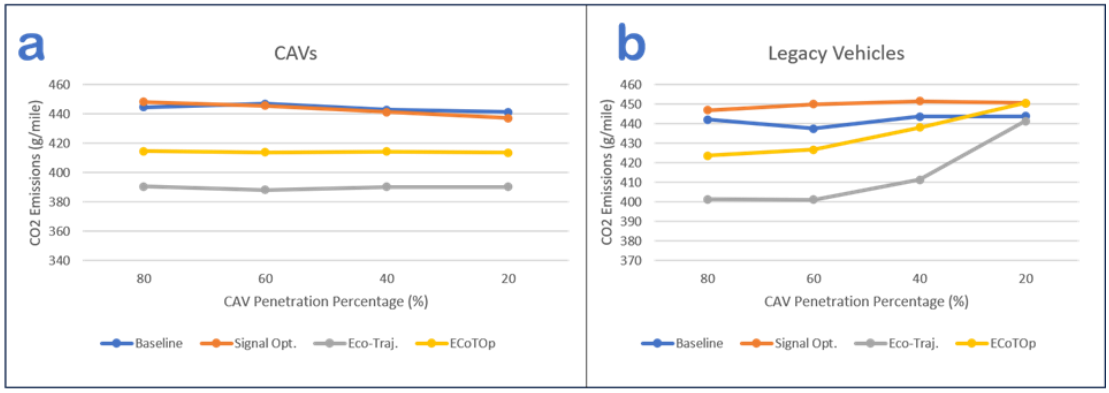

Figure 6.4. Plot of CO_2 output across different CAV penetration percentages, (a) CAV; (b) Legacy vehicles.

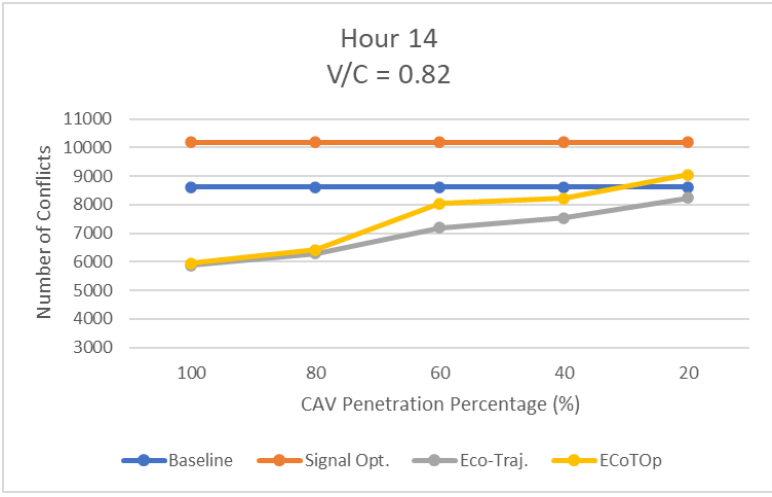

Figure 6.5. Number of Conflict plotted over different CAV penetration percentages.

Safety: Surprisingly, the signal optimization module alone scenario provided the most conflicts. It was expected that the eco-trajectory module alone scenario would have the least conflicts, and that the ECoTOp scenario would be in-between the eco-trajectory module alone and signal optimization module alone scenarios. Figure 6.5 shows the trend for each scenario over each CAV penetration percentage. Similar to throughput and CO_2 output, the eco-trajectory module alone approaches the baseline and the ECoTOp system approaches the signal optimization module alone, as the CAV percentage decreases. Table 6.3 provides a summary of the safety of each scenario for each CAV penetration percentage.

Table 6.3. Safety results for signal optimization module, eco-trajectory module, and ECoTOp compared to baseline.

CAV %	**Baseline**	**Signal Opt. Safety**		**Eco-Traj. Safety**		**ECoTOp Safety**	
	Conflicts	Conflicts	Improve %	Conflicts	Improve %	Conflicts	Improve %
20	8615.6	10191.9	-18.3	8234.5	4.4	9048.5	-5.0
40	8615.6	10191.9	-18.3	7538.1	12.5	8225.1	4.5
60	8615.6	10191.9	-18.3	7189.9	16.5	8036.9	6.7
80	8615.6	10191.9	-18.3	6300.6	26.9	6418.2	25.5
100	8615.6	10191.9	-18.3	5886.5	31.7	5947.7	31.0

The rise in number of conflicts for the signal optimization module alone could be due to the increased speeds and shorter time gaps, leading to more conflicts and potential collisions. Or due to the approach assuming all vehicles are identical and have same speed, acceleration, and braking characteristics. The eco-trajectory module alone often smoothed out vehicle trajectories and reduced queuing leading to fewer conflicts. The ECoTOp approach makes trade-offs between signal optimization and eco-trajectory planning resulting in more conflicts than eco-trajectory module alone but less conflicts than the signal optimization module alone.

Figures 6.6, 6.7, and 6.8 show a sample of the trajectories for each scenario, where a. is baseline, b. is signal optimization alone, c. is eco-trajectory module alone, and d. is ECoTOp. For Figures 6.6, 6.7, and 6.8, black lines represent legacy vehicles, red lines represent CAVs, grey lines represent right turning legacy vehicles, and pink lines represent right turning CAVs. Figure 6.6 shows the trajectories for 100% CAV penetration, Figure 6.7 shows the trajectories for 60% CAV penetration, and Figure 6.8 shows the trajectories for 20% CAV penetration. In Figure 6.6a, the blue arrows show instances where vehicles missed the green light interval and had to stop and wait for the next green interval, and in Figure 6.6c, the green arrows show instances where vehicles knew they would miss the green interval and slowed to pass through the next green interval. Figure 6.6b shows all waiting vehicles passing through the intersection, but vehicles for the next green interval have to stop. Figure 6.6d shows passing smoothly through each green interval.

Figures 6.7a and 6.7b shows the same trajectories as 6.6a and 6.6b, but show which vehicles are CAV equivalent in eco-trajectory module and ECoTOp. Figure 6.7c shows legacy vehicles having to stop and wait at red lights, while CAVs slow to pass through the next green interval. Figure 8d shows legacy vehicles having to stop and wait at red lights. The green arrows in Figures 6.7c and 6.7d show instances where legacy vehicles are behind CAVs and are forced to follow the eco-trajectories resulting in some legacy vehicles lowering CO_2 output.

Similar to Figure 6.7, Figures 6.8a and 6.8b shows the same trajectories as 6.6a and 6.6b, but the red lines are the CAV equivalent vehicles. Figure 6.8c shows the eco-trajectory planning module alone scenario becoming more like the baseline scenario. The blue arrows in Figure 6.8c show instances of vehicles missing the green interval, similar to baseline Figures 6.6a, 6.7a, and 6.8a, while the green arrow shows instances of CAVs slowing to pass through the next green interval. Figure 6.8d shows the ECoTOp scenario becoming like the signal optimization module alone scenario, Figures 6.6b, 6.7b, and 6.8b. The blue arrow in Figure 6.8d shows an instance where

the green interval was extended enough for the vehicle to pass through the intersection, where that same vehicle in Figure 6.8c had to stop and wait for the next green interval.

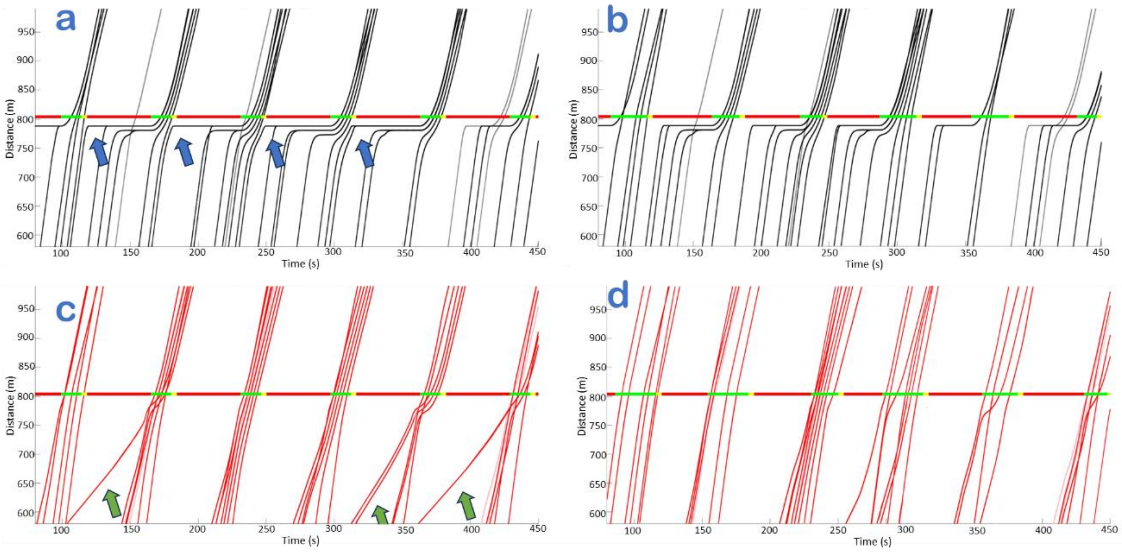

Figure 6.6. Trajectory plots for 100% CAV penetration

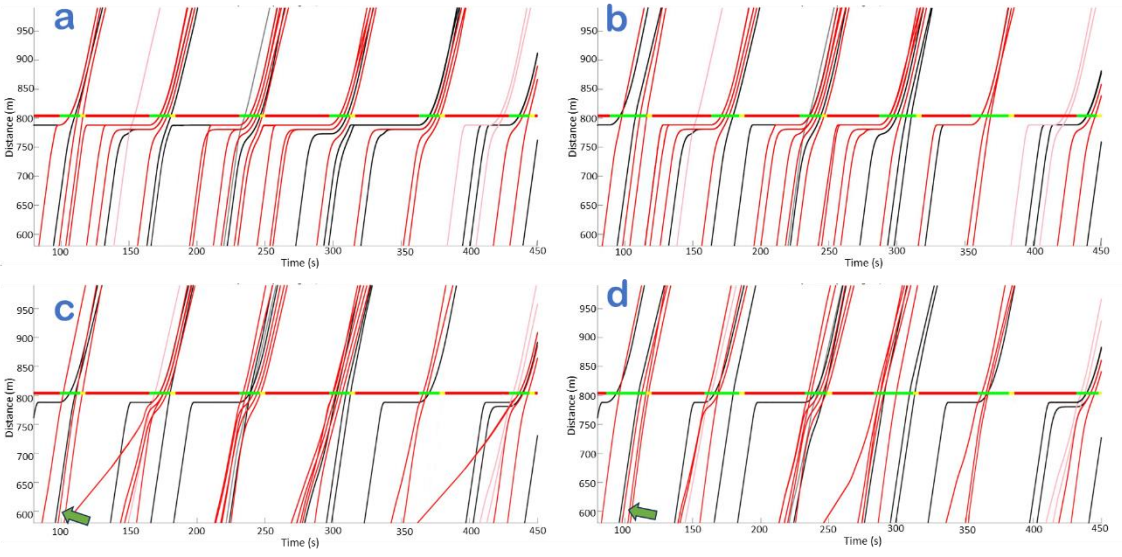

Figure 6.7. Trajectory plots for 60% CAV penetration.

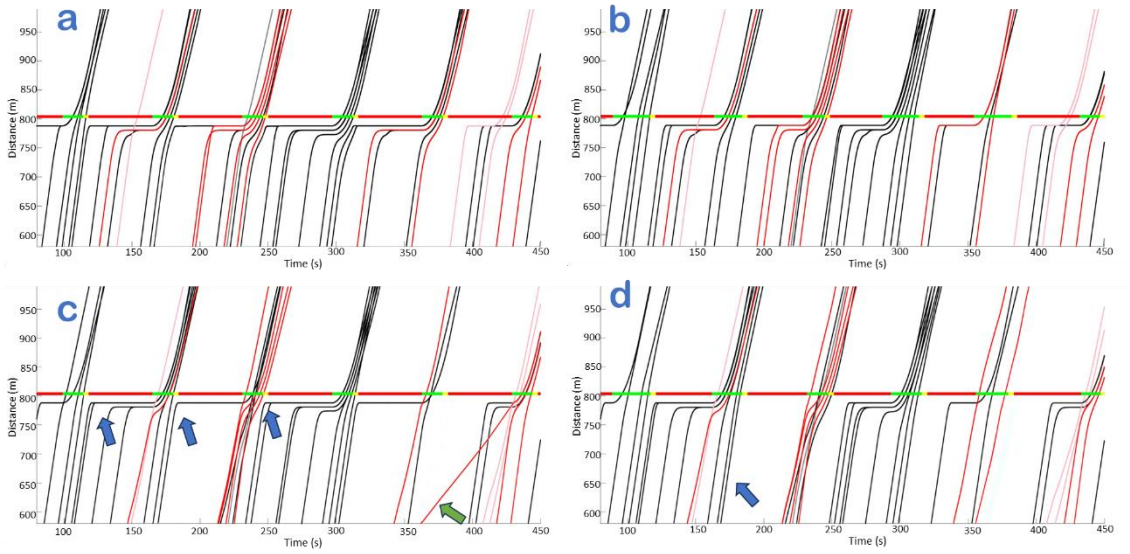

Figure 6.8. Trajectory Plots for 20% CAV penetration.

Figure 10 shows an illustrated version of the conclusion of the results. Figure 10a shows that as signal optimization increases, the mobility (throughput) increases, but the emissions (CO_2 output) also increase. As the eco-trajectory planning increases, the emissions decrease, but the mobility also decreases. The darker shade of green shows the ECoTOp system sitting in the middle where mobility and emission output both outperform baseline.

Figure 10b shows a similar conclusion but with safety and mobility. As signal optimization increases, the mobility increases, but the number of conflicts increase. As eco-trajectory planning increases, the number of conflicts decrease, but the mobility also decreases. The darker shade of green shows the ECoTOp system in the middle where mobility and safety each outperform baseline.

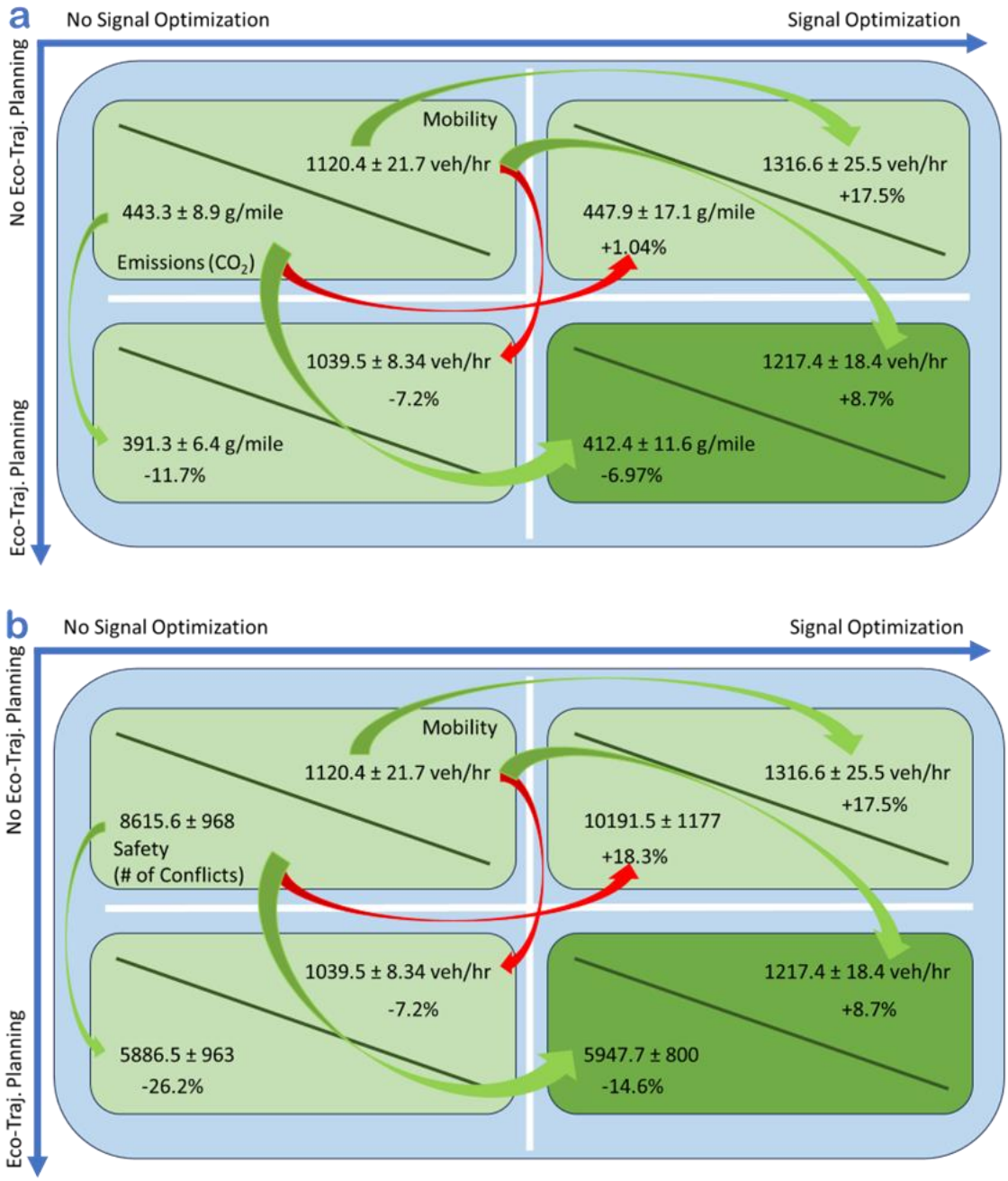

Figure 6.9. Visualization of dynamic optimization strategies. (a) Emissions and mobility; (b) Safety and mobility.

6.1.4 Conclusions and Future Work

6.1.4.1 Research Contributions

In this chapter, we proposed an Eco-friendly Cooperative Traffic Optimization (ECoTOp) system. The approach leverages the information on vehicle trajectories to optimize the traffic signals in real-time, with the goal of increasing total throughput while ensuring a fair distribution of green time intervals among different approaches, and decreasing emissions output.

The proposed ECoTOp approach was evaluated through extensive case studies using the traffic simulation software SUMO. The results of the ECoTOp approach were compared with a traffic signal optimization approach and an eco-trajectory planning approach. The results showed that the ECoTOp system showed better mobility than baseline and the eco-trajectory planning, and lower emissions output than baseline and the traffic signal optimization approach.

The proposed approach was also found to be robust and effective in adapting to different traffic volumes and demand patterns. The simulation results demonstrated the potential of the proposed approach for improving intersection performance and reducing traffic congestion at isolated signalized intersections.

The contributions of this research can be summarized as follows:

- Development of a novel co-optimization approach (ECoTOp) for traffic signals and vehicle trajectories at isolated signalized intersections.
- Demonstration of the effectiveness and potential of the proposed approach against traffic signal optimization alone, and vehicle trajectory optimization alone, through extensive case studies using a traffic simulation software.
- Provision of a foundation for further research in the area of dynamically adjusting eco-driving approaches based on traffic and environmental conditions.

6.1.4.2 Limitations and Future Directions

While the proposed ECoTOp approach has shown promising results, there are several limitations and future directions to be considered. First, the proposed approach assumes a fixed and known intersection geometry. In reality, intersection geometry can vary over time, and different approaches may have different traffic characteristics. Therefore, future research may investigate the robustness and adaptability of the proposed approach to changing traffic conditions. Second, the proposed approach does not consider the effects of non-motorized traffic and pedestrians. Future research may extend the proposed approach to accommodate these users and investigate their impacts on intersection performance. Third, the proposed approach was evaluated using a traffic simulation software, and its applicability to real-world scenarios has yet to be demonstrated. Future research may investigate the feasibility of implementing the proposed approach in real-world settings and evaluate its effectiveness using field data.

6.1.4.3 Final Remarks

Our experimental results demonstrate the effectiveness of the proposed ECoTOp approach compared to baseline, traffic signal timing optimization, and eco-trajectory planning. While there are limitations and future directions to be considered, our ECoTOp system presents a promising avenue for improving intersection performance and reducing traffic congestion. The approach has the potential to be applied in real-world scenarios and can be extended to incorporate additional objectives, such as environmental and social considerations. We hope this chapter will inspire further research in this area and contribute to the development of more efficient and sustainable transportation systems.

Chapter 7

ECoTOp and Electric Vehicles

This chapter focuses on the integration of electric vehicles (EVs) into the co-optimization framework, with the aim of examining their impact on the performance of the system. By incorporating market-predicted EV penetration percentages and leveraging real-world EV trajectories obtained from the SUMO traffic simulation platform, this chapter explores the effectiveness of the co-optimization approach in the presence of EVs and compares it to the performance of vehicle trajectory optimization alone and traffic signal optimization alone. The insights gained from these comparisons lay the foundation for the future development of an adaptive optimization strategy capable of dynamically selecting the most suitable optimization approach based on real-time traffic conditions and environmental considerations.

To accurately represent the anticipated increase in EVs on the road, market-predicted EV penetration percentages are incorporated into the simulations. These percentages are based on industry forecasts and provide a realistic representation of the expected growth in EV usage. By considering different EV penetration levels, ranging from conservative estimates to more aggressive projections, we gain insights into the performance of the co-optimization approach under various EV adoption scenarios. Four EV penetration levels were chosen: 18%, EVs could account for 18% of total car sales in 2023 [105]; 50%, United States are pushing to reach 50% EV sales in 2030 [106]; 80%, the share of EV sales is expected to reach over 80% in many countries by 2040 [107]; and 100%, California wants 100% zero-emission vehicle sales by 2035 [108].

Real-world EV trajectories recorded from the SUMO simulation platform are utilized to capture the actual driving patterns and behaviors of EVs. These trajectories, combined with energy usage estimation using MATLAB's EV reference application in Simulink, tailored specifically for

the Cadillac Lyriq, enable a comprehensive analysis of the energy implications and performance of the co-optimized vehicle trajectories and traffic signal timings.

The experimental results presented in this chapter provide valuable insights into the performance of the ECoTOp approach in the presence of EVs. By comparing the outcomes of the co-optimization strategy with those of vehicle trajectory optimization alone and traffic signal optimization alone, we assess the benefits and challenges associated with the integration of EVs into the transportation system. This comparative analysis aids in establishing a baseline understanding of the advantages and trade-offs of different optimization strategies and sets the stage for the development of an adaptive optimization strategy that dynamically selects the most suitable approach based on real-time traffic conditions, EV penetration levels, and environmental considerations.

The findings from this chapter contribute to the understanding of the interactions between EVs and the ECoTOp approach, shedding light on the energy implications, vehicle flow, and overall transportation efficiency achieved with different optimization strategies. These insights provide a foundation for future research and policymaking efforts aimed at promoting sustainable transportation systems that effectively incorporate electric vehicles.

In summary, this chapter investigates the integration of electric vehicles into the ECoTOp framework and examines their influence on the performance of the system. By incorporating market-predicted EV penetration percentages and real-world EV trajectories, we compare the outcomes of the ECoTOp approach with vehicle eco-trajectory planning alone and traffic signal optimization alone. These comparisons lay the groundwork for the future development of an adaptive optimization strategy, which dynamically selects the most appropriate optimization approach based on real-time traffic conditions, EV penetration levels, and environmental

considerations. The insights gained from this chapter contribute to the advancement of sustainable transportation systems that effectively accommodate the growing presence of electric vehicles.

7.1 Simulink Electric Vehicle Model

In this study, the MATLAB EV reference application for Simulink was utilized to estimate the energy use of electric vehicles (EVs) within the co-optimization framework. The MATLAB EV reference application [109] is a powerful tool that allows for accurate modeling and simulation of EV behavior and energy consumption. Figure 7.1 shows the Simulink model outer layer.

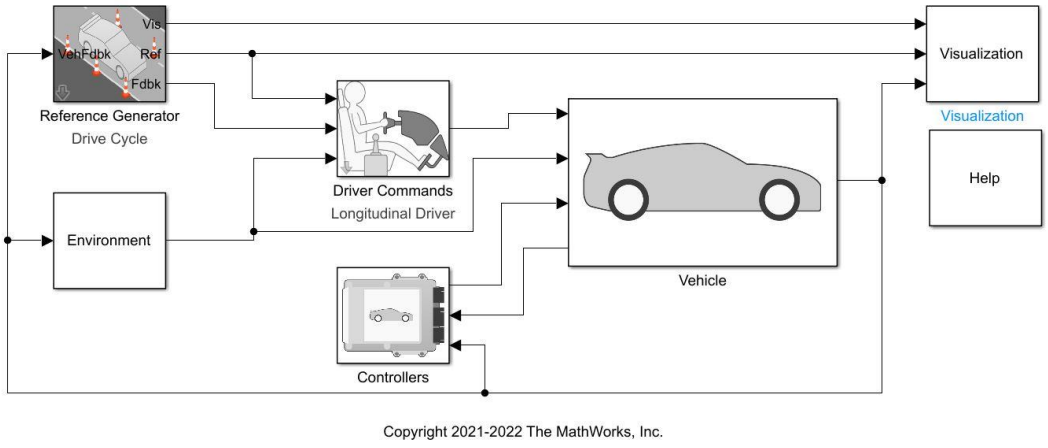

Figure 7.1. MATLAB EV reference application Simulink model.

The reference application in Simulink provides a comprehensive set of blocks and models specifically designed for simulating EVs. It incorporates various components and characteristics of an EV, including the battery, electric motor, drivetrain, and vehicle dynamics. These components are modeled using physics-based equations and empirical data to capture the real-world behavior of EVs.

One key advantage of the MATLAB EV reference application is its flexibility and customization options. The application allows researchers to tailor the model parameters to specific EV makes and models, providing a more accurate representation of the vehicle being studied. In

this research, the reference application was specifically tuned for the Cadillac Lyriq, an electric vehicle model used in the experiments.

By integrating the EV trajectories recorded from the Simulation of Urban MObility (SUMO) platform with the MATLAB EV reference application, it was possible to estimate the energy consumption of the EVs under different traffic signal timing scenarios. This enabled a comprehensive assessment of the energy-saving potential of the co-optimization approach.

The use of the MATLAB EV reference application in this study ensures a rigorous and accurate representation of EV energy consumption. By leveraging the capabilities of Simulink, the author was able to simulate realistic driving conditions, account for variations in traffic patterns, and evaluate the impact of different optimization strategies on EV energy use.

The results obtained from the MATLAB EV reference application provide valuable insights into the energy efficiency of EVs and the effectiveness of the co-optimization approach. They contribute to a deeper understanding of the potential benefits of integrating EVs into the optimization framework and inform the development of future adaptive optimization strategies.

7.2 Simulation and Results

The simulation setup for EVs was the same as the simulation setup in section 6.1.3, except the eco-trajectory planning module was trained specifically for EVs. We tested four different penetration rates: 18% EVs, 50% EVs, 80% EVs, and 100% EVs. Each penetration rate was tested at the 20%, 60%, and 100% CAV penetration rates, and at the hour 14 v/c ratio. The results showed that the ECoTOp approach was more effective in increasing throughput and battery efficiency as the penetration rate of CAVs and EVs increased. For example, at low CAV penetration rate, the efficiency improvement for EVs achieved by the ECoTOp approach was only around 10% for each EV penetration, while at high CAV penetration rate, it increased to around 20%. This indicates that the ECoTOp approach is more effective in a future traffic network with a higher share of CAVs and

EVs, but still performs well in lower CAVs. The safety and mobility were similar to that of no EVs, as was the CO_2 emissions for ICE vehicles.

Figure 7.2 shows the trend for battery efficiency over the three CAV penetrations, 100%, High CAV (60%) and Low CAV (20%) for each EV penetration rate; Figure 7.2a is for 18% EVs, 7.2b for 50% EVs, 7.2c for 80% EVs, and 7.2d for 100% EVs. Table 7.1 shows the results for EV efficiency, Table 7.2 shows the vehicle flow results, and Table 7.3 shows the safety results.

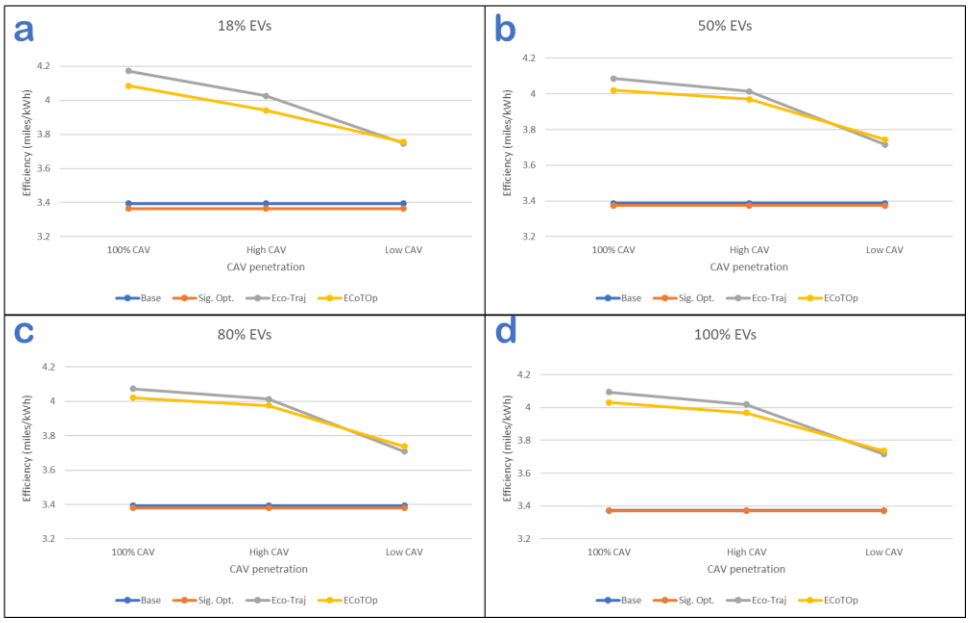

Figure 7.2. EV efficiencies output across different CAV penetration percentages.

Figure 7.3 shows the EV efficiency for each CAV penetration rate across the four EV penetration rates; Figure 7.3a is 20% CAV rate, 7.3b is 60%, and 7.3c is 100%. Interestingly, for 50% EVs and above, the average efficiency was almost the same; this was the case for each CAV penetration rate. Meaning, for Low CAV rate, 50%, 80% and 100% EVs penetrations had similar average efficiencies, and the same for High CAV rate and 100% CAV rate.

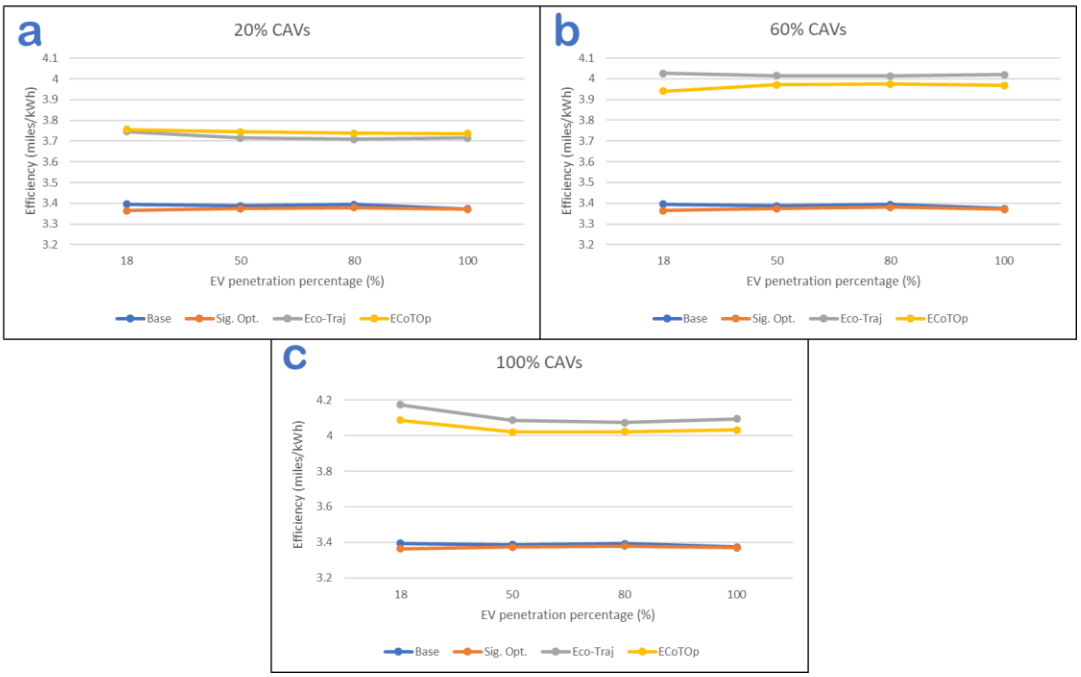

Figure 7.3. EV efficiencies across different EV penetration rates.

Figure 7.4 shows the EV efficiencies for CAVs and legacy EVs (non-connected EVs) for High CAV rate (60%) and Low CAV rate (20%). Figure 7.4a is CAVs for High CAV rate, 7.4b is legacy EVs for High CAV rate, 7.4c is CAVs for Low CAV rate, and 7.4d is legacy EVs for High CAV rate. It should be noted that for Figure 7.4, the Baseline and Signal Opt. vehicles plotted are the equivalent vehicles in the eco-trajectory module alone and ECoTOp scenarios. In other words, the legacy vehicles from baseline and signal optimization that became CAVs in eco-trajectory planning and ECoTOp are plotted against each other, and the legacy vehicles that stayed legacy vehicles are plotted against each other. For eco-trajectory planning alone and ECoTOp, the CAVs improved efficiency, which is expected, but the legacy vehicles also improved efficiency. This is because of the CAVs forcing the legacy vehicles to follow their trajectories sometimes, as the green arrows point out in Figure 6.7.

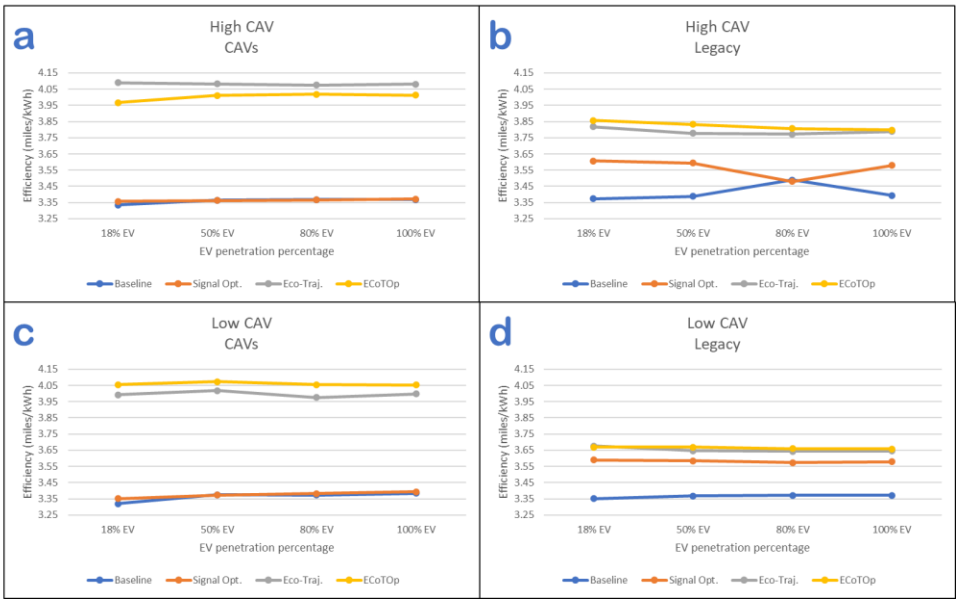

Figure 7.4. EV efficiencies for CAVs and legacy vehicles.

Table 7.1. EV energy efficiency results.

EV %	CAV %	Baseline	Signal Opt.		Eco-Trajectory Planning		ECoTOp	
		Efficiency (mi/kWh)	Efficiency (mi/kWh)	% Improve (vs. Baseline)	Efficiency (mi/kWh)	% Improve (vs. Baseline)	Efficiency (mi/kWh)	% Improve (vs. Baseline)
18	20	3.3946	3.3641	-0.9	3.7464	10.4	3.7551	10.6
	60	3.3946	3.3641	-0.9	4.0261	18.6	3.9403	16.1
	100	3.3946	3.3641	-0.9	4.1729	22.9	4.0852	20.3
50	20	3.3870	3.3738	-0.4	3.7154	9.7	3.7445	10.6
	60	3.3870	3.3738	-0.4	4.0140	18.5	3.9705	17.2
	100	3.3870	3.3738	-0.4	4.0854	20.6	4.0194	18.7
80	20	3.3932	3.3797	-0.4	3.7089	9.3	3.7376	10.1
	60	3.3932	3.3797	-0.4	4.0126	18.3	3.9748	17.1
	100	3.3932	3.3797	-0.4	4.0732	20.0	4.0213	18.5
100	20	3.3733	3.3708	-0.8	3.7148	10.1	3.7364	10.8
	60	3.3733	3.3708	-0.8	4.0195	19.2	3.9681	17.6
	100	3.3733	3.3708	-0.8	4.0931	21.3	4.0311	19.5

Table 7.2. Flow rate results for different EV penetration rates.

EV %	CAV %	Baseline	Signal Opt.		Eco-Trajectory Planning		ECoTOp	
		Vehicle Flow (veh/hr)	Vehicle Flow (veh/hr)	% Improve (vs. Baseline)	Vehicle Flow (veh/hr)	% Improve (vs. Baseline)	Vehicle Flow (veh/hr)	% Improve (vs. Baseline)
18	20	1120.4	1316.6	17.5	1108.1	-1.1	1302.8	16.3
	60	1120.4	1316.6	17.5	1046.2	-6.6	1250.8	11.6
	100	1120.4	1316.6	17.5	1026.8	-8.4	1209.1	7.9
50	20	1120.4	1316.6	17.5	1101.5	-1.7	1292.8	15.4
	60	1120.4	1316.6	17.5	1016.2	-9.3	1220.8	8.9
	100	1120.4	1316.6	17.5	980.1	-12.5	1199.1	7.0
80	20	1120.4	1316.6	17.5	1091.5	-2.5	1279.5	14.2
	60	1120.4	1316.6	17.5	1009.6	-9.9	1204.2	7.5
	100	1120.4	1316.6	17.5	966.8	-13.7	1182.4	5.5
100	20	1120.4	1316.6	17.5	1074.8	-4.1	1266.1	13.0
	60	1120.4	1316.6	17.5	999.6	-10.8	1194.2	6.6
	100	1120.4	1316.6	17.5	951.0	-15.1	1177.3	5.1

Table 7.3. Safety results for different EV penetration rates.

EV %	CAV %	Baseline	Signal Opt.		Eco-Trajectory Planning		ECoTOp	
		Conflicts	Conflicts	% improvement (vs. Baseline)	Conflicts	% improvement (vs. Baseline)	Conflicts	% improvement (vs. Baseline)
18	20	8615.6	10191.9	-18.3	8537.9	0.9	9514.4	-5.0
	60	8615.6	10191.9	-18.3	8126.2	5.7	9020.3	6.7
	100	8615.6	10191.9	-18.3	6611.1	23.3	7147.5	30.9
50	20	8615.6	10191.9	-18.3	8561.5	0.6	8462.6	1.7
	60	8615.6	10191.9	-18.3	8041.6	6.6	8010.9	7.0
	100	8615.6	10191.9	-18.3	6620.5	23.2	7142.8	17.1
80	20	8615.6	10191.9	-18.3	8303.9	3.6	8481.4	1.6
	60	8615.6	10191.9	-18.3	8079.2	6.2	7916.7	8.1
	100	8615.6	10191.9	-18.3	6629.9	23.6	7133.4	17.2
100	20	12458.1	13572.3	-8.9	11729.0	5.8	12411.8	0.3
	60	12458.1	13572.3	-8.9	10809.9	13.2	12237.5	1.8
	100	12458.1	13572.3	-8.9	10123.8	18.7	11311.8	9.2

7.3 Conclusions

This chapter presented the integration of electric vehicles (EVs) into the co-optimization framework for vehicle trajectories and traffic signal timing. Through the use of the MATLAB EV reference application in Simulink, the energy consumption of EVs was estimated, allowing for a comprehensive analysis of their performance within the optimization framework. The key findings and implications from this chapter can be summarized as follows:

1. Energy Efficiency: The energy consumption of EVs under different optimization strategies was evaluated, providing insights into the potential energy-saving benefits of the co-optimization approach. By considering the specific characteristics of EVs and their interactions with traffic signal timing, the optimization framework demonstrated the ability to improve the energy efficiency of EVs.
2. Comparative Analysis: The comparison between the co-optimization approach, vehicle trajectory optimization alone, and traffic signal optimization alone revealed the strengths and limitations of each strategy. While vehicle trajectory optimization alone achieved the best energy efficiency, the co-optimization approach showed promising results by striking a balance between energy consumption and overall traffic flow efficiency.
3. Foundation for Adaptive Optimization: The integration of EVs into the co-optimization framework serves as a foundational step towards the future development of an adaptive optimization strategy. By considering real-time traffic conditions, EV penetration rates, and environmental factors, the adaptive strategy can dynamically select the most suitable optimization approach to maximize overall system performance.

The findings from this chapter contribute to the advancement of sustainable transportation systems by demonstrating the potential benefits of integrating EVs into the optimization

framework. The results highlight the importance of considering EV energy consumption and its interaction with traffic signal timing for achieving efficient and eco-friendly transportation networks. The study revealed that the integration of electric vehicles (EVs) did not significantly impact traffic flow and safety compared to the results obtained without EVs. However, concerning energy efficiency, it was observed that traffic signal optimization alone showed a marginal difference of merely 1% from the baseline, irrespective of the EV penetration rate. Furthermore, the ECoTOp approach demonstrated remarkable proximity to eco-trajectory planning alone, with ECoTOp achieving an improvement of 10-20% over the baseline, while eco-trajectory planning alone achieved 10-22%, depending on the connected and automated vehicle (CAV) penetration rate.

Moving forward, future research should focus on refining the co-optimization framework to better address the unique characteristics and requirements of EVs. This includes incorporating real-time EV data, considering charging infrastructure constraints, and further investigating the trade-offs between energy efficiency and traffic flow optimization.

By continuing to explore and enhance the co-optimization approach with EV integration, we can pave the way for the development of intelligent and adaptive optimization strategies that optimize the performance of transportation systems while promoting sustainability and energy efficiency.

Chapter 8

Additional ECoTOp Case Studies

The final chapter of this dissertation presents additional case studies that further investigate the ECoTOp framework. These case studies explore different traffic volumes, mixed vehicle type scenarios, and electric vehicle (EV) considerations, providing valuable insights into the performance and effectiveness of the ECoTOp approach under various conditions.

1. Variation in Traffic Volumes: To assess the robustness of the co-optimization approach, different traffic volumes are tested. By simulating varying levels of traffic demand, ranging from low to high volume scenarios, the performance of the ECoTOp approach can be evaluated under different levels of congestion and traffic flow.
2. Mixed Vehicle Type Scenarios: Two distinct mixed vehicle type scenarios are examined in the case studies. The first scenario reflects the real-world distribution of heavy-duty vehicles (HDV), medium-duty vehicles (MDV), and light-duty vehicles (LDV) from the Innovation Corridor [41]. This scenario allows for an assessment of the ECoTOp approach's performance when considering the typical vehicle composition on the road. The second scenario involves a fabricated ratio that is more truck-dominated, providing insights into the approach's adaptability to different vehicle mix scenarios.
3. CAV Penetration Rates: The case studies also investigate the impact of connected and automated vehicle (CAV) penetration rates on the performance of the co-optimization approach. By simulating different CAV penetration levels, ranging from low to high, the effectiveness of the approach in leveraging CAV technologies for enhanced traffic management can be assessed.

4. EV Considerations: The case studies also include specific test scenarios that focus on electric vehicles (EVs). Different traffic volumes are considered to evaluate the performance of the co-optimization approach in the context of EVs. This analysis provides insights into the interaction between EVs, traffic signal timing, and overall system performance.

By conducting these additional case studies, a comprehensive understanding of the ECoTOp approach's performance across different traffic volumes, vehicle types, CAV penetration rates, and EV considerations can be obtained. The results of these case studies will further contribute to the evaluation and refinement of the ECoTOp approach, facilitating its potential implementation in real-world transportation systems.

Overall, these case studies provide important insights into the versatility and adaptability of the ECoTOp approach, demonstrating its effectiveness in a range of scenarios and paving the way for future advancements in the field of intelligent transportation systems.

8.1 Simulation Setup

The simulation setup for EVs was the same as the simulation setup in section 6.1.3, and section 7.2 for EVs. The simulations were performed using the SUMO (Simulation of Urban Mobility) traffic simulation platform, which provides a realistic environment to model and analyze traffic dynamics at isolated signalized intersections.

1. Traffic Volumes: Different traffic volumes were considered to assess the performance of the ECoTOp approach under varying levels of demand. The selected traffic volumes represent different demand levels for different hours of the day using real-world data. Specifically, we tested the performance of the approach at hour 10 with a volume-to-capacity (v/c) of 0.52, hour 14 (v/c = 0.82), and an over-saturated case, hour 17 (v/c =

1.09). These varying volumes allowed for a comprehensive analysis of the ECoTOp system's effectiveness across different traffic conditions.

2. Connected and Automated Vehicle (CAV) Penetration: To assess the impact of CAV technology, different CAV penetration rates were simulated in the experiments. The CAV penetration rates were: 20%, 40%, 60%, 80%, and 100%. This allowed for the evaluation of how the ECoTOp approach performs under different levels of CAV deployment and interaction with conventional vehicles.
3. Mixed Vehicle Types: Two different scenarios were considered to evaluate the co-optimization approach's performance with different vehicle mixes. The first mix comprised of 3% HDV, 20% MDV, and 77% LDV. The second mix was 30% HDV, 30% MDV and 40% LDV. We evaluated the two mixes at three different levels of connected and automated vehicle (CAV) penetration: 20%, 60%, and 100%. The tests were conducted at hours 10, 14, and 17 v/c ratios.
4. Electric Vehicles (EVs): The influence of electric vehicles on the co-optimization approach was also investigated by considering different traffic volumes specific to EVs. These volumes were based on market predictions of EV penetration percentages: 18% EVs, 50% EVs, 80% EVs, and 100% EVs. Each EV penetration rate was tested at low CAV penetration (20%), high CAV penetration (60%), and 100% CAV penetration. Also, each EV/CAV penetration scenario was tested at the hours 10, 14, and 17 v/c ratios.

The calculation of intersection volume-to-capacity ratios is based on critical lane groups, with noncritical lane groups not constraining traffic signal operations. The determination of critical lane groups follows rules set out in HCM 2000. The v/c ratio, which is also known as degree of saturation, represents the ability of an intersection to handle the vehicular demand. A v/c ratio of less than 0.85 usually suggests that sufficient capacity is available, and drivers are not expected to

encounter significant queues and delays. As the v/c ratio approaches 1.0, traffic flow can become unstable, leading to delay and queuing conditions. Once the demand surpasses the capacity (a v/c ratio greater than 1.0), traffic flow becomes unstable, and significant delay and queuing are expected. In such cases, vehicles may require more than one signal cycle to navigate the intersection, a scenario referred to as cycle failure [16].

The simulation setup parameters were carefully selected to create a diverse set of scenarios that represent real-world conditions and potential future trends in traffic composition. By examining various traffic volumes, vehicle types, CAV penetration rates, and EV scenarios, the simulation experiments aimed to provide comprehensive insights into the performance and effectiveness of the ECoTOp approach.

8.2 Results

In this section, we present the results of the simulation experiments conducted to evaluate the ECoTOp framework under various scenarios. The analysis focuses on key performance metrics, including traffic flow, CO_2 output, EV miles per kilowatt-hour, and potential traffic conflicts, to assess the effectiveness of the ECoTOp approach in improving traffic efficiency and sustainability. The results are discussed for each specific case, considering different traffic volumes, mixed vehicle types, CAV penetration rates, and EV scenarios.

First, we examine the performance of the ECoTOp approach across different traffic volume scenarios. we conducted experiments with different demand levels for different hours of the day using real-world data. Specifically, we tested the performance of the approach at hour 10 with a volume-to-capacity (v/c) ratio of 0.524, hour 14 (v/c = 0.82), and hour 17 (v/c = 1.09). Those hours were chosen in order to test at one medium capacity, one high capacity, and one over-saturated capacity. The hour 14 with v/c ratio is the same scenario as section 7.2, and is shown in this section for comparison purposes.

The results are shown in Figure 8.1 and show the safety, mobility, and emission output for the three v/c ratios tested at several different CAV penetration percentages. The ECoTOp approach is often in-between the eco-trajectory module alone and signal optimization module alone, but still performing better than baseline. Where the medium traffic (v/c=0.524), when compared to baseline, signal optimization safety improves by 4.1%, and mobility improves by 25.7%, and emissions worsen by 0.5%; eco-trajectory improves safety by 13-60%, mobility worsens by 1.9-5.8%, and emissions improve by 8.2-16.9%; ECoTOp improves safety by 25-54%, mobility improves by 18-24%, and emissions improve by 5.5-14%. However, the over-saturated case did provide some irregularities. For instance, emissions in the over-saturated case more closely resembles that of the signal optimization alone, and worse than the baseline emissions. Also, for all cases, the mobility was significantly less in the over-saturated case. Tables 8.1, 8.2, and 8.3 show all the results for safety, mobility and emissions respectively.

Figure 8.1. Safety, mobility, and emissions results for varying traffic demands.

Next, we investigate the co-optimization approach's effectiveness in managing mixed vehicle type scenarios. Two different scenarios were considered: one reflecting the real-world distribution of heavy-duty vehicles (HDVs), medium-duty vehicles (MDVs), and light-duty vehicles (LDVs), and the other representing a truck-dominated scenario with a higher proportion of HDVs. The results for the real-world distribution are shown in Figure 8.2 and show the safety, mobility, and emission output for these scenarios. Adding HDVs and MDVs made it so that there was very little variation between the different traffic volumes. The number of conflicts in Figure 8.2a was significantly lower for the lower traffic volume, but the throughput in Figure 8.2b and the emissions in 8.2c showed similar results across the three v/c ratios simulated. Tables 8.4, 8.5, and 8.6 show all the results for safety, mobility and emissions respectively.

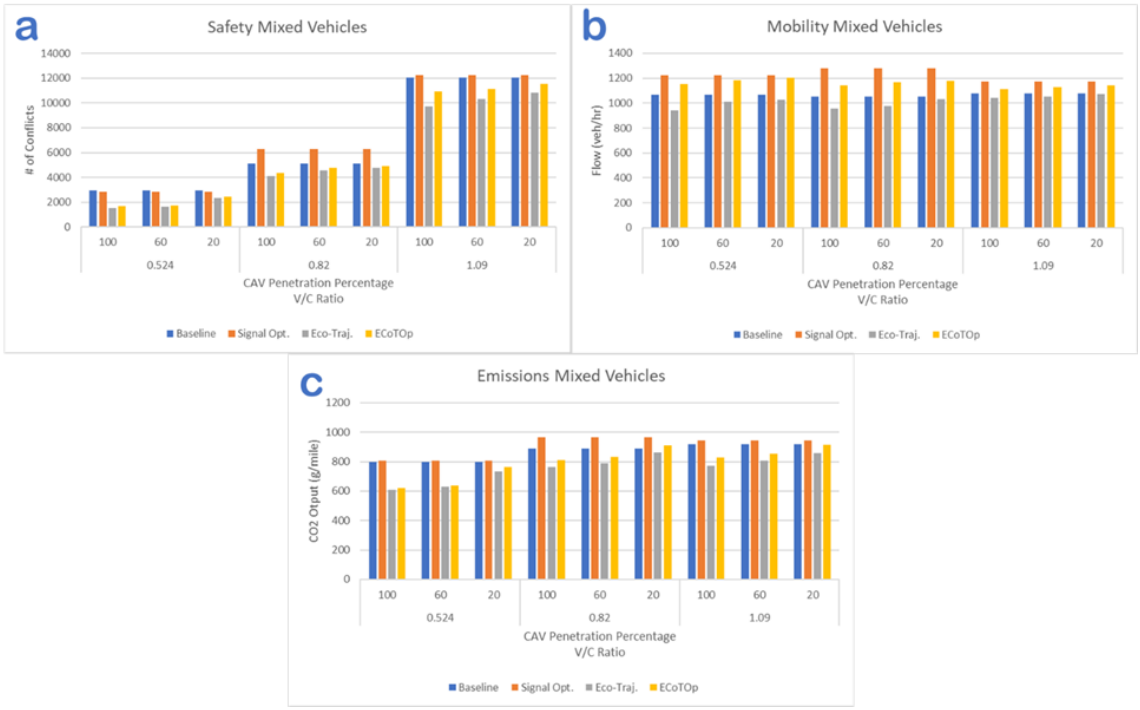

Figure 8.2. Safety, mobility, and emissions results for mixed vehicle types across varying traffic demands.

Table 8.1. CO_2 output results for mixed traffic – real-world distribution.

V/C Ratio	CAV %	Baseline	Signal Opt.		Eco-Trajectory Planning		ECoTOp	
		CO_2 Output (g/mile)	CO_2 Output (g/mile)	% improvement (vs. Baseline)	CO_2 Output (g/mile)	% improvement (vs. Baseline)	CO_2 Output (g/mile)	% improvement (vs. Baseline)
0.524	20	798.8	804.9	-0.7	732.6	8.3	763.6	4.4
	60	798.8	804.9	-0.7	627.6	21.4	638	20.1
	100	798.8	804.9	-0.7	606.8	24.1	621.9	22.1
0.82	20	888.7	964.3	-8.5	862.6	2.9	909.9	-2.4
	60	888.7	964.3	-8.5	791.1	10.9	831.6	6.4
	100	888.7	964.3	-8.5	763.1	14.1	810.6	8.8
1.09	20	919.7	945	-2.7	857.7	6.7	916.4	0.4
	60	919.7	945	-2.7	807.9	12.2	853.3	7.2
	100	919.7	945	-2.7	771	16.2	828.9	9.9

Table 8.2. Flow rate results for mixed traffic – real-world distribution.

V/C Ratio	CAV %	Baseline	Signal Opt.		Eco-Trajectory Planning		ECoTOp	
		Vehicle Flow (veh/hr)	Vehicle Flow (veh/hr)	% improvement (vs. Baseline)	Vehicle Flow (veh/hr)	% improvement (vs. Baseline)	Vehicle Flow (veh/hr)	% improvement (vs. Baseline)
0.524	20	1067.5	1220.7	14.4	1028.7	-3.6	1200.7	12.5
	60	1067.5	1220.7	14.4	1010.4	-5.3	1183.9	10.9
	100	1067.5	1220.7	14.4	942.3	-11.7	1150.3	7.8
0.82	20	1050.3	1276.6	21.5	1029.4	-1.99	1178.6	12.2
	60	1050.3	1276.6	21.5	975.8	-7.1	1167.9	11.2
	100	1050.3	1276.6	21.5	954.1	-9.2	1144.4	8.9
1.09	20	1077.7	1171.3	6.7	1072.9	-0.4	1140.9	5.9
	60	1077.7	1171.3	6.7	1053.4	-2.2	1127.6	4.6
	100	1077.7	1171.3	6.7	1039.9	-3.5	1113.8	3.3

Table 8.3. Safety results for mixed traffic – real-world distribution.

V/C Ratio	CAV %	Baseline	Signal Opt.		Eco-Trajectory Planning		ECoTOp	
		Conflicts	Conflicts	% improvement (vs. Baseline)	Conflicts	% improvement (vs. Baseline)	Conflicts	% improvement (vs. Baseline)
0.524	20	2962.8	2866.9	3.2	2339.6	21.1	2429.1	18.0
	60	2962.8	2866.9	3.2	1652.4	44.2	1722.7	41.8
	100	2962.8	2866.9	3.2	1521.4	48.6	1665.2	43.8
0.82	20	5107.7	6273.3	-22.8	4774.3	6.5	4899.7	4.1
	60	5107.7	6273.3	-22.8	4563.6	10.6	4747.7	7.1
	100	5107.7	6273.3	-22.8	4104.9	19.6	4104.9	14.9
1.09	20	12019.8	12216.3	-1.6	10816.6	10.0	11524.6	4.1
	60	12019.8	12216.3	-1.6	10333.7	14.1	11139.9	7.3
	100	12019.8	12216.3	-1.6	9732.1	19.1	10935.3	9.0

The truck-dominated mixed traffic scenario results were similar to the real-world distribution, and shown in Figure 8.3. The only difference was that the emissions were much high overall for the truck-dominated scenario. Tables 8.7, 8.8, and 8.9 show all the results for safety, mobility and emissions respectively.

Table 8.4. CO_2 output results for mixed traffic – truck dominated distribution.

V/C Ratio	CAV %	Baseline	Signal Opt.		Eco-Trajectory Planning		ECoTOp	
		CO_2 Output (g/mile)	CO_2 Output (g/mile)	% improvement (vs. Baseline)	CO_2 Output (g/mile)	% improvement (vs. Baseline)	CO_2 Output (g/mile)	% improvement (vs. Baseline)
0.524	20	1753.5	1810.1	-3.2	1664.6	5.1	1693.6	3.4
	60	1753.5	1810.1	-3.2	1487.4	15.2	1505.2	14.2
	100	1753.5	1810.1	-3.2	1270.99	27.5	1286.9	26.6
0.82	20	2126.5	2162.9	-1.7	1866.4	12.2	1948.9	8.3
	60	2126.5	2162.9	-1.7	1719.6	19.1	1764.2	17.0
	100	2126.5	2162.9	-1.7	1595.5	24.9	1658.5	22.0
1.09	20	1832.3	1832.6	-0.01	1761.1	3.9	1792.2	2.2
	60	1832.3	1832.6	-0.01	1685.2	8.0	1729.7	5.6
	100	1832.3	1832.6	-0.01	1633.6	10.8	1662.6	9.2

Table 8.5. Flow rate results for mixed traffic – truck dominated distribution.

V/C Ratio	CAV %	Baseline	Signal Opt.		Eco-Trajectory Planning		ECoTOp	
		Vehicle Flow (veh/hr)	Vehicle Flow (veh/hr)	% improvement (vs. Baseline)	Vehicle Flow (veh/hr)	% improvement (vs. Baseline)	Vehicle Flow (veh/hr)	% improvement (vs. Baseline)
0.524	20	900.1	1074.1	19.3	889.1	-1.2	1056.6	17.4
	60	900.1	1074.1	19.3	864.8	-3.9	1023.2	13.7
	100	900.1	1074.1	19.3	836.2	-7.1	998.0	10.9
0.82	20	698.0	961.8	37.7	694.8	-0.5	896.1	28.4
	60	698.0	961.8	37.7	658.4	-5.7	819.9	17.5
	100	698.0	961.8	37.7	640.8	-8.2	820.1	17.5
1.09	20	820.1	1030.1	25.6	818.3	-0.2	1000.2	21.9
	60	820.1	1030.1	25.6	794.7	-3.1	900.3	9.78
	100	820.1	1030.1	25.6	758.8	-7.5	900.1	9.76

Table 8.6. Safety results for mixed traffic – truck dominated distribution.

V/C Ratio	CAV %	Baseline	Signal Opt.		Eco-Trajectory Planning		ECoTOp	
		Conflicts	Conflicts	% improvement (vs. Baseline)	Conflicts	% improvement (vs. Baseline)	Conflicts	% improvement (vs. Baseline)
0.524	20	3359.1	3451.8	-2.8	2381.1	29.1	2601.6	22.5
	60	3359.1	3451.8	-2.8	2320.4	30.9	2413.4	28.2
	100	3359.1	3451.8	-2.8	2087.1	37.9	2125.4	36.7
0.82	20	5019.7	5515.8	-9.9	4350.3	13.3	4721.0	5.9
	60	5019.7	5515.8	-9.9	3878.2	22.7	4363.6	13.1
	100	5019.7	5515.8	-9.9	3678.1	26.7	4123.5	17.9
1.09	20	11483.7	11770.2	-2.5	10587.4	7.8	11008.9	4.1
	60	11483.7	11770.2	-2.5	9728.0	15.3	10706.1	6.8
	100	11483.7	11770.2	-2.5	9118.2	20.6	10108.6	11.9

Additionally, we examine the influence of electric vehicles (EVs) on the ECoTOp approach. By considering different traffic volumes specific to EVs, based on market-predicted EV penetration percentages, the results demonstrated the successful integration of EVs into the traffic stream. The ECoTOp approach effectively improved EV energy efficiency, and minimized the impact of EV charging on overall traffic flow. The safety and mobility measures were very similar to that of no EVs. These findings highlight the ECoTOp approach's potential to facilitate the seamless integration of EVs into the transportation system, promoting sustainable mobility. The results, along with the results for EVs for eco-trajectory planning alone and signal optimization alone, are shown for 18% and 100% EV penetration rate in Figures 8.4 and 8.5, and all EV energy efficiency results are shown in Table 8.10. In Figures 8.4 and 8.5, a is safety, b is mobility, and c is EV efficiency.

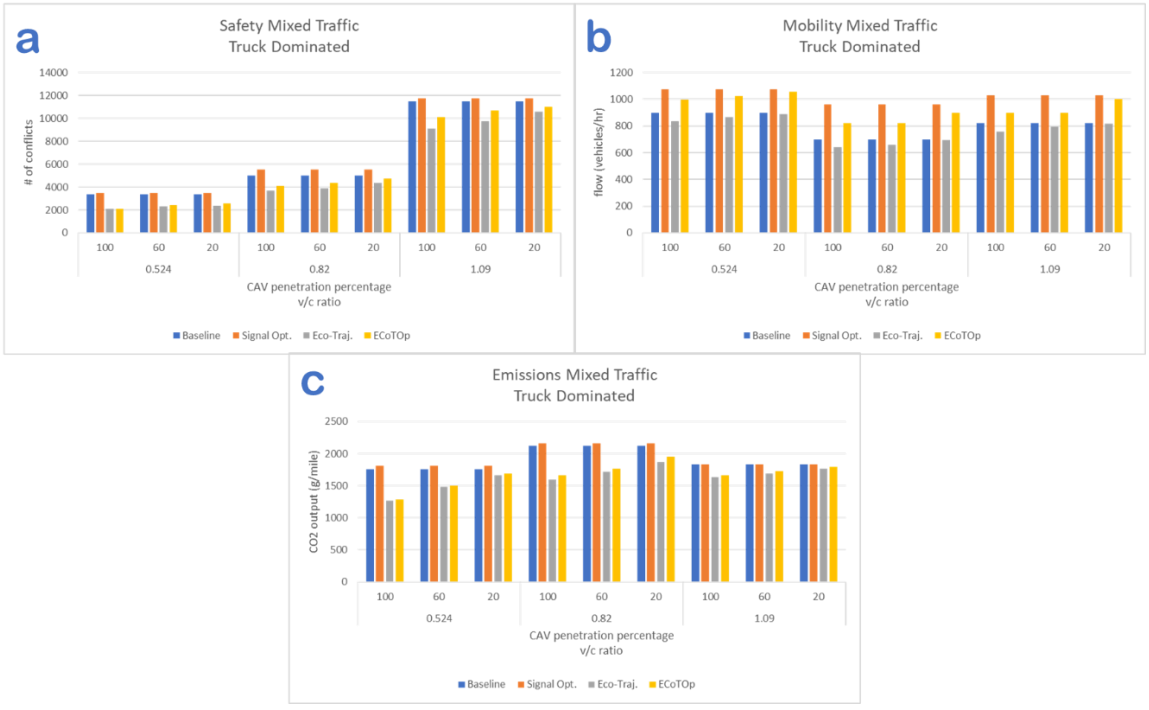

Figure 8.3. Safety, mobility, and emissions results for truck dominated mixed vehicle types across varying traffic demands.

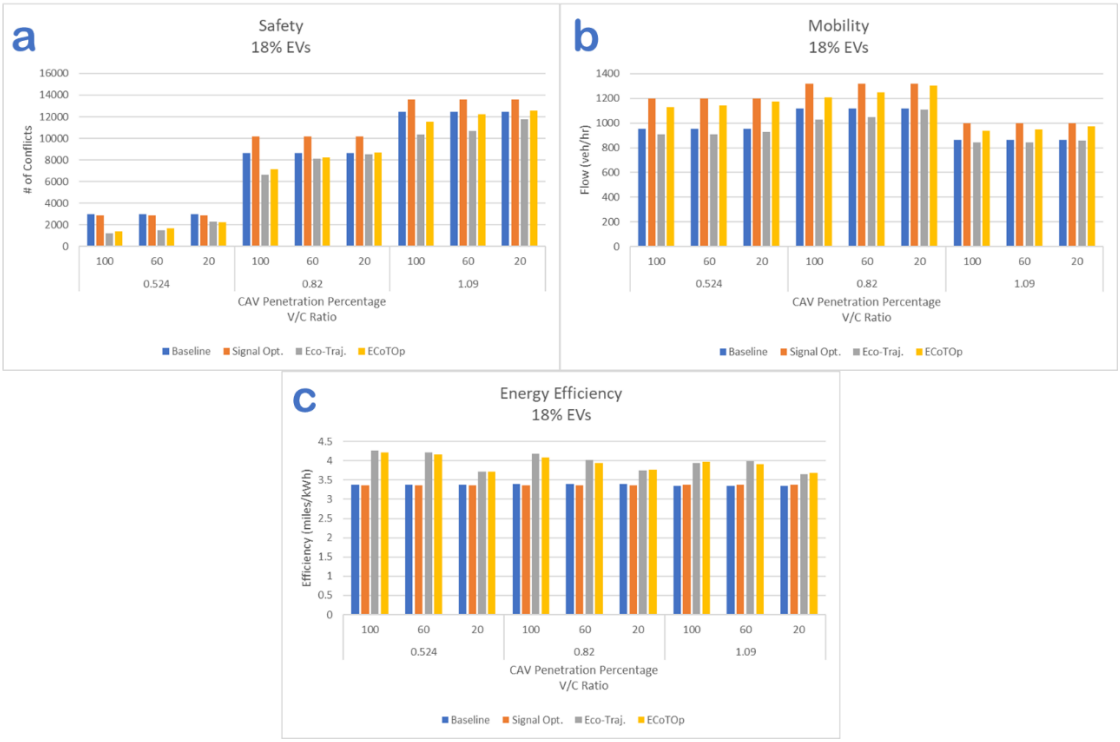

Figure 8.4. Safety, mobility, and energy efficiency results for 18% EVs across varying traffic demands.

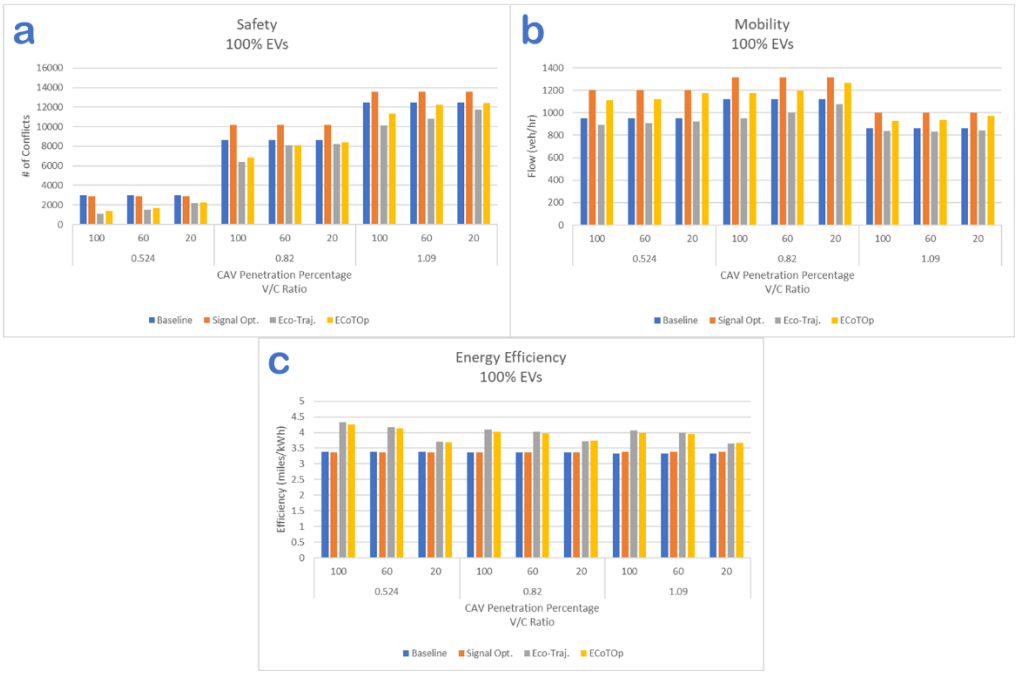

Figure 8.5. Safety, mobility, and energy efficiency results for 100% EVs across varying traffic demands.

Table 8.7. EV energy efficiency across varying CAV and EV penetration rates.

EV %	V/C	CAV %	Baseline	Signal Opt.		Eco-Trajectory Planning		ECoTOp	
			Efficiency (mi/kWh)	Effic. (mi/kWh)	% Improve	Effic. (mi/kWh)	% Improve	Effic. (mi/kWh)	% Improve
18	0.52	20	3.3787	3.3626	-0.5	3.7082	9.7	3.7129	9.9
		60	3.3787	3.3626	-0.5	4.2205	24.9	4.1575	23.1
		100	3.3787	3.3626	-0.5	4.2619	26.1	4.2092	24.6
	0.82	20	3.3946	3.3641	-0.9	3.7464	10.4	3.7551	10.6
		60	3.3946	3.3641	-0.9	4.0261	18.6	3.9403	16.1
		100	3.3946	3.3641	-0.9	4.1729	22.9	4.0852	20.3
	1.09	20	3.3377	3.3815	1.5	3.6538	9.5	3.6895	10.5
		60	3.3377	3.3815	1.5	3.9463	18.2	3.9022	16.9
		100	3.3377	3.3815	1.5	3.9917	19.6	3.9738	19.1
50	0.52	20	3.3878	3.3998	-0.4	3.6955	9.1	3.6873	8.8
		60	3.3878	3.3998	-0.4	4.1673	23.0	4.1133	21.4
		100	3.3878	3.3998	-0.4	4.3138	27.3	4.2622	25.8
	0.82	20	3.3870	3.3738	-0.4	3.7154	9.7	3.7445	10.6
		60	3.3870	3.3738	-0.4	4.0140	18.5	3.9705	17.2
		100	3.3870	3.3738	-0.4	4.0854	20.6	4.0194	18.7
	1.09	20	3.3338	3.3827	1.3	3.6394	9.2	3.6712	10.1
		60	3.3338	3.3827	1.3	3.9463	19.7	3.9623	18.8
		100	3.3338	3.3827	1.3	4.0192	20.6	3.9781	19.3
80	0.52	20	3.3892	3.3855	-0.1	3.7110	9.5	3.6940	9.0
		60	3.3892	3.3855	-0.1	4.1676	22.9	4.1350	22.0
		100	3.3892	3.3855	-0.1	4.3047	27.0	4.2346	24.9
	0.82	20	3.3932	3.3797	-0.4	3.7089	9.3	3.7376	10.1
		60	3.3932	3.3797	-0.4	4.0126	18.3	3.9748	17.1
		100	3.3932	3.3797	-0.4	4.0732	20.0	4.0213	18.5
	1.09	20	3.3291	3.3859	1.7	3.6625	10.0	3.6786	10.5
		60	3.3291	3.3859	1.7	3.9965	20.0	3.9591	18.9
		100	3.3291	3.3859	1.7	4.0089	20.4	3.9786	19.5
100	0.52	20	3.3765	3.3682	-0.2	3.7107	9.9	3.6958	9.5
		60	3.3765	3.3682	-0.2	4.1669	23.4	4.1404	22.6
		100	3.3765	3.3682	-0.2	4.3356	28.4	4.2586	26.1
	0.82	20	3.3733	3.3708	-0.8	3.7148	10.1	3.7364	10.8
		60	3.3733	3.3708	-0.8	4.0195	19.2	3.9681	17.6
		100	3.3733	3.3708	-0.8	4.0931	21.3	4.0311	19.5
	1.09	20	3.3311	3.3824	1.5	3.6486	9.5	3.6777	10.4
		60	3.3311	3.3824	1.5	3.9918	19.8	3.9568	18.8
		100	3.3311	3.3824	1.5	4.0678	22.1	3.9916	19.8

Overall, the simulation experiments provide compelling evidence of the ECoTOp approach's effectiveness in enhancing traffic performance and sustainability across a wide range of scenarios. The results showcased its adaptability to diverse traffic conditions, vehicle compositions, and emerging technologies. These findings underscore the potential of the ECoTOp approach as a promising strategy for improving traffic operations in the context of evolving transportation systems. The simulation experiments also consistently show that as the eco-trajectory planning increases, the emissions/efficiency improves, but the mobility worsens. As signal optimization increases, the mobility (throughput) improves, but the emissions/efficiency worsen. As signal optimization increases, the mobility improves, but the number of conflicts worsen. As eco-trajectory planning increases, the number of conflicts improves, but the mobility also worsens.

In the next section, we discuss the implications of these results and draw key conclusions from the simulation experiments.

8.3 Implications and Conclusions

The findings from the simulation experiments comparing different optimization approaches for vehicle eco-trajectory planning and traffic signal timing at isolated signalized intersections have important implications for transportation planning and optimization strategies. This section discusses the key implications of the results and draws conclusions, emphasizing the establishment of a foundation for the future development of an adaptive optimization strategy capable of dynamically selecting the most appropriate optimization approach based on real-time traffic conditions and environmental considerations.

One significant implication of this study is the identification of the strengths and limitations of different optimization approaches. By comparing the ECoTOp system with the individual approaches of eco-trajectory planning alone and traffic signal optimization alone, the study

highlights the trade-offs and performance differences across these methods. The ECoTOp approach demonstrates superior performance in terms of intersection throughput and emissions compared to the baseline. However, it is also important to acknowledge that as the eco-trajectory planning increases, the emissions/efficiency improves but the mobility worsens, and as signal optimization increases, the mobility improves but the emissions/efficiency worsens indicating the need for an adaptive optimization strategy that can dynamically select the most suitable approach based on the prevailing conditions.

The adaptability and versatility of the ECoTOp approach are crucial aspects of its implementation. The ability to dynamically adjust vehicle trajectories and traffic signal timings based on real-time traffic conditions, vehicle types, and environmental factors is essential for effective traffic management. By considering different scenarios, such as varying traffic volumes, mixed vehicle types, and different CAV penetration rates, the study demonstrates the flexibility of the ECoTOp approach. This adaptability is a key requirement for the future development of an adaptive optimization strategy that can respond to changing traffic conditions and emerging technologies.

Furthermore, the study underscores the importance of considering environmental factors and the increasing presence of electric vehicles (EVs) in transportation planning and optimization. The ECoTOp approach showcases its potential in promoting sustainable mobility by incorporating EVs into the optimization framework. The findings highlight the impact of EVs on vehicle throughput and energy consumption, providing valuable insights for the integration of EVs into transportation systems. The future development of an adaptive optimization strategy will play a crucial role in accommodating EVs and ensuring their efficient and sustainable operation.

Chapter 9

Conclusions and Future Work

In this dissertation, we have embarked on a transformative journey to propose a groundbreaking co-optimization approach for vehicle eco-trajectory planning and traffic signal timing at isolated signalized intersections. This approach is called the Eco-friendly Cooperative Traffic Optimization (ECoTOp) framework. The primary aim was to achieve superior performance in terms of safety, mobility, and emissions. However, our ambition went beyond conventional optimization paradigms. We sought to establish a foundation for the future development of an adaptive optimization strategy capable of dynamically selecting the most suitable approach based on real-time traffic conditions and environmental considerations.

Through meticulous comparative analyses, we unveiled the strengths and limitations of individual eco-trajectory planning and traffic signal timing optimization. The results not only confirmed the efficacy of the ECoTOp approach but also shed light on its unique attributes. The ECoTOp approach demonstrated the ability to achieve a balanced trade-off between improved traffic throughput and reduced emission output, a feat that trajectory and signal optimization alone could not match.

Our journey extended beyond conventional optimization methods as we examined the integration of electric vehicles (EVs) into the ECoTOp framework. By meticulously gathering EV penetration percentages from market-predicted estimates and considering different traffic volumes, we explored the adaptability and effectiveness of our approach in a diverse range of scenarios.

The ECoTOp approach yielded remarkable results, showcasing a substantial improvement of up to 24% in vehicle throughput and a notable reduction of up to 14% in CO_2 emissions when

compared to the baseline. Notably, ECoTOp approach consistently outperformed eco-trajectory planning in terms of traffic throughput, while presenting less effectiveness in CO_2 reduction.

Moreover, our findings indicated that the ECoTOp approach consistently outperformed traffic signal optimization alone in CO_2 reduction, while exhibiting less efficiency in terms of vehicle throughput. In contrast, traffic signal optimization often performed on par with the baseline or experienced up to a 9% decline in CO_2 emissions, whereas eco-trajectory planning demonstrated up to a 17% reduction in CO_2 emissions.

Additionally, the results revealed that traffic signal optimization achieved up to a 38% improvement in traffic throughput, while eco-trajectory planning at times performed similarly to the baseline, or in some cases, up to 12% worse than the baseline.

The comparisons between the ECoTOp system and individual optimization strategies served as a crucial stepping stone for our future ambitions. By laying the foundation for an adaptive optimization strategy, we seek to revolutionize transportation systems. The vision of a dynamic approach capable of responding to real-time traffic conditions and environmental impacts will transform the way we optimize intersections, creating a more efficient, sustainable, and intelligent mobility landscape.

An adaptive optimization strategy would transition from the ECoTOp approach to a traffic signal optimization approach under specific traffic conditions and environmental considerations. The switch could be triggered when traffic volume is relatively low, and the presence of connected and automated vehicles (CAVs) is limited. In such scenarios, the benefits of the ECoTOp approach, which leverages CAV technologies and complex vehicle trajectory planning, might not be fully realized due to reduced traffic interactions.

Additionally, environmental considerations play a crucial role in the adaptive optimization strategy. If the focus is primarily on reducing greenhouse gas emissions and fuel consumption, the

ECoTOp approach may remain more favorable, especially in high-density traffic scenarios with significant CAV penetration. However, in situations where emissions reduction is the primary goal, and traffic flow efficiency is of lesser concern, the eco-trajectory planning approach might be prioritized. Figure 9.1 shows a Venn diagram of the relationship between safety, mobility, and environmental impact, and where the ECoTOp framework, eco-trajectory planning, and traffic signal optimization falls in it. ECoTOp is nearly in the middle of the Venn diagram, but an adaptive optimization strategy could choose between the three strategies depending on the situation, as in Figure 9.2. Ultimately, the adaptive optimization strategy seeks to strike a balance between traffic flow efficiency and environmental sustainability, adapting to the dynamic conditions of the transportation network. By continually assessing real-time data, such as traffic volumes, vehicle types, CAV penetration rates, and emission levels, the adaptive strategy can make informed decisions to optimize traffic management and enhance overall system performance.

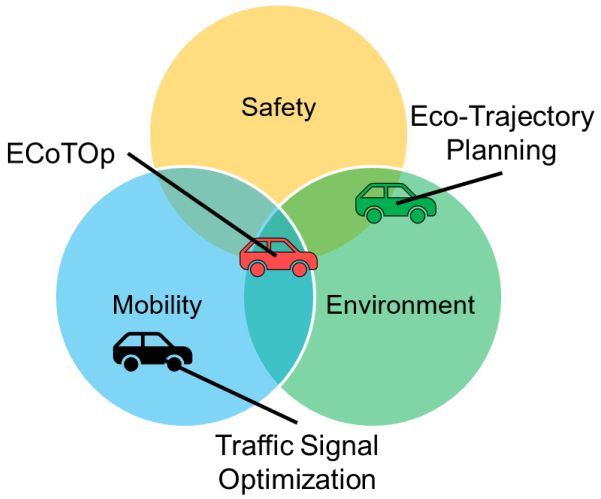

Figure 9.1. Venn diagram of the relationship between safety, mobility, and environmental impact.

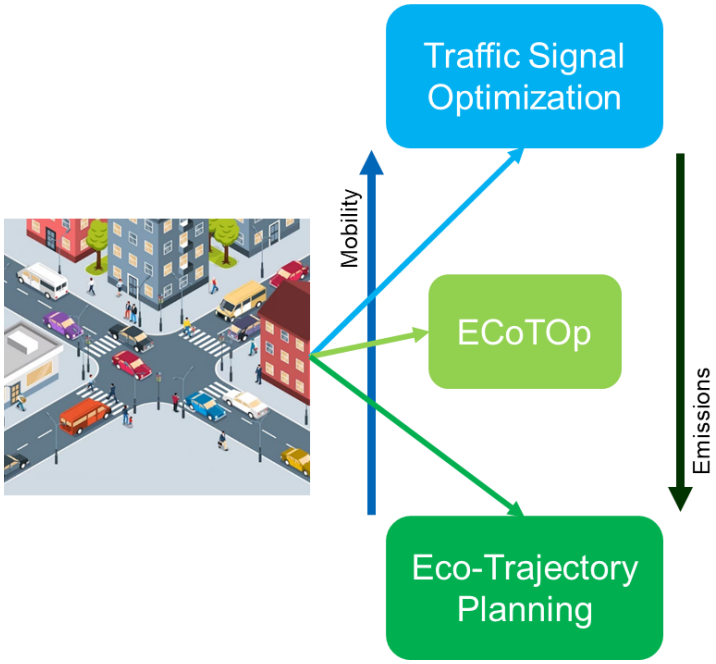

Figure 9.2. Depiction of intersection and the choices based on environment and traffic scenario.

In conclusion, this dissertation contributes not only a pioneering ECoTOp framework but also a roadmap for the future. As we look ahead, we anticipate further research and advancements that will harness the power of adaptive optimization. We envision a future where transportation systems seamlessly adapt to the evolving dynamics of our cities, providing efficient and sustainable mobility solutions for generations to come. The journey does not end here; it merely marks the beginning of a transformative era in transportation optimization.

9.1 Future Work

The completion of this dissertation opens up promising directions for future research, aiming to further enhance co-optimization strategies in traffic management. One important avenue to explore is the dynamic adaptation of optimization strategies based on real-time traffic conditions. Developing algorithms that continuously analyze traffic data and automatically select the most suitable optimization approach would significantly improve the system's responsiveness and

efficiency. Another avenue is to expand the ECoTOp approach from individual intersections to a network of signalized intersections is a natural progression. Investigating how co-optimization strategies can be scaled up and applied to larger urban road networks will be essential for developing practical applications for smart cities.

The integration of machine learning techniques into the co-optimization process presents another exciting opportunity. By leveraging historical traffic data, machine learning algorithms can identify patterns and trends, leading to more adaptive and predictive optimization strategies.

Environmental impact assessments can be extended beyond CO_2 emissions to include other pollutants, providing a comprehensive understanding of the ECoTOp approach's overall contributions to sustainable transportation.

Validating the ECoTOp approach in real-world scenarios and operational road networks is a crucial next step. Collaboration with transportation agencies and stakeholders can facilitate the transition from simulation-based experiments to practical applications.

Furthermore, researchers can explore how to incorporate resilience and safety considerations into the ECoTOp framework, ensuring its viability in unexpected events or emergencies while maintaining traffic efficiency and safety.

As the co-optimization strategies have the potential to impact traffic behavior and travel patterns, future research should examine public acceptance, behavioral changes, and policy implications when implementing these strategies in urban environments.

By pursuing these research avenues, the field of traffic management and optimization will advance, leading to more sustainable, efficient, and resilient transportation systems in the cities of the future.

9.2 Papers Resulting from this Research

Oswald, D., Scora, G., Williams, N., Hao, P. and Barth, M., 2019, October. "Evaluating the environmental impacts of connected and automated vehicles: Potential shortcomings of a binned-based emissions model." In 2019 IEEE intelligent transportation systems conference (ITSC) (pp. 3639-3644). IEEE.

Oswald, D., Hao, P., Williams, N., and Barth, M., "Development of an Innovation Corridor Testbed for Shared Electric Connected and Automated Transportation". UC Davis: National Center for Sustainable Transportation, 2021. http://dx.doi.org/10.7922/G21C1V6T Retrieved from https://escholarship.org/uc/item/99q6w075.

Oswald, D., Vu, A., Williams, N., Boriboonsomsin, K., Barth, M.J., Kunimura, Y., Nagaya, T., Yoshimatsu, H. and Fukuoka, N., 2021, September. "Real-world Efficacy of a Haptic Accelerator Pedal-based Eco-driving System. In 2021 IEEE International Intelligent Transportation Systems Conference (ITSC) (pp. 1541-1546). IEEE.

Oswald, D., Hao, P., Wu, G., and Barth, M., "Eco-friendly Cooperative Traffic Optimization (EcoTOp) at Signalized Intersections with Mixed Connected Traffic", Transportation Research Board Annual Meeting, Washington, DC, January 2023.

Liao, X., **Oswald, D.**, Wang, Z., Wu, G., Boriboonsomsin, K., Barth, M.J., Han, K., Kim, B. and Tiwari, P., "Cooperative Ramp Merging with Vehicle-to-Cloud Communications: A Field Experiment."

Wang, Z., Liao, X., Wang, C., **Oswald D.**, Wu, G., Boriboonsomsin, K., Barth, M.J., Han, K., Kim, B., Tiwari, P., "Driver behavior modeling using game engine and real vehicle: A learning-based approach." IEEE Transactions on Intelligent Vehicles. 2020 May 1;5(4):738-49.

Farrell, J.A., Wu, G., Hu, W., Oswald, D., and Hao, P., 2023. "Lane-Level Localization and Map Matching for Advanced Connected and Automated Vehicle (CAV) Applications." UC Davis: National Center for Sustainable Transportation, 2022.

Bibliography

[1] D. Schrank, B. Eisele, T. Lomax, "2019 Urban Mobility Report," Published by The Texas A&M Transportation Institute, Aug. 2019.

[2] "Sources of Greenhouse Gas Emissions," US Environmental Protection Agency, Accessed on: Dec. 10, 2019. [online]. Available: https://www.epa.gov/ghgemissions/sources-greenhouse-gas-emissions.

[3] "Where Does Air Pollution Come From?," National Park Service, Jan. 17, 2018. Accessed on: Dec. 16, 2019. [online]. Available: https://www.nps.gov/subjects/air/sources.htm.

[4] C. Shirley, R. Gecan, J. Kile, D. Adler, D. Austin, N. Chase, B. Hopkins, A. Krupkin, T. Prendergast, R. Reese, J. Rosenberg, N. Tawil, S. Willie, M. Dwyer, R. Lattanzio, J. Kling, R. Sunshine, B. Peery, and R. L. Rebach. "Emissions of Carbon Dioxide in the Transportation Sector," Congressional Budget Office, December 2022. Accessed on: June 14, 2023. [online]. Available: https://www.cbo.gov/publication/58861

[5] T. Houser and H. Pitt, Preliminary US Emissions Estimates for 2019, Rhodium Group, Jan 07, 2020. Accessed on Feb 12, 2020. [online]. Available: https://rhg.com/research/preliminary-us-emissions-2019/

[6] K. Boriboonsomsin, A. Vu, M. J. Barth, "Eco-Driving: Pilot Evaluation of Driving Behavior Changes Among U.S. Drivers," UC Berkeley: University of California Transportation Center. Aug. 01, 2010. Retrieved from https://escholarship.org/uc/item/9z18z7xq

[7] N. Lu, N. Cheng, N. Zhang, X. Shen, and J. W. Mark, "Connected Vehicles: Solutions and Challenges," IEEE Internet of Things Journal, vol. 1, no. 4, pp. 289-299, Aug. 2014.

[8] "How an Automated Car Platoon Works," US Department of Transportation, [online]. Available: https://www.transportation.gov/connections/how-automated-car-platoon-works

[9] M. Barth and K. Boriboonsomsin, "Energy and emissions impacts of a freeway-based dynamic eco-driving system," Transportation Research Part D: Transport and Environment, vol. 14, no. 6, pp. 400-410, 2009.

[10] Mandava, S., Boriboonsomsin, K. and Barth, M. Arterial Velocity Planning based on Traffic Signal Information under Light Traffic Conditions. *The 12th International IEEE Conference on Intelligent Transportation Systems*, St. Louis, MO, October 2009.

[11] B. Asadi and A. Vahidi, "Predictive cruise control: utilizing upcoming traffic signal information for improving fuel economy and reducing trip time," International IEEE Conf. on Control Systems Technology, 2011, pp. 707-714.

[12] H. Rakha and R. K. Kamalanathsharma, "Eco-driving at signalized intersections using v2i communication," International IEEE Conf. on Intelligent Transportation Systems, 2011, pp. 341-346.

[13] P. Michandani and L. Head, “A real-time traffic control system: architecture, algorithms, and analysis,” Transportation Research Part C, vol. 9, pp. 415-432, 2001.

[14] Y. Feng, L. Head, S. Khoshmagham, and M. Zamanipour, “A real-time adaptive signal control in a connected vehicle environment,” Transportation Research Part C, vol. 55, pp. 460-473, 2015.

[15] Lopez, P.A., Behrisch, M., Bieker-Walz, L., Erdmann, J., Flotterod, Y.P., Hilbrich, R., Lucken, L., Rummel, J. Wagner, P., Wiessner, E., 2018. Microscopic traffic simulation using sumo. IEEE Intelligent Transportation Systems Conference. https://doi.org/10.1109/ITSC.2018.8569938.

[16] “MOVES and Other Mobile Source Emissions Models,” US-EPA, Accessed 2021, https://www.epa.govf/moves

[17] E. Bavarez, and G. F. Newell. “Traffic Signal Synchronization on a one-way street.” Transportation Science, vol. 1, no. 2, pp. 55-73, 1967.

[18] U.S. Department of Transportation, 2021. Traffic signal timing manual (Report No. FHWA-HOP-08-024). National Highway Traffic Safety Administration.

[19] M. Brown. “The World’s First Traffic Lights in London.” Londonist. https://londonist.com/london/history/here-s-what-the-world-s-first-traffic-lights-in-westminster-looked-like, (2023).

[20] M. Gordon. “Traffic devices: historical aspects thereof.” Washington Institute of Traffic Engineers publications, OCLC 278619, pp. 27-28, 1971.

[21] G. Duncan, L. Head, and R. Puvvala, “Multi-Modal Intelligent Traffic Signal System — Safer and More Efficient Intersections Through a Connected Vehicle Environment,” IMSA Journal, Sep. 2014.

[22] “Multi-Modal Intelligent Traffic Safety System (MMITSS),” Intelligent Transportation Systems Joint Program Office, US Department of Transportation, [online]. Available: https://www.its.dot.gov/research_archives/dma/bundle/mmitss_plan.htm

[23] W. Sun, Y. Wang, G. Yu, and H. X. Liu, “Quasi-optimal feedback for a system of oversaturated intersections,” Transportation Research Part C, vol. 57, pp. 224-240, 2015.

[24] X. He, H. X. Liu, and X. Liu, “Optimal vehicle speed trajectory on a signalized arterial with consideration of queue,” Transportation Research Part C, vol. 61, pp. 106-120, 2015.

[25] X. Huang and H. Peng, “Speed trajectory planning at signalized intersections using sequential convex optimization,” American Control Conference, 2017, pp. 2992-2997.

[26] H. Xia et al., “Field Operational Testing of ECO-Approach Technology at a Fixed-Time Signalized Intersection,” International IEEE Conf. on Intelligent Transportation Systems, 2012, pp. 188-193.

[27] O. D. Altan, G. Wu, M. J. Barth, K. Boriboonsomsin, and J. A. Stark, “GlidePath: Eco-Friendly Automated Approach and Departure at Signalized Intersections,” IEEE Transactions on Intelligent Vehicles, vol. 2, no. 4, pp. 266-277, Dec. 2017.

[28] P. Hao, G. Wu, K. Boriboonsomsin, and M. J. Barth, “Preliminary Evaluation of Field Testing on Eco-Approach and Departure (EAD) Application for Actuated Signals,” 2015 International Conference on Connected Vehicles and Expo (ICCVE), Shenzhen, 2015, pp. 279-284.

[29] P. Hao, G. Wu, K. Boriboonsomsin and M. J. Barth, "Eco-Approach and Departure (EAD) Application for Actuated Signals in Real-World Traffic," in IEEE Transactions on Intelligent Transportation Systems, vol. 20, no. 1, pp. 30-40, Jan. 2019.

[30] Hao, P., Boriboonsomsin, K., Wang, C., Wu, G., Barth, M.J., 2021a. Connected eco-approach and departure system for diesel trucks. SAE Int. J. Commer. Veh. 14 (2), 217-227. https://doi.org/10.4271/02-14-02-0017.

[31] Esaid, D., Hao, P., Wu, G., Fei, Y., Wei, Z., Boriboonsomsin, K., Barth, M.J., 2021. Machine learning-based eco-approach and departure: real-time trajectory optimization at connected signalized intersection. SAE J. STEEP 3 (1), 41-53. https://doi.org/10.4271/13-03-01-0004.

[32] Chang, M.F., Evans, L., Herman, R., Wasielewski, P., 1976. Gasoline consumption in urban traffic. Trans. Research Record 566, 25-30.

[33] Akcelik, R., 1980. Fuel efficiency and other objectives in traffic system management. Traffic Engineering and Control, 22 (2), 54-65.

[34] Newman, P.W.G., Kenworthy, J.R., 1988. The transport energy trade-off: fuel-efficient traffic versus fuel efficient cities. Transport. Res. A: General, 22 (3), 163-174. https://doi.org/10.1016/0191-2607(88)90034-9.

[35] Tong, H.Y., Hung, W.T., Cheung, C.S., 2000. On-road motor vehicle emissions and fuel consumption in urban driving conditions. Journal of the Air and Waste Management Assoc., 50 (4), 543-554. https://doi.org/10.1080/10473289.2000.10464041.

[36] Malakorn, K.J., Park, B., 2010. Assessment of mobility, energy, and environment impacts of intellidrive-based cooperative adaptive cruise control and intelligent traffic signal control. IEEE International Symposium on Sustainable Systems and Technology. https://doi.org/10.1109/ISSST.2010.5507709.

[37] Yu, C., Feng, Y., Liu, H.X., Ma, W., Yang, X., 2018. Integrated optimization of traffic signals and vehicle trajectories at isolated urban intersections. Transport. Res. B: Methodol. 112, 89-112. https://doi.org/10.1016/j.trb.2018.04.007.

[38] Xu, B., Ban, X.J., Bian, Y., Li, W., Wang, J., Li, S.E., Li, K., 2019. Cooperative method of traffic signal optimization and speed control of connected vehicles at isolated intersections. IEEE Trans. On Intelligent Transportation Systems, 20 (4), 1390-1403. https://doi.org/10.1109/TITS.2018.2849029.

[39] Guo, Y., Ma, J., Xiong, C., Li, X., Zhou, F., Hao, W., 2019. Joint optimization of vehicle trajectories and intersection controllers with connected automated vehicles: combined dynamic programming and shooting heuristic approach. Trans. Res. C: Emerging Tech. 98, 54-72. https://doi.org/10.1016/j.trc.2018.11.010.

[40] Du, Y., ShangGuan, W., Chai, L., 2021. A coupled vehicle-signal control method at signalized intersections in mixed traffic environment. IEEE Trans. On Vehicular Tech. 70 (3), 2089-2100. https://doi.org/10.1109/TVT.2021.3056457.

[41] Sun, P., Nam, D., Jayakrishnan, R., Jin, W., 2022. An eco-driving algorithm based on vehicle to infrastructure (v2i) communications for signalized intersections. Trans. Res. C: Emerging Tech. 144, 103876. https://doi.org/10.1016/j.trc.2022.103876.

[42] D. Oswald, P. Hao, N. Williams, M. Barth, "Development of an Innovation Corridor Testbed for Shared Electric Connected and Automated Transportation". UC Davis: National Center for Sustainable Transportation, 2021. http://dx.doi.org/10.7922/G21C1V6T Retrieved from https://escholarship.org/uc/item/99q6w075.

[43] Liao, X., Oswald, D., Wang, Z., Wu, G., Boriboonsomsin, K., Barth, M.J., Han, K., Kim, B. and Tiwari, P., Cooperative Ramp Merging with Vehicle-to-Cloud Communications: A Field Experiment.

[44] Wang Z, Liao X, Wang C, Oswald D, Wu G, Boriboonsomsin K, Barth MJ, Han K, Kim B, Tiwari P. Driver behavior modeling using game engine and real vehicle: A learning-based approach. IEEE Transactions on Intelligent Vehicles. 2020 May 1;5(4):738-49.

[45] Hu, W., Neupane, A. and Farrell, J.A., 2022. Using PPP Information to Implement a Global Real-Time Virtual Network DGNSS Approach. IEEE Transactions on Vehicular Technology, 71(10), pp.10337-10349.

[46] Teunissen, P.J. and Montenbruck, O. eds., 2017. Springer handbook of global navigation satellite systems (Vol. 10, pp. 978-3). Cham, Switzerland: Springer International Publishing.

[47] Farrell, J., 2008. Aided navigation: GPS with high rate sensors. McGraw-Hill, Inc..

[48] PTV Group PTV VISSIM, 2022. (https://www.ptvgroup.com/)

[49] Farrell, J.A., Wu, G., Hu, W., Oswald, D. and Hao, P., 2023. Lane-Level Localization and Map Matching for Advanced Connected and Automated Vehicle (CAV) Applications. UC Davis: National Center for Sustainable Transportation, 2022.

[50] Oswald, D., Scora, G., Williams, N., Hao, P. and Barth, M., 2019, October. Evaluating the environmental impacts of connected and automated vehicles: Potential shortcomings of a binned-based emissions model. In 2019 IEEE intelligent transportation systems conference (ITSC) (pp. 3639-3644). IEEE.

[51] Oswald, D., Vu, A., Williams, N., Boriboonsomsin, K., Barth, M.J., Kunimura, Y., Nagaya, T., Yoshimatsu, H. and Fukuoka, N., 2021, September. Real-world Efficacy of a Haptic

Accelerator Pedal-based Eco-driving System. In 2021 IEEE International Intelligent Transportation Systems Conference (ITSC) (pp. 1541-1546). IEEE.

[52] Y. Zhang, P. A. Ioannou, "Environmental impact of combined variable speed limit and lane change control: a comparison of MOVES and CMEM model," International Federation of Automatic Control, Vol. 49, no. 3, pp 323-328, 2016.

[53] S. Bai, D. Eisinger, D. Niemeier, "MOVES vs. emfac: a comparison of greenhouse gas emissions using los angeles county," In Proceedings of the Transportation Research Board 88th Annual Meeting, Washington, DC, USA, 11–15 January 2009.

[54] G. Scora, B. Morris, C. Tran, M. Barth, M. Trivedi, "Real-time roadway emissions estimation using visual traffic measurements," IEEE Forum on Integrated and Sustainable Transportation Systems, Vienna, Austria, 2011.

[55] A. Cappiello, I. Chabini, E. K. Nam, A. Lue, M. Abou Zeid, "A statistical model of vehicle emissions and fuel consumption." IEEE 5th International Conference on Intelligent Transportation Systems, Singapore, 2002.

[56] H. Rakha, K. Ahn, A. Trani, "Comparison of mobile5a, mobile6, vt-micro, and cmem models for estimating hot-stabilized light-duty gasoline vehicle emissions," Canadian Journal of Civil Engineering, Vol. 30, no. 6, pp 1010-1021, 2003.

[57] R. Chamberlin, B. Swanson, E. Talbot, J. Dumont, S. Pesci, "Analysis of moves and cmem for evaluating the emissions impacts of an intersection control change," Transportation Research Board 90th Annual Meeting, 11-0673, 2011.

[58] H. Abou-Senna, E. Radwan, K. Westerlund, C. D. Cooper, "Using a traffic simulation model (vissim) with an emissions model (MOVES) to predict emissions from vehicles on a limited-access highway," Journal of the Air & Waste Management Association, Vol. 63, no. 7, pp 819-831, 2013.

[59] J. Liu, K. M. Kockelman, A. Nichols, "Anticipating the emissions impacts of smoother driving by connected and autonomous vehicles, using the MOVES model," In Proceedings of the Transportation Research Board 96th Annual Meeting, Washington, DC., 2017.

[60] Y. Xu, H. Li, H. Liu, M. O. Rodgers, R. L. Guensler, "Eco-driving for transit: An effective strategy to conserve fuel and emissions," Applied Energy, Vol. 194, pp 784-797, 2017.

[61] L. El-Shawarby, K. Ahh, and H. Rakha, "Comparative field evaluation of vehicle cruise speed and acceleration level impacts on hot stabilized emissions," Transportation Research Part D, vol. 10, no. 1, Jan. 2005, pp. 13-30.

[62] Kobayashi, Yosuke, et al. "Development of a Prototype Driver Support System With Accelerator Pedal Reaction Force Control and Driving and Braking Force Control." SAE Transactions, vol. 115, 2006, pp. 268–272. JSTOR, www.jstor.org/stable/44700050. Accessed 01 Mar. 2021.

[63] R. Hayashi, F. Yin, P. Raksincharoensak, M. Nagai, S. Sannodo and M. Hoshino, "Study on acceleration and deceleration maneuver guidance for driver by gas pedal reaction force control," 13th International IEEE Conference on Intelligent Transportation Systems, Funchal, Portugal, 2010, pp. 1428-1434, doi: 10.1109/ITSC.2010.5625142.

[64] "ECO Pedal," Nissan Motor Corporation, https://www.nissan-global.com/EN/TECHNOLOGY/OVERVIEW/eco_pedal.html. Accessed Mar. 2021.

[65] F. U. Syed, D. Filev and Hao Ying, "Real time Advisory System for Fuel Economy Improvement in a Hybrid Electric Vehicle," NAFIPS 2008 - 2008 Annual Meeting of the North American Fuzzy Information Processing Society, New York, NY, USA, 2008, pp. 1-6, doi: 10.1109/NAFIPS.2008.4531275.

[66] F. U. Syed, D. Filev, F. Tseng and Hao Ying, "Adaptive real-time advisory system for fuel economy improvement in a hybrid electric vehicle," NAFIPS 2009 - 2009 Annual Meeting of the North American Fuzzy Information Processing Society, Cincinnati, OH, USA, 2009, pp. 1-7, doi: 10.1109/NAFIPS.2009.5156404..

[67] Hanna Larsson and Eva Ericsson, "The effects of an acceleration advisory tool in vehicles for reduced fuel consumption and emissions," Transportation Research Part D, vol. 14, no. 2, 2009, pp. 141-146. ISSN 1361-9209, https://doi.org/10.1016/j.trd.2008.11.004.

[68] S. Azzi, G. Reymond, F. Merienne, and A. Kemeny, "Eco-driving performance assessment with in-car visual and haptic feedback assistance," Driving Simulation Conference, Paris, France, Sep. 2010, pp. 181-190. Hal-01343184.

[69] A. H. Jamson, D. L. Hibberd, and N. Merat, "Interface design considerations for an in-vehicle eco-driving assistance system, Transportation Research Part C, vol. 58, part D, Sep. 2015, pp.642-656.

[70] Federal Highway Administration, Table DL-22 – Highway Statistics 2017. Accessed 17 Mar. 2021, https://www.fhwa.dot.gov/policyinformation/statistics/2017/dl22.cfm.

[71] H. Nishiuchi and T. Yoshii, "A Study of the Signal Control for the Minimization of CO2 Emission," Proceedings of the 12th World Congress on Intelligent Transport Systems, San Francisco, CA, 2005.

[72] Wu, G., Hao, P., et al. Eco-Approach and Departure along Signalized Corridors Considering Powertrain Characteristics. SAE International Journal of Sustainable Transportation, Energy, Environment & Policy, Vol. 2, No. 1, 2021, pp. 25 – 40.

[73] H. Yang, F. Almutairi, and H. Rakha. "Eco-driving at signalized intersections: a multiple signal optimization approach," IEEE Transactions on Intelligent Transportation Systems, vol. 22, no. 5, pp. 2943 – 2955, 2021.

[74] Hedges, C. and Perry, F., "Overview and Use of SAE J2735 Message Sets for Commercial Vehicles," SAE Technical Paper 2008-01-2650, 2008, https://doi.org/10.4271/2008-01-2650.

[75] Jiang, D., Taliwal, V., Meier, A., Holfelder, W. and Herrtwich, R., 2006. Design of 5.9 GHz DSRC-based vehicular safety communication. *IEEE wireless communications*, 13(5), pp.36-43.

[76] Ge, X., Tu, S., Mao, G., Wang, C.X. and Han, T., 2016. 5G ultra-dense cellular networks. *IEEE Wireless Communications*, 23(1), pp.72-79.

[77] Santa, J., Gómez-Skarmeta, A.F. and Sánchez-Artigas, M., 2008. Architecture and evaluation of a unified V2V and V2I communication system based on cellular networks. *Computer Communications,* 31(12), pp.2850-2861.

[78] Kim, H., Han, J., Kim, S.H., Choi, J., Yoon, D., Jeon, M., Yang, E., Pham, N., Woo, S., Park, J. and Kim, D., 2017, June. IsV2C: An integrated road traffic-network-cloud simulator for V2C connected car services. In 2017 *IEEE International Conference on Services Computing (SCC)* (pp. 434-441). IEEE.

[79] Mahler, G., Winckler, A., Fayazi, S.A., Filusch, M. and Vahidi, A., 2017, October. Cellular communication of traffic signal state to connected vehicles for arterial eco-driving. In 2017 IEEE 20th International Conference on Intelligent Transportation Systems (ITSC) (pp. 1-6). IEEE.

[80] Z. Xu, X. Li, X. Zhao, M. H. Zhang, and Z. Wang. "DSRC versus 4g-lte for connected vehicle applications: a study on field experiments of vehicular communication performance," Journal of Advanced Transportation, Aug. 2017.

[81] A. Vinel. "3GPP lte versus ieee 802.11p/wave: which technology is able to support cooperative vehicular safety applications?," IEEE Wireless Communications Letters, vol. 1, no. 2, April 2012.

[82] A. Rayamajhi, A. Yoseph, A. Balse, Z. Huang, E. M. Leslie, V. Fessmann. "Preliminary performance baseline testing for dedicated short-range communication (dsrc) and cellular vehicle-to-everything (c-v2x)," IEEE 92nd Vehicular Technology Conference, pp. 1-5, 2020.

[83] Puterman, M., 1977. Dynamic programming and its applications. Proc. Of the International Conference on Dynamic Programming and its Applications.

[84] Wei, Y., Avci, C., Liu, J., Belezamo, B., Aydin, N., Li, P., Zhou, X., 2017. Dynamic programming-based multi-vehicle longitudinal trajectory optimization with simplified car following models. Trans. Res. B: Methodol. 106, 102-129. https://doi.org/10.1016/j.trb.2017.10.012.

[85] Witten, I.H., Frank, E., Hall, M.A., Pal, C.J., 2016. Data mining: practical machine learning tools and techniques, 3rd edition. Morgan Kaufmann Publishers.

[86] Chauhan, N.K., Singh, K., 2022. Performance assessment of machine learning classifiers using selective feature approaches for cervical cancer detection. Wireless Personal Communications 124, 2335-2366. https://doi.org/10.1007/s11277-022-09467-7.

[87] Ho, T.K., 1995. Random Decision Forests. Proc. Of 3rd International Conf. on Document Analysis and Recognition. https://doi.org/10.1109/ICDAR.1995.598994.

[88] Kraft, D., 1988. A software package for sequential quadratic programming. Forschungsbericht-Deutsche Forschungs-und Versuchsanstalt fur Luft- und Raumfahrt.

[89] Murray, W., Prieto, F.J., 1995. A sequential quadratic programming algorithm using an incomplete solution of the subproblem. Society for Industrial and Applied Mathematics 5 (3), 590-640. https://doi.org/10.1137/0805030.

[90] Han, S.P., 1980. Least-squares solution of linear inequalities. Wisconsin Univ.- Madison Mathematics Research Center.

[91] Burke, J.V., Han, S.P., 1989. A robust sequential quadratic programming method. Mathematical Programming 43, 277-303. https://link.springer.com/article/10.1007/BF01582294.

[92] Nocedal, J., Wright, S.J., 1999. Numerical optimization. New York, NY: Springer New York. https://link.springer.com/content/pdf/10.1007/0-387-22742-3_18.pdf

[93] Virtanen, P. et al., 2020. SciPy 1.0: fundamental algorithms for scientific computing in python. Nature Methods 17 (3), 261-272. https://doi.org/10.1038/s41592-019-0686-2.

[94] Kell, J.H., Fullerton, I.J., 1991. Manual of traffic signal design, second edition. https://trid.trb.org/view/349378

[95] Franz, W.J., Hartenstein, H., Bochow, B., 2001. Internet on the road via inter-vehicle communications. GI Jahrestagung (1), 577-584.

[96] Luo, J., Hubau, J.P., 2004. A survey of inter-vehicle communication. Technical Report, IC/2004/24. https://infoscience.epfl.ch/record/28039.

[97] Lopez, P.A., Behrisch, M., Bieker-Walz, L., Erdmann, J., Flotterod, Y.P., Hilbrich, R., Lucken, L., Rummel, J. Wagner, P., Wiessner, E., 2018. Microscopic traffic simulation using sumo. IEEE Intelligent Transportation Systems Conference. https://doi.org/10.1109/ITSC.2018.8569938.

[98] Pu, L., Joshi, R., and Siemens Energy, 2008. Surrogate safety assessment model—software user manual. (Report No. FHWA-HRT-08-050). Turner-Fairbank Highway Research Center.

[99] Treiber, M., Hennecke, A., Helbing, D., 2000. Congested traffic states in empirical observations and microscopic simulations. Physical Review E 62 (2), 1805-1824. https://doi.org/10.1103/PhysRevE.62.1805.

[100] Gettman, D., Pu, L., Sayed, T., Shelby, S., 2008. Surrogate safety assessment model and validation: final report (Report no. FHWA-HRT-08-051). National Highway Traffic Safety Administration. https://rosap.ntl.bts.gov/view/dot/39210.

[101] Zhou, S., Li, K., Sun, J., Han, P., 2010. Calibration and validation procedure for intersection safety simulation using ssam and vissim. Integrated Trasportation Systems-Green, Intelligent, Reliable. https://doi.org/10.1061/41127(382)64.

[102] Fan, R., Yu, H., Liu, P., Wang, W., 2011. Using vissim simulation model and surrogate safety assessment model for estimating field measured traffic conflicts at freeway merge areas. IET Intelligent Transport Systems 7 (1), 68-77. https://doi.org/10.1049/iet-its.2011.0232.

[103] Huang, F., Liu, P., Yu, H., Wang, W., 2013. Identifying if vissim simulation model and ssam provide reasonable estimates for field measured traffic conflicts at signalized intersections. Accident Analysis and Prevention 50, 1014-1024. https://doi.org/10.1016/j.aap.2012.08.018

[104] Wu, J., Radwan, E., Abou-Senna, H., 2018. Determination if vissim and ssam could estimate pedestrian-vehicle conflicts at signalized intersections. Journal of Transportation Safety and Security 10 (6), 572-585. https://doi.org/10.1080/19439962.2017.1333181

[105] E. Connelly and A. Dasgupta, "Electric car sales break new records with momentum expected continue through 2023." Electric vehicles – IEA. June 2023. https://www.iea.org/energy-system/transport/electric-vehicles, Accessed, June 2023.

[106] S. Searle and J. Miller, "To Put the United States on Track to Reach 50% Electric Vehicle Sales in 2030, Cut the Greenhouse Gas Target in Half." The International Council on Clean Transportation. 7 September, 2022. https://theicct.org/us-ghg-standards-ev-sales-sep22/, Accessed, June 2023.

[107] "Electric vehicles are forecast to be half of global car sales by 2035." Goldman Sachs. 10 Feb, 2023. https://www.goldmansachs.com/intelligence/pages/electric-vehicles-are-forecast-to-be-half-of-global-car-sales-by-2035.html. Accessed, June 2023.

[108] "California moves to accelerate to 100% new zero-emission vehicle sales by 2035." California Air Resources Board, 25 August, 2022. https://ww2.arb.ca.gov/news/california-moves-accelerate-100-new-zero-emission-vehicle-sales-2035. Accessed, June 2023.

[109] "EV Reference Application." MathWorks. https://www.mathworks.com/help/autoblks/ug/electric-vehicle-reference-application.html. Accessed December 2022.